Nina Jäger, BSc

Tracking-Down Molecular Interactions in an Amorphous Solid Dispersion and Investigating their Role in Dissolution Testing

MASTER'S THESIS

to achieve the university degree of

Diplom-Ingenieurin

Master's degree programme: Chemical and Pharmaceutical Engineering

submitted to

Graz University of Technology

Supervisor

Univ.-Prof. Dipl.-Ing. Dr. techn. Johannes Khinast

Institute of Process and Particle Engineering

Graz, February 2017

AFFIDAVIT

I declare that I have authored this thesis independently, that I have not used other than the declared sources/resources, and that I have explicitly indicated all material which has been quoted either literally or by content from the sources used. The text document uploaded to TUGRAZonline is identical to the present master‘s thesis.

Date

Signature

Acknowledgement

First of all I want to express my gratitude to my supervisor Professor Johannes Khinast for granting me the opportunity to conduct my master's thesis at Research Center Pharmaceutical Engineering GmbH. My appreciation also extends to my other supervisor, Amrit Paudel for his scientific input and his time throughout the whole process.

A special thank goes to my technical supervisor Theresa Hörmann for her great support and her motivation.

I also want to use this opportunity to thank the amazing RCPE lab-team for their support and for making the time during my thesis a great one.

Finally, I want to thank all my family and my dear friends for believing in me and supporting me and of course for their encouragement and lifelong support for reaching my goals.

Kurzfassung

Die Herstellung von festen Dispersionen ist ein vielversprechender Ansatz zur Löslichkeitsverbesserung von schwerlöslichen Wirkstoffen. Bei festen Dispersionen handelt es sich um einen oder mehrere Wirkstoffe, die amorph vorliegen und in einer Trägermatrix (z.B. Polymere) dispergiert sind. Eine Möglichkeit, diese industriell herzustellen, ist die Anwendung von Schmelzextrusion. Formulierungen für die Schmelzextrusion mit den gewünschten Eigenschaften zu finden ist sehr zeitintensiv. Vor Beginn dieser Arbeit ist bereits ein Dreistoffsystem ausgewählt worden, welches stabil ist und das gewünschte Freisetzungsprofil aufweist. Dissolutiontests haben gezeigt, dass der Wirkstoff schneller von einem Dreistoffsystem freigesetzt wird, als vom Zweistoffsystem mit HPMC. Somit ist es notwendig, den Zusammenhang der Wirkstofffreisetzung in verschiedenen Systemen und die molekularen Interaktionen zu untersuchen.

Untersucht werden der Wirkstoff Nimodipin und die Matrixkunststoffe Eudragit® E und Methocel™ E5. Das Verfahren des Vakuumkompressionsformens (VCM) wird angewandt, um Proben mit unterschiedlichen Mengen von Wirkstoff und Kunststoffen herzustellen. Die dazu verwendeten Pulvermischungen werden in einem vorhergehenden Schritt kryogemahlen, um möglichst homogene Tabletten zu formen. Diese Herstellungsmethode soll den Extrusionsprozess im kleinen Maßstab abbilden und dabei Zeit und Material sparen. Die Tabletten und Pulvermischungen werden bezüglich ihrer Wirkstofffreisetzung, Phasenzusammensetzung und Molekülanordnung untersucht. Dies wird mit Dissolutiontests, dynamischer Differenzkalorimetrie und Infrarot Spektroskopie durchgeführt.

Aus den Ergebnissen geht hervor, dass der Wirkstoff amorph vorliegt. Die IR-Spektren geben Aufschluss darüber, dass die Wirkstoffmoleküle in der Trägermatrix dispergiert sind, jedoch zeigen sie keine Interaktionen zwischen den unterschiedlichen Molekülen von Nimodipin und Kunststoffen. Die Thermogramme zeigen bessere Mischbarkeit bei ausgeglichenen Kunststoffmengen, im Gegensatz zu sehr unterschiedlichen Kunststoffmengen. Außerdem weisen sie keine Schmelzpeaks auf, was den amorphen Zustand des Wirkstoffs bestätigt. Die Dissolutiontests werden mit den VCM Tabletten und Extrudaten durchgeführt. Zunächst wird die intrinsische Freisetzungsrate bestimmt (hauptsächlich mit 10 % Wirkstoff). Danach werden Schmelzextrudate von Formulierungen, die von besonderem Interesse sind, getestet. Diese Freisetzungsraten werden miteinander verglichen, um danach eine Aussage darüber zu treffen, ob Vakuumkompressionsformen zur Formulierungsentwicklung geeignet ist.

Abstract

The formation of amorphous solid dispersions (ASDs) is one of the most promising ways to enhance the solubility of poorly water soluble drugs. They are defined as one or more active pharmaceutical ingredient(s) (API) existing in their amorphous form, dispersed in a carrier matrix (e.g. polymers). One of the industrially used manufacturing processes of such is hot-melt extrusion (HME). Identifying formulations for HME that achieve the desired product properties is a time-consuming process. An immediate release formulation consisting of a poorly soluble API and two polymers which achieves a stable amorphous system is investigated in the present study. Dissolution studies show that the API is released faster from a ternary system than from a binary system with HPMC. Thus, the connection between the API release of different systems during dissolution testing and the molecular interactions needs to be investigated.

The API used in this work is nimodipine and the carriers are Eudragit® E and Methocel™ E5. Vacuum compression molding (VCM) is employed to prepare specimen with different amounts of API and polymers. The powder blends used for VCM are cryo-milled beforehand to achieve homogeneous tablets. This preparation method should imitate the extrusion process on a small scale consuming less time and material. The dissolution behavior, the phase composition and the molecular arrangement are investigated. This is made via dissolution studies, differential scanning calorimetry (DSC) and Fourier transform infrared spectroscopy (FTIR).

The material characterization of VCM tablets and physical blends of the binary and ternary systems leads to the conclusion that the API is in its amorphous form. The FTIR-spectra reveal that the drug molecules are dispersed in the carrier matrix, however, evidence of molecular interactions is not given. The DSC-thermograms show that the miscibility is better when equal ratios of the polymers are used instead of using binary systems and unequal ratios. Further, there are no crystalline melting peaks detected, confirming the amorphous state of the API. The drug release studies are made with the VCM tablets and with extrudates and results show that the solubility is significantly increased compared to the crystalline form of the API. At first, the intrinsic dissolution rate of different formulations is determined. Then, some formulations of interest are hot-melt extruded and also tested. The release rate is compared to the intrinsic ones. This is done to compare the VCM technology to extrusion and to evaluate this technology as a possible way to test formulations in an early development phase.

Index

1 Aims and Objectives 1

2 Theoretical Background 2

2.1 Aspects of Preformulation 2
2.2 Amorphous Solid Dispersions 6
2.3 Manufacturing Methods of ASDs 8
2.3.1 Hot-Melt Extrusion 9
2.4 Characterization of ASDs 13
2.4.1 Thermal Analysis 13
2.4.2 Spectroscopy 16
2.4.3 Drug Release Studies 18

3 Materials and Methods 20

3.1 Materials 20
3.1.1 Nimodipine 20
3.1.2 Polymeric Carriers 21
3.1.3 Drug-Polymer Mixtures 23
3.1.4 Dissolution Studies 24
3.2 Methods 24
3.2.1 Vacuum Compression Molding 24
3.2.2 Tabletop Extrusion 25
3.2.3 In-Vitro Dissolution Testing 26
3.3 Analytical Methods 28
3.3.1 Differential Scanning Calorimetry (DSC) 28
3.3.2 Fourier Transform Infrared Spectroscopy (FTIR) 28
3.3.3 UV-Visible Spectroscopy 29

4 Results, Discussion and Conclusion 30

4.1 Characterization of Drug-Polymer Interactions 30
4.1.1 Phase Composition Studies (DSC) 30
4.1.2 Molecular Arrangement (FTIR-Spectroscopy) 38
4.2 Characterization of Drug Release 45
4.2.1 Intrinsic Dissolution Studies 45
4.2.2 Dissolution Studies of Pellets 47
4.2.3 Dissolution Studies under Non-Sink Conditions 49

5 Summary and Outlook 52

6 Appendix 54

6.1 Additional DSC-Thermograms 54
6.1.1 First Heating Run 54
6.1.2 Second Heating Run 58
6.1.3 Experimental and Empirical T_g Values 62
6.2 Additional FTIR-Spectra 63
6.3 Dissolution Testing of VCM Tablets 67

7 References 71

Figure Index

Figure 2-1 Illustration of differences of crystalline and amorphous forms 6

Figure 2-2 Illustration of screw geometry [15]..... 11

Figure 2-3 Schematic illustration of a co-rotating twin-screw extruder [18]..... 12

Figure 2-4 Schematic DSC-thermogram 15

Figure 2-5 Regions of a FTIR-spectrum 17

Figure 2-6 Scheme of surface erosion and bulk erosion and their controlled release profiles [36] 18

Figure 3-1 Chemical structure of NMD [39] 20

Figure 3-2 Chemical structure of Eudragit® E; x:y:z = 2:1:1 (x = dimethylaminoethyl methacrylate, y = butyl methacrylate, z = methyl methacrylate) [42]..... 21

Figure 3-3 Chemical structure of Methocel™ E5; cellulose backbone with hydroxypropoxyl and methoxyl side groups [44]..... 22

Figure 3-4 Vacuum compression molding setup: left – hot plate with VCM tool, middle – vacuum pump, right – cooler with VCM tool [45] 24

Figure 3-5 Sectional view of VCM tool; left – description of all parts, right – front view of the assembled tool [45] 25

Figure 3-6 Picture of a VCM tablet (d = 10 mm) in the used PTFE-fixation for intrinsic dissolution experiments..... 27

Figure 3-7 Schematic drawing of a dissolution vessel showing the position of the PFTE-fixation 27

Figure 4-1 DSC-thermogram: first heating run of the binary system NMD and EE (10% API)..... 31

Figure 4-2 DSC-thermogram: first heating run of the binary system NMD and HPMC (10% API)..... 31

Figure 4-3 DSC-thermogram: first heating run of the ternary system NMD and EE:HPMC 3:2 (10% API)..... 32

Figure 4-4 Evaluated area of melting peak (NMD) versus EE content; dashed line - NMD pure substance 32

Figure 4-5 Onset temperature of area versus EE content; dashed line - NMD pure substance 32

Figure 4-6 DSC-thermogram: second heat run - reversing heat flow of the binary system NMD and EE (10% API) and their derivatives (1.7 and 2.7) 34

Figure 4-7 DSC-thermogram: second heating run of the binary system NMD and HPMC (10% API) and their derivatives (1.7 and 2.7) 35

Figure 4-8 DSC-thermogram: second heating run of NMD and EE:HPMC 1:1 (10% API) and their derivatives (1.7 and 2.7) 35

Figure 4-9 Experimental values (-) of T_g versus theoretical values (♦) using Gordon-Taylor model for ternary mixtures..... 37

Figure 4-10 Experimental values (-) of T_g versus theoretical values (▲) using Gordon-Taylor model for binary mixtures (NMD and EE) 37

Figure 4-11 Chemical structure of NMD – groups of interest are tagged..... 38

Figure 4-12 Averaged FTIR-spectra (n=3) of crystalline (dotted line) and amorphous (solid line) NMD revealing characteristic differences in two regions..... 39

Figure 4-13 Averaged FTIR-spectra (n=3) of crystalline (dotted line) and amorphous (solid line) NMD – detailed view of the single bond stretch region 40

Figure 4-14 Averaged FTIR-spectra (n=3) of crystalline (dotted line) and amorphous (solid line) NMD - detailed view of the double bond stretch region..... 40

Figure 4-15 Averaged FTIR-spectra (n=3) of EE powder (dotted line) and VCM prepared sample (solid line) 41

Figure 4-16 Averaged FTIR-spectra (n=3) of HPMC powder (dotted line) and VCM prepared sample (solid line) 41

Figure 4-17 Averaged FTIR-spectra (n=3) of pure substances: amorphous NMD (grey, solid line), VCM prepared polymers – EE grey, dashed line; HPMC grey, chain dotted line, binary mixtures: API + EE black, solid = ASD, dotted = digital blend, API + HPMC green, solid = ASD, dotted = digital blend, ternary system: API + EE:HPMC 1:1, red solid line 42

Figure 4-18 Averaged FTIR-spectra (n=3) of pure amorphous substances (grey, NMD solid, EE dotted, HPMC chain dotted), prepared (solid) and digital (dotted) binary systems (black for EE; green for HPMC) and the ternary system EE:HPMC 1:1 (red) – detailed view (3000 – 3500 cm^{-1})..... 43

Figure 4-19 Averaged FTIR-spectra (n=3) of pure amorphous substances (grey, NMD solid, EE dotted, HPMC chain dotted), prepared (solid) and digital (dotted) binary systems (black for EE; green for HPMC) and the ternary system EE:HPMC 1:1 (red) – detailed view (1400 – 2000 cm^{-1})..... 43

Figure 4-20 Averaged FTIR-spectra (n=3) of pure amorphous NMD (grey, solid) prepared (solid) and digital (dotted) ternary systems (black for more EE; green for more HPMC) – detailed view (3000- 3500 cm^{-1})..... 44

Figure 4-21 Averaged FTIR-spectra (n=3) of pure amorphous NMD (grey, solid) prepared (solid) and digital (dotted) ternary systems (black for more EE; green for more HPMC) – detailed view (1400- 2000 cm^{-1})..... 44

Figure 4-22 dissolution profiles of formulations with 10% API and more EE: (▲) EE; (□) 4:1 EE:HPMC; (●)2:1 EE:HPMC; (○)3:2 EE:HPMC; (♦)1:1 EE:HPMC 45

Figure 4-23 dissolution profiles of formulations with 10% API and more HPMC: (●) 1:2 EE:HPMC; (□)1:4 EE:HPMC; (○)2:3 EE:HPMC; (♦)1:1 EE:HPMC; (Δ) HPMC 45

Figure 4-24 VCM prepared sample of NMD (10 %) and HPMC (90 %) 46

Figure 4-25 VCM prepared sample of HPMC (pure polymer) 46

Figure 4-26 VCM prepared sample of NMD (10 %) and HPMC (90 %) after dissolution testing 46

Figure 4-27 PLM before dissolution testing 46

Figure 4-28 PLM after 20' dissolution testing 46

Figure 4-29 PLM after 45' dissolution testing 46

Figure 4-30 PLM after 70' dissolution testing 46

Figure 4-31 Plot of the intrinsic dissolution rates against the EE content..... 47

Figure 4-32 Pellet dissolution profiles of formulations with 10% API: (▲) EE; (●) 2:1 EE:HPMC ; (♦)1:1 EE:HPMC; (○)2:3 EE:HPMC; (Δ) HPMC 48

Figure 4-33 Intrinsic dissolution profiles (VCM) of formulations with 10% API: (▲) EE; (●) 2:1 EE:HPMC ; (♦)1:1 EE:HPMC; (○)2:3 EE:HPMC; (Δ) HPMC 48

Figure 4-34 Dissolution profiles under non-sink condition: (○) 2:3 EE:HPMC ASD; (●)2:3 EE:HPMC physical mixture 49

Figure 4-35 Dissolution profiles of formulations with 10% API: (●) 2:1 EE:HPMC ; (♦)1:1 EE:HPMC; (○)2:3 EE:HPMC; (Δ) HPMC 49

Figure 6-1 DSC-thermogram: first heating run of the ternary system EE:HPMC 4:1 (10% API)..... 54

Figure 6-2 DSC-thermogram: first heating run of the ternary system EE:HPMC 2:1 (10% API)..... 54

Figure 6-3 DSC-thermogram: first heating run of the ternary system EE:HPMC 3:2 (10% API)..... 55

Figure 6-4 DSC-thermogram: first heating run of the ternary system EE:HPMC 2:3 (10% API)..... 55

Figure 6-5 DSC-thermogram: first heating run of the ternary system EE:HPMC 1:2 (10% API)..... 56

Figure 6-6 DSC-thermogram: first heating run of the ternary system EE:HPMC 1:4 (10% API)..... 56

Figure 6-7 DSC-thermogram: first heating run of the ternary system EE:HPMC 1:1 (20% API) 57

Figure 6-8 DSC-thermogram: first heating run of the ternary system EE:HPMC 1:1 (30% API) 57

Figure 6-9 DSC-thermogram: second heating run of the ternary system EE:HPMC 4:1 (10% API) and their derivatives (1.7 and 2.7) 58

Figure 6-10 DSC-thermogram: second heating run of the ternary system EE:HPMC 2:1 (10% API) and their derivatives (1.7 and 2.7) 58

Figure 6-11 DSC-thermogram: second heating run of the ternary system EE:HPMC 3:2 (10% API) and their derivatives (1.7 and 2.7) 59

Figure 6-12 DSC-thermogram: second heating run of the ternary system EE:HPMC 2:3 (10% API) and their derivatives (1.7 and 2.7) 59

Figure 6-13 DSC-thermogram: second heating run of the ternary system EE:HPMC 1:2 (10% API) and their derivatives (1.7 and 2.7) 60

Figure 6-14 DSC-thermogram: second heating run of the ternary system EE:HPMC 1:4 (10% API) and their derivatives (1.7 and 2.7) 60

Figure 6-15 DSC-thermogram: second heating run of the ternary system EE:HPMC 1:1 (20% API) and their derivatives (1.7 and 2.7) 61

Figure 6-16 DSC-thermogram: second heating run of the ternary system EE:HPMC 1:1 (30% API) and their derivatives (1.7 and 2.7) 61

Figure 6-17 Averaged FTIR-spectra (n=3) of binary mixture (NMD and EE); dotted line – powder blend, solid line – VCM prepared sample 63

Figure 6-18 Averaged FTIR-spectra (n=3) of binary mixture (NMD and HPMC); dotted line – powder blend, solid line – VCM prepared sample..... 63

Figure 6-19 Averaged FTIR-spectra (n=3) of ternary mixtures (10% API 1:2 EE:HPMC); (black) solid line – VCM sample, (grey) dotted line – physical mixture..... 64

Figure 6-20 Averaged FTIR-spectra (n=3) of ternary mixtures (10% API 2:3 EE:HPMC); (black) solid line – VCM sample, (grey) dotted line – physical mixture..... 64

Figure 6-21 Averaged FTIR-spectra (n=3) of ternary mixtures (10% API 1:1 EE:HPMC); (black) solid line – VCM sample, (grey) dotted line – physical mixture..... 65

Figure 6-22 Averaged FTIR-spectra (n=3) of ternary mixtures (10% API 3:2 EE:HPMC); (black) solid line – VCM sample, (grey) dotted line – physical mixture..... 65

Figure 6-23 Averaged FTIR-spectra (n=3) of ternary mixtures (10% API 2:1 EE:HPMC); (black) solid line – VCM sample, (grey) dotted line – physical mixture..... 66

Figure 6-24 Averaged FTIR-spectra (n=3) of ternary mixtures (20% API 1:1 EE:HPMC); (black) solid line – VCM sample, (grey) dotted line – physical mixture..... 66

Figure 6-25 Averaged FTIR-spectra (n=3) of ternary mixtures (30% API 1:1 EE:HPMC); (black) solid line – VCM sample, (grey) dotted line – physical mixture..... 67

Figure 6-26 10% API with EE; picture taken after dissolution testing (70‘) 68

Figure 6-27 10% API with 4:1 EE:HPMC; picture taken after dissolution testing (70‘) 68

Figure 6-28 10% API with 2:1 EE:HPMC; picture taken after dissolution testing (70‘) 68

Figure 6-29 10% API with 3:2 EE:HPMC; picture taken after dissolution testing (70‘) 69

Figure 6-30 10% API with HPMC; picture taken after dissolution testing (70‘)..... 69

Figure 6-31 10% API with 1:4 EE:HPMC; picture taken after dissolution testing (70‘) 69

Figure 6-32 10% API with 1:2 EE:HPMC; picture taken after dissolution testing (70‘) 70

Figure 6-33 10% API with 2:3 EE:HPMC; picture taken after dissolution testing (70‘) 70

Figure 6-34 10% API 1:1 EE:HPMC; picture taken after dissolution testing (70‘) 70

Table Index

Table 2-1 Biopharmaceutical classification system [3] 3

Table 2-2 Description of symbols used in equation 2-1 3

Table 2-3 Approaches to improve solubility [5] 5

Table 2-4 List of API properties that need to be considered in process selection [11], [12] 7

Table 2-5 Hot-melt extrusion and spray drying – advantages and limitations 8

Table 2-6 Screw extruder classification adapted from [17] 10

Table 2-7 Thermal analysis methods used to characterize ASDs in pharmaceutical industry [3] 13

Table 3-1 Chemical data of NMD [40] 20

Table 3-2 Chemical data of Eudragit® E [6] 21

Table 3-3 Chemical data of Methocel™ E5 [6] 22

Table 3-4 Tested compositions of API and polymeric carriers in weight percent and the ratio of the carries 23

Table 3-5 Bands of interest in IR-spectra (taken from spectra of pure substances) 29

Table 4-1 Description of symbols used in equation 4-1 and equation 4-2 36

Table 4-2 Bands of interest in IR-spectra 39

Table 4-3 Bands of interest in IR-spectra of polymers 40

Table 4-4 Dissolution results of extruded pellets compared to intrinsic dissolution results 48

Table 4-5 Description of symbols used in equation 4-3 50

Table 6-1 Experimental and empirical *Tg* values 62

Table 6-2 Released API content and intrinsic dissolution rate 67

List of Abbreviations

API	Active pharmaceutical ingredient
ASD	Amorphous solid dispersion
ATR	Attenuated total reflection
BCS	Biopharmaceutical classification system
DSC	Differential scanning calorimetry
EE	Eudragit® E
FTIR	Fourier transform infrared (spectroscopy)
HME	Hot-melt extrusion
HPMC	Methocel™ E5
MSE	Multi screw extruder
NCE	New chemical entities
NMD	Nimodipine
PM	Physical mixture
PTFE	Polytetraflouroethylene
SLS	sodium lauryl sulfate
SSE	Single screw extruder
TA	Thermal analysis
T_g	Glass transition temperature
T_m	Melting temperature
TSE	Twin screw extruder
USP	United states pharmacopeia
VCM	Vacuum compression molding

1 Aims and Objectives

Continuous manufacturing in pharmaceutical industry offers many advantages compared to conventional batch processes, such as decreased fluctuations in production and quality, higher yields, lower time consumption and cost reduction.

A manufacturing process namely hot-melt extrusion (HME) is a continuous process with increasing importance for pharmaceutical industry, because it provides a promising way to enhance poor solubility of drug molecules via the formation of an amorphous solid dispersion (ASD). HME process has also long been used in manufacturing controlled/sustained release polymeric formulations for oral and non-oral products.
In HME, the materials are generally molten up and mixed intensively. Afterwards, the melt is formed into desired shape and cooled down. During cooling down, recrystallization of the active pharmaceutical ingredient (API) has to be avoided when designing ASD. If the API is well soluble in the polymeric carrier in the molten and in the solid state, this can be achieved easily. If the API concentration is above the solubility limit in the selected polymeric carrier, the cooling must be done fast, in order to kinetically freeze the API molecules and their mobilities between the polymer molecules. This way the formation of API crystals can be retarded dramatically due to the hindered diffusion of the API in the mixture. Thus, the solid amorphous dispersion is stable.

Variability of the drug dissolution profile of a formulation for HME containing API and two carriers is observed. The profile matches either immediate or sustained release depending on the ratio between the two carriers. The reason for such an effect needs to be thoroughly investigated. Both carriers have side groups in their molecular structure which appear to cause concentration-dependent interactions with the API molecules. Still, a clear reason for this observation is not fully understood. Therefore, different material characterization methods like infrared spectroscopy and differential scanning calorimetry are used to find relations between the API release of different mixtures during dissolution testing and the molecular interactions detected during characterization.

2 Theoretical Background

This chapter gives background about solubility enhancement of poorly soluble drugs, the approach of forming amorphous solid dispersions (ASDs), a manufacturing process for ASDs, namely hot-melt extrusion (HME), and characterization methods of ASDs.

2.1 Aspects of Preformulation

After the production of the raw materials in the primary manufacturing process, an active pharmaceutical ingredients (APIs) needs to be converted into a final product. This happens in the secondary manufacturing process.

Dosage Forms

The final products marketed for use are called dosage forms. The design of dosage forms is mainly based on the chemical properties of the API, the onset of action required and convenience of intake by the patient and costs. Depending on the route of administration and the physical state, many configurations are available. Routes of administration can be mainly divided into two groups, namely the enteral and parenteral route. The enteral route of administration refers to the intestine hence includes dosage forms that pass the gastrointestinal tract. Oral, sublingual or rectal administered drugs for instance belong to this group. Parenteral administered means bypassing the alimentary canal via injections (e.g. intravenous, intramuscular, subcutaneous) or injection independent like transdermal, intranasal and via inhalation. Examples for enteral administered dosage forms are tablets, capsules, syrups, elixirs, suppositories. Parenteral dosage forms must be prepared sterile. Examples are injections, infusions, inhalers, patches and implants. [1]

In this work an oral solid dosage form of a biopharmaceutics classification system (BCS) class II API is investigated.

Biopharmaceutics Classification System

This system classifies drugs according to their permeability through the intestinal membrane and solubility in gastro-intestinal fluid, tested and analysed under specified conditions. According to the biopharmaceutics classification system, highly soluble means that a drug (the highest clinical dose) can be dissolved in 250 ml aqueous media or less at pH 1 to 7.5. A drug is considered to be highly permeable when the fraction absorbed of an administered dose exceeds 90%.[2]

If an API is ranked to be a class II drug, it means that permeability is sufficient, but the solubility is low which leads to low and/or variable bioavailability issues [3]. Solubility is a chemical property giving information about how much of the drug can be dissolved in a given volume of media and follows a thermodynamic process. Dissolution is closely connected to solubility and describes the rate and extent of the process when a solution is formed from a solute (e.g. drug) dissolving in a solvent (e.g. water). This is a kinetic process.[4]

Table 2-1 Biopharmaceutical classification system [3]

	Permeability	**Solubility**
Class I	high	high
Class II	high	low
Class III	low	high
Class IV	low	low

The dissolution rate can be described using the modified Noyes–Whitney equation, offering information about relevant parameters for the dissolution process. [4]

$$\frac{dm}{dt} = \frac{A \cdot D \cdot (c_s - c)}{d} \qquad \textbf{Equation 2-1}$$

The symbols used in equation 2-1 are described in table 2-2

Table 2-2 Description of symbols used in equation 2-1

Symbol		Unit
$\frac{dm}{dt}$	Dissolution rate	[kg/s]
A	Surface area	[m²]
D	Diffusion coefficient	[m²/s]
c_s	Solubility of solute in dissolution medium	[mol/L]
c	Concentration of drug at time *t*	[mol/L]
d	Thickness of diffusion boundary layer	[m]

From the Noyes-Whitney equation, the following correlations can be read [4]:

- The dissolution rate (*dm/dt*) will increase with an increasing surface area (*A*) relative to the volume. This can be achieved by reducing the particle size.
- The diffusion coefficient (*D*) is depending on the viscosity of the solvent. *D* increases with decreasing solvent viscosity and due to that the dissolution rate increases too.
- The solubility concentration (C_s) can be influenced with ionisable solutes as they can cause pH changes of the solvent and thus the dissolution rate is higher or lower.
- Stirring and agitation has impact on the diffusion gradient (*d*). When decreasing *d* during dissolution the dissolution rate increases.

For poorly soluble APIs, the solubility concentration is critical. At very low solubility, the driving concentration gradient is low and dissolution is slow. There are several approaches to cope with the challenge of poorly soluble drugs. The generation of ASDs is one possibility to improve this issue. The following table gives an overview of the most common strategies to overcome this challenge.

Table 2-3 Approaches to improve solubility [5]

Strategy	Product(s)	Remarks	Illustration*
Amorphous solid dispersions	Kaletra® Sporanox®	Drug-polymer mix used to stabilize amorphous drug	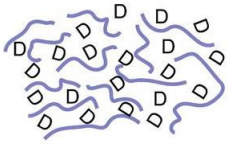
Co-crystals	AMG 517	Change of crystal lattice due to formation of molecular complex	
Cosolvents	Prograf® Valium®	Cosolvents disturb intermolecular H-bonding formation in aqueous systems	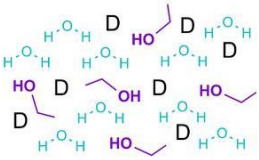
Cyclodextrins	Vfend® Sporanox® IV	Drug and cyclodextrins are forming complexes	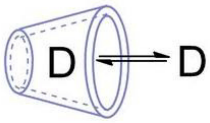
Lipid-based systems	Neoral® Agenerase®	Solubilized drug in liquid or thermo softening fillings in capsules	
Particle size reduction	Emend® Rapamune®	Mechanical treatment (milling, grinding)	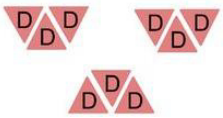
Polymorphs		Formation of different molecular arrangement (crystal structure variation)	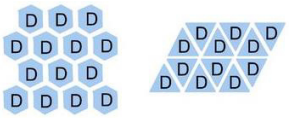
Salts	Ziprasidone HCl Diclofenac sodium	Isolation of salt forms of API	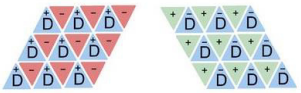
Surfactants	Taxol® Prograf®	Drug is linked to surfactant micelles	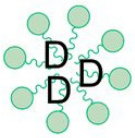

*) D…drug molecule

2.2 Amorphous Solid Dispersions

Amorphous State

Based on the degree of structural order, pharmaceutical solids can be classified into crystalline and amorphous forms. Crystalline substances show a characteristic three dimensional long-range order of repeating units structured through several molecular and supramolecular interactions, whereas amorphous substances only show short-range order over a few molecular dimensions. The lack of the repeating unit results into different properties of amorphous substances in comparison to their crystalline form [6]. Amorphous solids have increased enthalpies (*H*), entropies (*S*), free energies (*G*), free volumes (*V*) and decreased densities (ρ) compared to crystalline solids. [7]

If the crystalline drug form is changed into the amorphous form, many hurdles can appear, like decreased physical or chemical stability. The lattice energy of the crystalline form causes a barrier for the dissolution of the drug molecules. Thus, advantage is taken from the disordered structure of the amorphous state as it has a higher free energy leading to increased water solubility, dissolution rate and oral absorption. [3] Figure 2-1 is a two dimensional illustration to visualize differences of crystalline and amorphous state of solids.

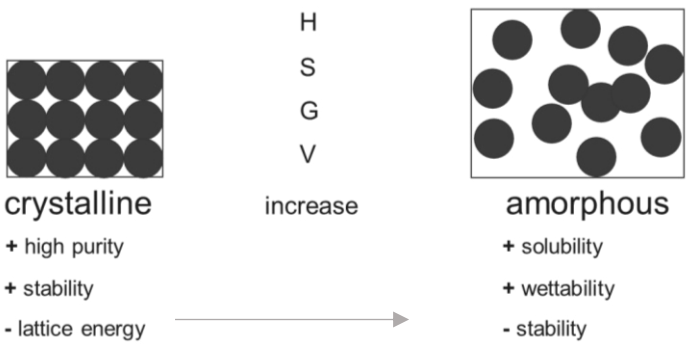

Figure 2-1 Illustration of differences of crystalline and amorphous forms

Solid Dispersions

Recently discovered drug candidates include an increasing number of poorly soluble active molecules [8]. Thus, the approach of forming solid dispersions has gained more importance. Amorphous solid dispersion is a broadly defined term in pharmaceutical industry. Dispersion itself implies phase immiscibility, however, solid solutions, specifically glass solutions (drug dispersed at molecular level giving a single phase) are also classified as ASDs. [9]

All types of solid dispersions contain API dispersed in carriers (chemically and pharmacologically inert matrices). The difference of the subtypes lies in the physical state of API and carrier. The API can either be dispersed as phase separated crystal or amorphous particle in the carrier or it forms a homogeneous phase with the carrier. [5]

Types of solid dispersions are [10]:

- Eutectic systems
- Amorphous API in crystalline carrier
- Amorphous API in amorphous carrier (phase separated system)
- Solid solutions (dissolved API in crystalline carrier)
- Glass solutions (API dissolved in amorphous carrier, completely ASD)

Lately, the term solid dispersion has shifted to describe amorphous drugs dispersed in amorphous or semi-crystalline carriers [6]. The formation of solid dispersions increases the drug dissolution via several mechanisms [5]:

- Reducing effective particle size
- Improving wettability
- Increasing solubilization
- Eliminating impact of lattice energy (as amorphous state is stabilized)

Considerations of API Properties to Choose Appropriate Process

HME and spray drying are two main industrial processes used in manufacturing ASD. The following table shows some of the properties that need to be regarded when choosing a process to generate ASDs.

Table 2-4 List of API properties that need to be considered in process selection [11], [12]

Biopharmaceutical properties	Physical and Chemical properties	Processability
Solubility in biorelevant media	Solubility of amorphous form	Solubility in organic solvents
Permeability	T_m, T_g, T_{cr}	T_m, T_g
Dose	Molecular weight	Stability
Absorption window	log P	
	pK_a	
	H-bonding capacity	

One of the main concerns with amorphous formulation systems is stability. Since the system is not in the energetically most preferable state, a transformation to other states (e.g. crystalline) has to be hindered, at least for a sufficient time scale equivalence to the shelf life of drug product. In terms of stability, melting-, glass transition-, crystallization temperature (T_m, T_g, T_{cr}) and solubility of amorphous form need to be considered. The pK_a-value and the H-bonding capacity can partially help deciding on which polymer to select as a carrier. Solubility in organic solvents is important when using spray drying to make ASDs. Heat sensitivity has to be regarded when using HME.

2.3 Manufacturing Methods of ASDs

ASDs are usually formulated as binary systems consisting of API and one carrier, even though the number of reported ternary systems and commercial products is increasing. Hot-melt extrusion and spray drying turn out to be the most important methods to process amorphous solid dispersions, which are commercially available. [10]

These two complementary technologies tend to cover the processability of a wide range of poorly soluble APIs. Table 2-5 sums up the most important advantages and limitations of both methods.

Table 2-5 Hot-melt extrusion and spray drying – advantages and limitations

	Hot-melt extrusion [11] **heat based method**	**Spray drying [13]** **solvent based method**
Advantages	Continuous process	Continuous process
	Cost efficient (solvent free, simpler equipment)	High mixing efficiency
	Possibility of direct shaping	Lower process temperature
Limitations	Heat/shear sensitive APIs	APIs with low solubility in organic solvents
	APIs with high T_m and/or low degradation temperature	Cost
	Lower mixing efficiency	Solvent handling, environmental impact

2.3.1 Hot-Melt Extrusion

Hot-melt extrusion goes back to the 1930s and is a well-established processing technology in plastic, rubber and food industry. Within the last decades, it has been increasingly used for pharmaceutical applications as well [11]. Differences between extruders of pharmaceutical applications and other applications are the materials and surface quality of contact parts and the scale. The surfaces are liable to regulatory requirements such as not being reactive, additive or absorptive with the product. At the same time, the equipment needs to meet the cleaning and validation requirements of pharmaceutical industry [14]. Concerning the scale, pharmaceutical manufacturing has significantly lower production volumes in compared to the plastics industry. Thus, mainly small-scale extruders are used. The next section will present the application of this technology for pharmaceutical products.

Process

In general, the extrusion process converts raw material into uniformly shaped products by melting and mixing of the material along one or more rotating screws and forcing it through a die [15]. In the extruder, the material undergoes a conveying – melting – mixing – (optionally) volatilization process. The API and the polymers can be blended before feeding or fed separately to the extruder (split feeding). Melting is achieved by thermal energy input through the barrel heating and by shear forces between the rotating screw(s) and the barrel wall. This shear stress again causes the generation of dissipative heat from the intermolecular friction. The dispersion of API molecules in carriers can take place when the glass transition of the polymers is exceeded and the chain mobility is increased. A volatilization step can be used to get extract residual moisture in the melt, volatiles or entrapped air. The extrudates are achieved by forcing the molten mixture through a die and cooling them afterwards. Subsequently, downstream processes, such as pelletisation, calendaring or sheet forming, can be applied [16].

Equipment

Generally, there are several types of extruders available, such as ram, radial screen, roll and screw extruders. The latter are the most used ones in pharmaceutical industry as the fed material is converted continuously to finished forms like rods, tubes or films [11]. Since screw extruders are used within this work they will be discussed in more detail. They can be classified concerning their number of screws, the rotational direction of them and the arrangement of the screw shafts.

Table 2-6 Screw extruder classification adapted from [17]

Single screw extruder	Twin-screw extruder			Multi-screw extruder	
	co-rotating		counter-rotating	rotating center shaft	static center shaft
	intermeshing		non-intermeshing		
	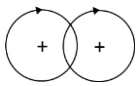	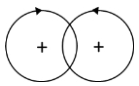	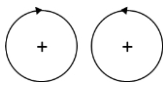	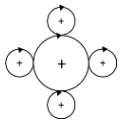	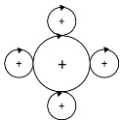

Single-screw extruders (SSE)

The mechanically simple single-screw extruder devices are widely applied in the plastics industry and used as high-pressure pumps for viscous material while mixing and melting. They consist of one rotating screw in a heated barrel and perform feeding, conveying, melting, volatilizing, pumping and shaping [14]. For pharmaceutical production they are rarely used, due to the advantages of the twin-screw extruder.

Twin-screw extruders (TSE)

TSEs have two screws that can either be co-rotating or counter-rotating and intermeshing or non-intermeshing. The processing zones along the processing length are the same as for the SSE. The advantages of the intermeshing screw design are the self-cleaning effect of the screws and thereby preventing the material from overheating due to flow stagnation. Moreover, better mixing can be achieved compared to the non-intermeshing screws. The non-intermeshing screw design, however, is employed when high shear forces are required to process highly viscous material and volatile substances have to be removed [14]. The difference between co- and counter-rotating screws is, that counter-rotating screws transport the material forward in enclosed portions between the two screws. For the co-rotating design, the material is transported from one screw to another along the barrel walls. Thus, the co-rotating design offers better back-mixing and also a larger variety of different possible screw element types. The tightly intermeshing co-rotating TSE is the most commonly used extrusion equipment in pharmaceutical industry. This is due to its high mixing efficiency, as it provides distributive and dispersive mixing, a short and well controlled residence time and the self-cleaning effect of the screws.[11]

Multi-screw extruders (MSE)

MSEs have more than two screws. Usually, extruders with 4 or 8 screws they are assembled circumferentially (table 2-6) and in case of 3 or 5 screws for example they are organized linearly. However, the setup is depending on requirements and applications. MSEs are preferred over SSEs since they are better in handling thermal sensitive materials at large throughputs. Since they are specialised for high throughputs, they are not used in the pharmaceutical industry.

Process Variables

Factors that influence the product properties are design variables, process settings and material properties. The design variables apply to the extruder, the screw and the die design. Extruders are classified using their length-to-diameter ratio (*L/D*). The die design determines the shape of the product. Figure 2-2 shows the geometry of a screw with all important parameters.

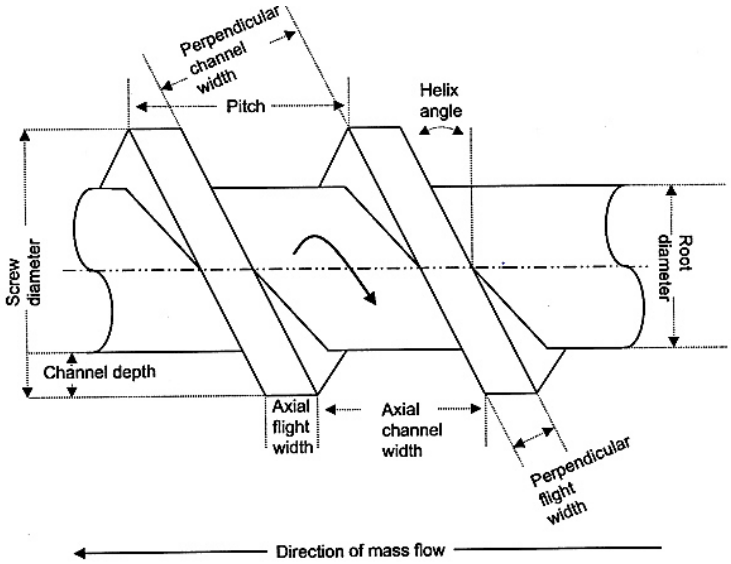

Figure 2-2 Illustration of screw geometry [15]

The extruder screw consists of screw elements which can be arranged freely for each specific material. Typical elements are conveying, kneading and toothed mixing elements varying in pitch size, helix angle, conveying direction and free cross-section.[15]

A typical screw configuration of a co-rotating TSE as used in pharmaceutical industry can be seen in figure 2-3. In the intake section, conveying elements with large pitch are applied to remove the material entering the screw immediately from the inlet to avoid a backlog in the intake zone. After that, the material is slowly compressed and entrapped air as removed by conveying elements with small pitch. Then, the melting zone is designed using kneading elements with high mechanical energy input, causing the material to melt due to high shear

forces. Then, there are several options for a screw design, depending on the processed material. An optional feed can be added in another conveying zone with large pitched elements. A distributive mixing zone can be employed by adding toothed mixing elements, or a dispersive mixing zone with another set of kneading blocks. If intensive mixing is needed, the kneading blocks can be of non-conveying design, where the blocks are arranged in an angle 90° to each other. For a volatilization zone again a large pitch is needed in order to provide as much surface for the extraction of volatiles as possible. Here it is also possible to apply vacuum for increased efficiency. At the end of the extruder conveying elements with a small pitch with a good pressure build-up characteristic are applied to force the material trough the die.

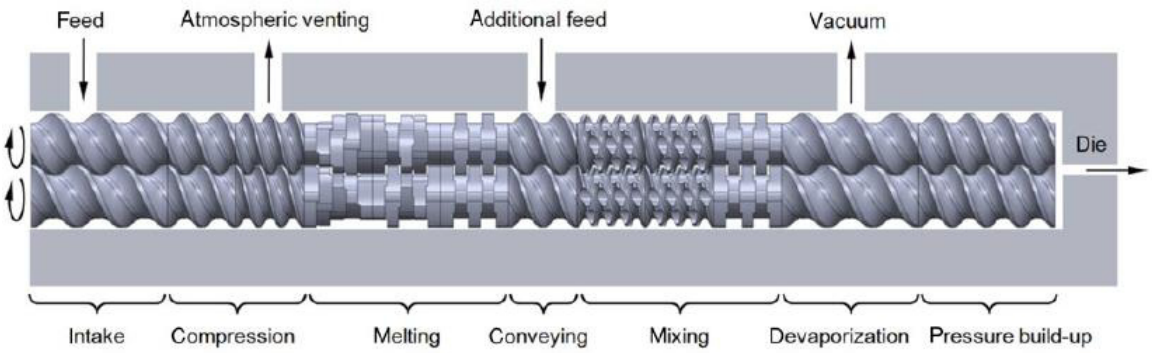

Figure 2-3 Schematic illustration of a co-rotating twin-screw extruder [18]

Process settings are screw rotation speed, the temperature profile of the barrels and the throughput. Dependent, or resulting variables are product temperature, die pressure, the extrusion torque and specific mechanical energy input and the residence time distribution.

Material properties important for the design of the extrusion setup and determining the material behaviour are powder properties, such as flowability and bulk density, thermal properties of the material, viscoelastic properties of the melt and the miscibility of components. [19]

2.4 Characterization of ASDs

Thermal analysis, X-ray diffraction, Fourier transform infrared spectroscopy and measurement of the drug release rate are among the most important methods to characterize ASDs. All used methods are explained in the following chapter.

2.4.1 Thermal Analysis

Thermal analysis (TA) describes a group of methods that characterize a substance as a function of temperature and time. These techniques aim at determining the properties (or the change of properties) of a substance during a defined temperature programme. [20] Table 2-7 lists the most used TA techniques in pharmaceutical industry.

Table 2-7 Thermal analysis methods used to characterize ASDs in pharmaceutical industry [3]

Method	Abbreviation	Information [21], [22]
Differential scanning calorimetry	DSC	T_g, transition temperatures, heats of reaction/transition, crystallinity, aging, degradation
Thermogravimetric analysis	TGA	Thermal + oxidative stability, degradation, shelf life/kinetics
Dynamic mechanical analysis	DMA	T_g, brittleness, anisotropy, crystallinity aging, residual cure + stress
Isothermal Microcalorimetry	IMC	(Very sensitive technique) thermodynamics of process, stability, crystallinity, wetting

Differential Scanning Calorimetry

Differential scanning calorimetry belongs to the thermal analysis techniques. It is used to identify substances, phase changes, purity of substances, reaction kinetics and thermal stability. [23] Determination of first-order transitions (melting) and second order endothermic transitions (glass transition) are the main objectives of this analytical technique [24].

It is among the most applied techniques to determine the thermal properties of pharmaceuticals. The principle of the analysis is, that the thermodynamic response (thermal

event) of the sample is measured and evaluated in terms of heat flow and temperature. More precisely, the enthalpy difference of a system is measured by comparing the temperature of the sample to the reference (e.g. empty crucible) [25].

There are two types of calorimeters:

- Heat-flux DSC
- Power-compensation DSC

The Heat-flux calorimeter (used within this work) has one single furnace for the sample and the reference and the crucibles are connected. The power-compensation calorimeter has a furnace for sample and reference respectively and thus the temperatures of the crucibles are controlled independently.[26]

Modulated DSC

Conventional DSC uses a linear change of temperature which can lead to analysis difficulties when events are overlapping at the same temperature. This challenge can be overcome via using modulated differential scanning calorimetry (MDSC). MDSC uses a linear and a sinusoidal (modulated) heating scan programme that enables a simultaneous analysis of the heat capacity of the sample. The total heat flow can be expressed by following equation:

$$\frac{dQ}{dt} = c_p \frac{dT}{dt} + f(t,T) \qquad \textbf{Equation 2-2}$$

This equation shows that the total heat flow (*dQ/dT*) consists of a heat capacity component (c_p*dT/dt*) which is heat rate dependent (reversing) and a kinetic component (*f(t,T)*) which is time dependent (non-reversing). Evaluation of the reversing heat flow signal gives information about glass transition and melting whereas the non-reversing heat flow signal allows to draw conclusions about enthalpy recovery, crystallization and decomposition for instance. [26]

Evaluation of DSC-thermograms

Figure 2-4 depicts a schematic thermogram with thermal events typically occurring when analysing a mixture of crystalline and amorphous components.

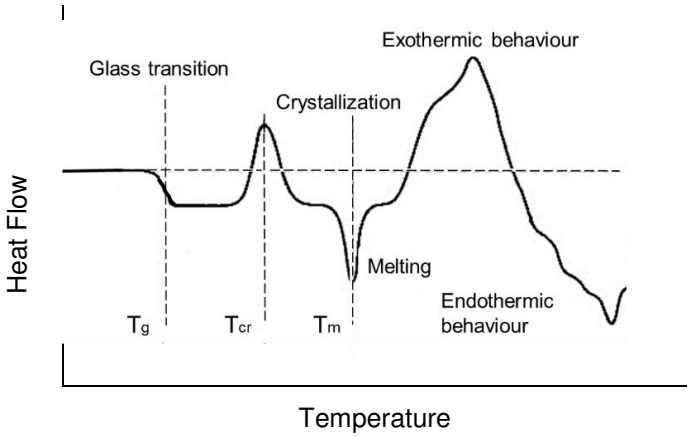

Figure 2-4 Schematic DSC-thermogram

Information that can be extracted from DSC thermograms [6]:

- Glass transition temperature
- Melting temperature and enthalpy of fusion
- Crystallization temperature and heat of crystallization
- Enthalpic recovery

Glass transition

DSC is one of the most common techniques for determining the glass transition temperature (T_g). The transition can be observed in thermograms as shown in figure 2-4. When cooling down a polymer from its softened/molten state, it can undergo glass transition at some point if it does not crystallize. In the thermogram, this is indicated by a point of inflection of heat capacity as a function of temperature. At this point, a change of the mechanical, electrical and rheological properties also occurs (basic principle for other measurement methods). Below this point, an elastic polymer is converted into a brittle one because the chain mobility is inhibited. The glass transition is an indicator for the amorphous state of a material [6].

Moreover, the T_g is observed as primary indicator of miscibility and compositional homogeneity when evaluating ASDs [6]. Dispersions which do not show a melting peak, but a glass transition, can be assumed as molecularly dispersed. This can be used as criterion to distinguish between solid solutions and crystalline dispersions [27].

Furthermore, the glass transition points in a solid mixture give insight in miscibility or phase separation. If a single T_g is detected, it can be assumed, that a homogenous amorphous system was generated. If more T_g*s* are present, this is an indicator for a multi-phase system.

Melting and crystallization

Melting is an endothermic process since heat is required. The process is isothermal under continued heating. If a melting event occurs in solid dispersion, it indicates the presence of

crystalline material. The enthalpy of fusion can be determined by the area under the melting peak. The enthalpy of fusion can be lowered in case of higher solubility or interaction of a crystalline material with the matrix material in a melt, or the melting peak can be shifted to the lower temperature. The latter is called melting point depression. Both effects are an indication for stronger mixing interaction between API-polymer and thus higher solubility of the API in the carrier polymer, when investigating ASDs.
Crystallization is an exothermic process as heat is set free. The heat of crystallization can be determined by the area under the curve of this thermal event. The non-isothermal crystallization event can be detected during heating ASDs or during the cooling phase of drug-carrier melt.

Enthalpic Recovery
Enthalpic recovery is an event observed in DSC for amorphous materials that reflects the recovery of energy released from the material during relaxation or aging process over time. In a thermogram, this endothermic event occurs usually in connection with the glass transition. Glassy amorphous materials are thermodynamically unstable trying to reach an equilibrium state. [28]

2.4.2 Spectroscopy

Spectroscopy deals with analytical methods based on interactions of electromagnetic radiation with matter. Electromagnetic radiation is a form of energy that moves at speed of light and can be UV-light, visible light or X-radiation, for example. Matter means the entire sample that is analysed such as ions, atoms or molecules. Spectroscopic methods are divided into atomic and molecular spectroscopy. The latter is mainly used for structural determination. [29]

Vibrational Spectroscopy/ Infrared (IR) Spectroscopy
Vibrational spectroscopy belongs to molecular spectroscopic methods and aims at detecting functional groups and structural determination. In principle, the absorption of IR light by molecules of a sample causes vibrations and rotations that are characteristic for a molecule and thus, the IR spectrum can be used for chemical identification. Interaction between matter and IR radiation only occurs when the vibration produces a change in a dipole moment (polar bonds). It is possible to detect linear or branched chains of a backbone (if a backbone exists) and to determine unsaturation, aromatic rings and specific functional groups. The identification is made via comparing the spectrum of the sample with reference spectra. [30]

Figure 2-5 shows typical regions of the IR spectrum and where to find characteristic functional groups of organic compounds. Wavenumbers [cm^{-1}] which are the reciprocal value of the wavelength, are used as unit on the x-axis. The absorbance or transmittance is plotted on the y-axis. Mid-infrared is mainly used for the molecular interaction studies.

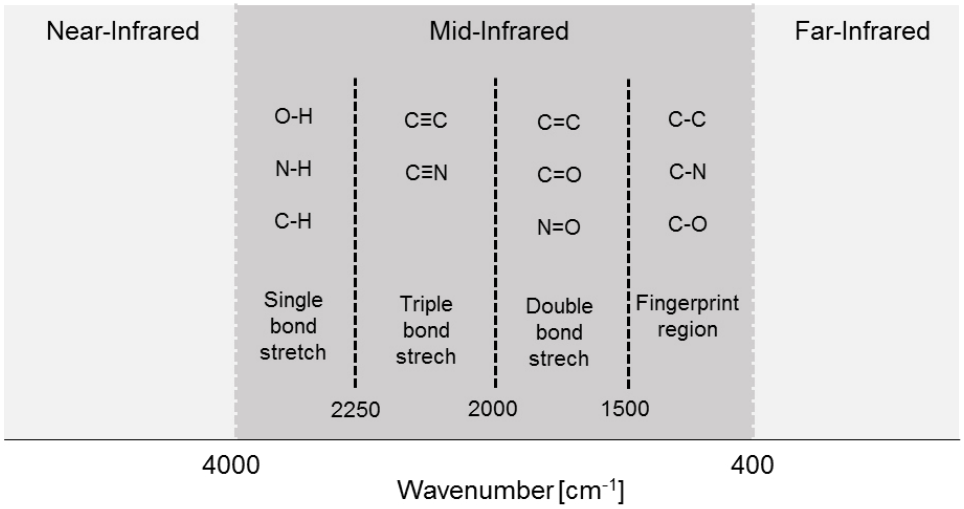

Figure 2-5 Regions of a FTIR-spectrum

In this work, a Fourier transform infrared (FTIR) spectrometer is used, which employs an optical device called interferometer. Interferometer produces a unique type of signal which encodes all infrared frequencies. The signal can be measured fast. Since the analysis requires a frequency spectrum (plot of intensity to each frequency) to make the identification, a decoding step is required to make the interpretation. Thus, the Fourier transformation (FT) is applied to transform the intensity as a function of the interferogram to a function of wavelengths. [31]

Evaluation of FTIR-spectra

The first step, when evaluating IR-spectra of ASDs is to record the spectra of the pure substances, in order to get an idea of bands of interest that occur and identifying those which are able to form intermolecular bonds. The spectra of physical mixtures and ASDs are recorded and compared to the ones of the pure substances.

Infrared spectra give information about the physical state of the drug, the presence of amorphous or crystalline form, possible interactions between the drug and the polymer, the nature and the strength of the interactions and recrystallization.

In general, the formation of H-bonding leads to shifts towards lower wavenumbers and to band broadening assigned to the carbonyl stretch [32]. Infrared spectra of amorphous

materials exhibit broader bands compared to their crystalline form. This refers to the lack of long-range order of the amorphous form [33].

2.4.3 Drug Release Studies

Dissolution is a process and needs to be investigated during the development of new solid oral dosage forms. *In vitro* dissolution testing is performed to compare dissolution profiles in the development phase of a drug or to evaluate the similarity to a target product. It aims at finding and predicting a relationship between in vitro and in vivo performance. However, in vitro dissolution tests do not always correlate to the performance of in vivo tests. Thus, in-vivo in-vitro correlation studies (IVIVC) need to be carried out. [1]

Erosion Mechanisms

Surface and bulk erosion are two different mechanisms that describe how a degrading polymer erodes during drug release/ dissolution. Surface erosion means release of polymer from the outer surface. The inside of the material does not migrate until all the surrounding material is migrated. Bulk erosion describes a mechanism in which the whole material degrades equally. The surface and the inside of the material degrade at same time. These erosion mechanisms are not exclusive. Several materials undergo a combination of the two. [34], [35]

The following figure depicts schematically how these mechanisms work.

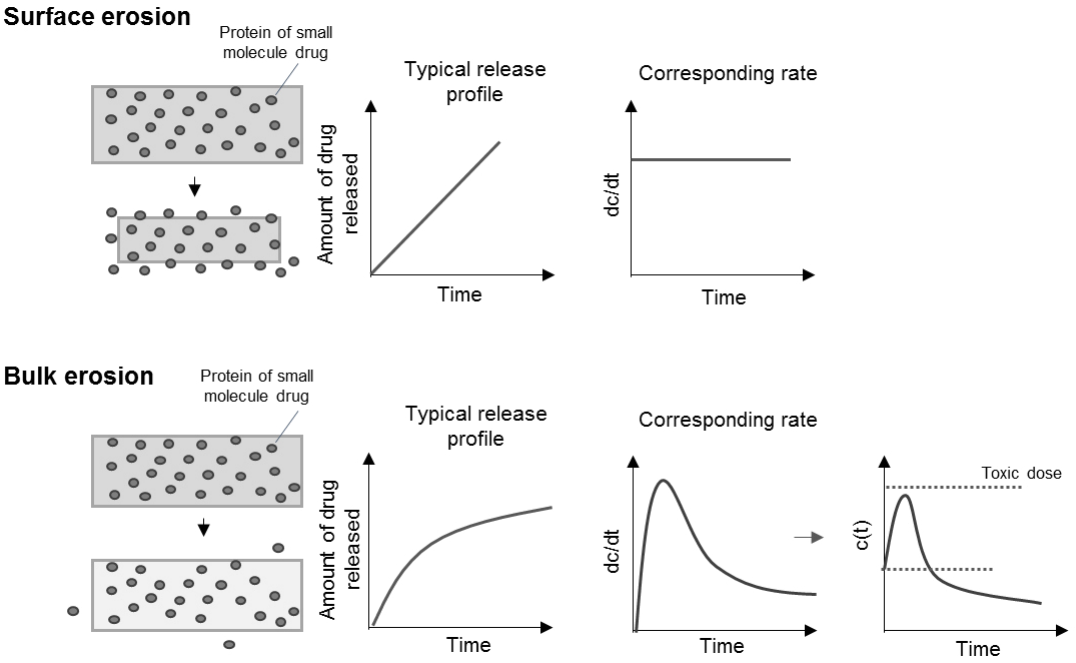

Figure 2-6 Scheme of surface erosion and bulk erosion and their controlled release profiles [36]

In addition to the surface and bulk erosion mechanisms several other factors control the dissolution of solid dispersions:

- The solid state of the drug: during dissolution, less energy is needed to break the structure of an amorphous API compared to the crystalline form.
- Stabilization function of the carrier: if the carrier is able to stabilize the API against recrystallization, a supersaturated solution state of the API can be achieved [37].
- surface area enlargement: dispersion the API at a molecular level provides a larger surface area for the dissolution process [33]
- Hydrophilicity: using hydrophilic carriers contributes to increase the dissolution rate.

3 Materials and Methods

This chapter provides an overview of materials used, the approach of sample preparation and methods used for characterising ASDs in the present thesis. As the used API (Nimodipine) is photosensitive (photo-degradable), all work is carried out under subdued light conditions [38].

3.1 Materials

The model API used within this thesis is Nimodipine, donated by Bayer AG, Germany. The polymeric carriers are a cationic polymethacrylate (Eudragit® EPO, Evonik AG, Germany) and hydroxypropyl methylcellulose (Methocel™ E5, Dow Chemical, USA). These two polymers were chosen in advance of this thesis, based on a screening of several polymers for stability of the ASD at accelerated conditions.

3.1.1 *Nimodipine*

Nimodipine (NMD) appears yellow and crystalline and belongs to the group of calcium channel blockers treating hypertension [39].

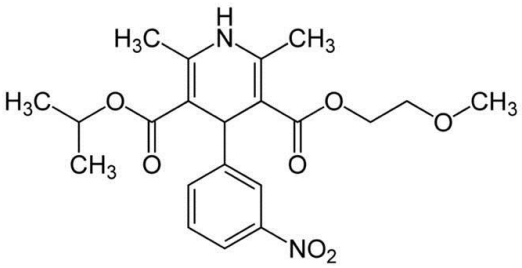

Figure 3-1 Chemical structure of NMD [39]

Chemical data from literature or experimental evaluation is specified in table 3-1.

Table 3-1 Chemical data of NMD [40]

	Abbreviation	Unit	Value
Molecular weight	*MW*	[g/mol]	418.44
Glass transition temperature	T_g	[°C]	14
Melting temperature	T_m	[°C]	116-127
Density	ρ	[g/cm³]	1.21

3.1.2 Polymeric Carriers

Eudragit® E

Eudragit® E (EE) is a cationic copolymer consisting of dimethylaminoethyl methacrylate, butyl methacrylate and methyl methacrylate monomers. It dissolves quickly in aqueous medium below pH values of 5 due to salt formation caused by the tertiary amino group [41].

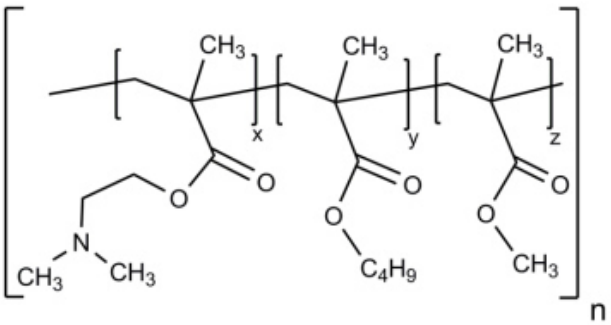

Figure 3-2 Chemical structure of Eudragit® E; x:y:z = 2:1:1 (x = dimethylaminoethyl methacrylate, y = butyl methacrylate, z = methyl methacrylate) [42]

Chemical data of interest is specified in table 3-2.

Table 3-2 Chemical data of Eudragit® E [6]

	Abbreviation	Unit	Value
Molecular weight	*MW*	[kDa]	147
Glass transition temperature	T_g	[°C]	48
pH solubility			<5
Density	ρ	[g/cm³]	1.11

HPMC E5

Methocel™ E5 or HPMC (hydroxyl propyl methyl cellulose) is a non-ionic cellulose ether with methoxyl and hydroxypropyl side groups. It enhances viscosity as it shows swelling behaviour in aqueous media which is retarding the drug liberation [43], [44]. Depending on the grade of HPMC, this retarding effect is stronger, or weaker. The grade used in this thesis is for fast release of the API.

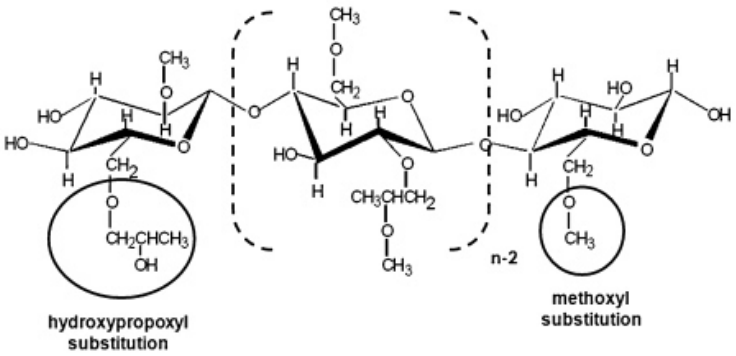

Figure 3-3 Chemical structure of Methocel™ E5; cellulose backbone with hydroxypropoxyl and methoxyl side groups [44]

Chemical data of interest is specified in table 3-3.

Table 3-3 Chemical data of Methocel™ E5 [6]

	Abbreviation	Unit	Value
Molecular weight	*MW*	[kDa]	10-50
Glass transition temperature	T_g	[°C]	170-180
pH solubility			1-10
Density	ρ	[g/cm³]	1.29

3.1.3 Drug-Polymer Mixtures

Physical mixtures and ASDs are prepared using drug to polymer ratios listed in the table below. Mostly, blends containing 10 % API are prepared. The drug amount is kept low to avoid stability problems and to make sure that the drug is completely dissolved. Two blends are binary mixtures, containing one polymer only to evaluate the impact of each polymer in the ternary systems. Ternary mixtures are prepared with different amounts of each polymer to find out how each polymer influences the drug release (in dissolution studies). Blends containing more than 10 % API are prepared with a 1:1 ratio of polymers to investigate the effect of the API on molecular interactions.

Table 3-4 Tested compositions of API and polymeric carriers in weight percent and the ratio of the carries

Number	Nimodipine [%]	Eudragit® E [%]	Methocel™ E5 [%]	Ratio of Polymers
1	10	90	0	-
2	10	72	18	4:1
3	10	60	30	2:1
4	10	54	36	3:2
5	10	36	54	2:3
6	10	30	60	1:2
7	10	18	72	1:4
8	10	0	90	-
9	10	45	45	1:1
10	20	40	40	1:1
11	30	35	35	1:1

3.1.4 Dissolution Studies

The dissolution studies are performed in a sodium acetate buffer with sodium acetate trihydrate (Sigma Aldrich, St. Louis, Missouri, USA), glacial acetic acid (Merck Millipore, Billerica, MA, USA), sodium lauryl sulfate (Carl Roth GmbH + Co. KG, Karlsruhe, Germany) and purified water (TKA MicroPure system, TKA GmbH, Niederelbert, Germany). For preparing the standards, methanol (HPLC grade, VWR, USA) is used as solvent for Nimodipine.

3.2 Methods

Material characterisation for a wide range of compositions needs a high number of samples. Since an extrusion process needs a rather high throughput (0.5 kg/h) in order to achieve consistent quality of the product, methods for the miniaturisation of the sample preparation are needed. In this thesis, vacuum compression molding is applied. The requirement of miniaturised methods is of course, that the large-scale production behaviour of the product can be mimicked. Thus, tabletop extrusion, being a small-scale version of the actual process, is used to assess the similarity of the product performance.

3.2.1 Vacuum Compression Molding

A novel vacuum compression molding (VCM) tool (MeltPrep GmbH, Austria), originally developed to prepare specimen for melt rheological studies, is employed to prepare amorphous, homogeneous samples that are used in dissolution studies and characterized via FTIR-spectroscopy in this work. Figure 3-4 and figure 3-5 show the setup of the device and a sectional view of the VCM tool. The idea is to produce samples in a cost and time efficient way with low consumption of drug material [45].

Figure 3-4 Vacuum compression molding setup: left – hot plate with VCM tool, middle – vacuum pump, right – cooler with VCM tool [45]

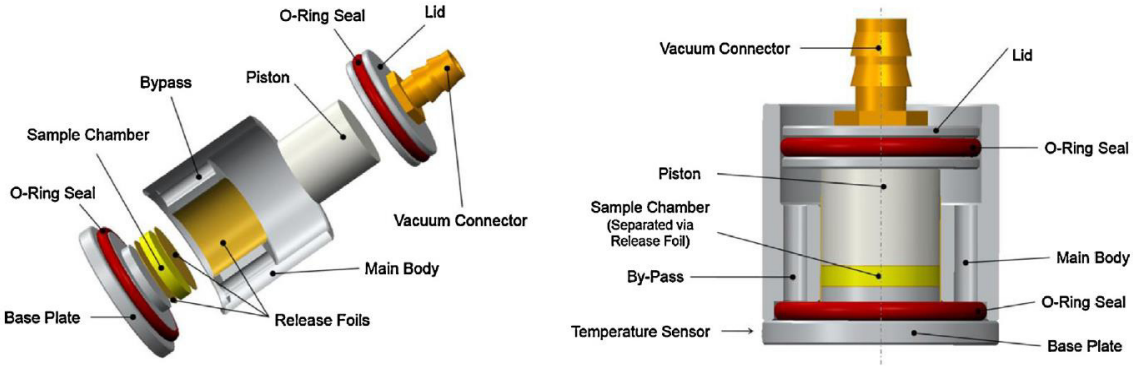

Figure 3-5 Sectional view of VCM tool; left – description of all parts, right – front view of the assembled tool [45]

The powder material is introduced into the sample chamber. Since the weight of the chamber is low it can be put on an analytical scale to determine the sample mass. Then vacuum is applied to build up a compressive force which removes volatiles and compacts the powder. After evacuating, the VCM tool is put on the hot plate to melt the powder material. Finally, the tool gets cooled on the cooling plate and the preparation of the specimen is completed. For dissolution testing in sink-conditions disc shaped VCM tablets with a diameter of 10 mm are prepared, using only about 60 mg of powder mixture. For non-sink conditions 25 mm tablets are prepared using 1 g of powder mixture. After filling the powder blends into the device an evacuation (5 min), heating (3 - 8 min) and cooling (3 – 5 min) process takes place to obtain homogeneous sample tablets with a diameter of 10 mm or 25 mm. The time duration is depending on the formulation and increases with the amount of Methocel™ E5, where longer time periods are necessary. The hot plate temperature is set between 170° - 180° C. Tablets of each composition are prepared.

In order to achieve very homogeneous VCM tablets, all physical mixtures were cryogenically milled using a nitrogen cooled CryoMill (Retsch, Germany). The grinding beaker is filled with 5 g of mixture and milled 3 cycles of 2:30 min at a milling frequency of 25 Hz. Intercooling is carried out for one minute at a frequency of 5 Hz.

3.2.2 Tabletop Extrusion

Extrudates of selected formulations are prepared using a co-rotating twin-screw tabletop Mini Extruder (ZE 9, Three Tec GmbH, Switzerland) with a *L/D* ratio of 20. The screw diameter is 9 mm and the extrusion die has a diameter of 1.5 mm. The three heated barrel zones are set to 140°C, 150°C and 150 °C, respectively. The screw speed is set to 150 rpm. The powder blends are fed manually into the hopper of the extruder and the extrudates are collected as rolled strands and cooled at ambient temperature. Pellets are made manually in order to perform dissolution testing experiments.

Before preparing the extrudates, all powder mixtures were weighed and blended using a tumble blender (Turbula® TypT2F, Willy Bachofen AG, Switzerland) for 10 min at 75 rpm.

3.2.3 In-Vitro Dissolution Testing

3.2.3.1 Preparation of the Dissolution Medium

Preparation of sodium acetate buffer (pH = 4.5 ± 0.1)

For preparing the buffer 15.4 g of sodium acetate trihydrate are weighed in a beaker and dissolved with purified water under constant stirring. After adding 8.6 mL glacial acetic acid the solution is transferred into a 5000 mL volumetric flask and filled up with purified water below the mark. The pH value is verified and adjusted to pH = 4.5 ± 0.1 with more glacial acetic acid if necessary. Then, the volumetric flask is filled up to the mark.

Preparation of 0.3% (w/v) sodium lauryl sulfate (SLS)-solution

For preparing a 0.3% SLS-solution 100 g of SLS are weighed in a 1000 mL beaker and dissolved with approximately 900 mL of purified water und constant stirring. The solution is stirred until the SLS is completely dissolved and then transferred into a 1000 mL volumetric flask and filled up to the mark with purified water.

Preparation of dissolution medium

The dissolution medium is made from solutions mentioned above. Therefore, 15 mL of SLS-solution are pipetted into a 500 mL graduated cylinder and filled up to the mark with acetate buffer.

3.2.3.2 Determination of the Solubility Concentration

Solubility studies of crystalline API are performed in dissolution medium by adding excess amount of drug crystal to the medium and letting it to saturate. The experiments are carried out in an incubator shaker for 24 h at 37 ± 0.5 °C in duplicate. Samples of 4 mL are withdrawn and filtered using mixed cellulose ester filters of 0.22 µm pore size. The concentration is determined using UV-Vis spectroscopy at a wavelength of 360 nm.

3.2.3.3 Dissolution Testing

Dissolution tests are performed for VCM tablets and pellets to determine the release profile of API. Intrinsic dissolution tests are performed to determine an API release rate per area and time in order to allow prediction of release profiles. Pellets are tested using an USP type I (basket, 100 rpm) and tablets using an USP type II (paddle, 75 rpm) apparatus. All tests are performed at a temperature of 37 ± 0.5 °C using 500 mL of dissolution medium.

Instrinsic dissolution tests (sink condition)

Experiments with VCM tablets of 60 mg and 10 mm diameter are carried out in a USP type II apparatus (Erweka DT820LH Dissolution Tester, Germany) using a rotational speed of 75 rpm. Intrinsic tests are performed with all formulations listed in table 3-4 in triplicates (n=3) aiming a “layer-wise” dissolution. Therefore, VCM tablets are put into heavy PTFE-fixations to cover the lateral and base area (top area stays uncovered) but also to guarantee that the tablets stay at the same spot during the experiment. Thus, proper hydrodynamic conditions can be achieved. Figure 3-6 shows a tablet in a fixation. Samples of 2 mL are taken manually every 10 min over a period of 70 min and filtered using 0.22 µm nylon filters. Concentrations are quantified via UV-Vis spectroscopy at 360 nm.

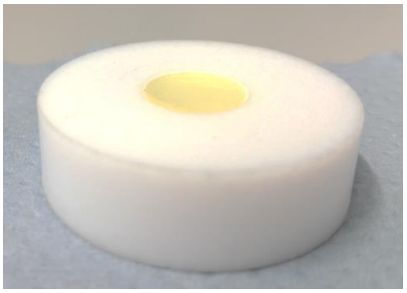

Figure 3-6 Picture of a VCM tablet (d = 10 mm) in the used PTFE-fixation for intrinsic dissolution experiments

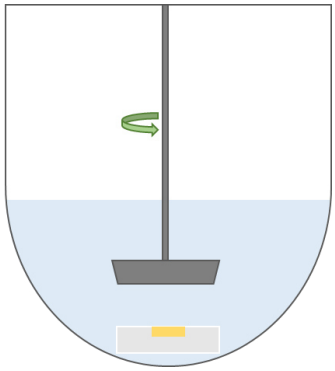

Figure 3-7 Schematic drawing of a dissolution vessel showing the position of the PFTE-fixation

Dissolution tests (non-sink condition)

Experiments with VCM tablets of 1 g and 25 mm diameter are carried out in a USP type II apparatus (Erweka DT820LH Dissolution Tester, Germany) using a rotational speed of 75 rpm. Tests are performed with selected formulations (number 3, 5, 8 and 9 listed in table 3-4) in triplicates (n=3). The non-sink conditions were selected according to the solubility of crystalline API determined experimentally. The solubility is exceeded threefold when using tablets of 1 g with 10 % API content. The physical mixture of one formulation is used for control. Samples of 1.5 mL are taken automatically after 0, 15 and 60 min and additionally after 2, 2.5, 3, 3.5, 4, 4.5 h over a period of 4.5 h. The samples are filtered using 0.10 µm poroplast filters and diluted appropriately. Concentrations are quantified via UV-Vis spectroscopy at 360 nm.

Dissolution tests (sink condition)

Experiments with pellets are carried out in a USP type I apparatus (Erweka DT820LH Dissolution Tester, Germany) using a rotational speed of 100 rpm. Tests are performed with

100 mg pellets of selected formulations (number 1, 3, 5, 8 and 9 listed in table 3-4) in triplicates (n=3). Samples of 1.5 mL are taken automatically after 0, 5, 15, 30, 45 and 60 min over a period of 60 min and filtered using 0.10 µm poroplast filters. Concentrations are quantified via UV-Vis spectroscopy at 360 nm.

3.3 Analytical Methods

3.3.1 Differential Scanning Calorimetry (DSC)

Dynamic and modulated DSC experiments are carried out to investigate the physical mixture samples using a differential scanning calorimeter (DSC 204F1 Phoenix®, Netzsch GmbH, Germany), standard aluminium crucibles and manually pierced lids. In the first heating run, all thermal events from the components can be detected. Amorphous solid dispersions are aimed to be achieved in a first heating and cooling run with a dynamic heating and cooling rate of 10 °C/min, a scan heating range from -10 °C to 180 °C and with pure nitrogen as purge gas at a flow rate of 50 mL/min. A second heating run is carried out using modulated DSC with a heating rate of 5 °C/min, a period of 40 s and an amplitude of ± 0.531 °C. The scan heating range is from -10 °C to 180 °C. The NETZSCH Proteus Thermal Analysis V.6.1.0 software is used for data evaluation.

3.3.2 Fourier Transform Infrared Spectroscopy (FTIR)

Attenuated total reflection (ATR) FTIR-spectroscopy is used to characterize the molecular arrangement of the pure substances and the VCM tablets. The absorbance spectra are recorded on a Bruker VERTEX 70 (Bruker, Germany) using an ATR unit and the following settings: spectral resolution 4 cm^{-1}, 64 scans, 4500 – 600 cm^{-1}. Spekwin32 – optical spectroscopy software V.1.72.2 and Microsoft Excel are used for spectra evaluation.

In order to record FTIR-spectra of amorphous nimodipine, the following procedure is applied: A small amount of crystalline drug is transferred into an aluminium DSC crucible, molten on a hot plate until a homogeneous melt is achieved and cooled down very fast in ice afterwards. The amorphous drug sample is immediately analysed.

Bands of interest of the substances used in this work are listed in table 3-5.

Table 3-5 Bands of interest in IR-spectra (taken from spectra of pure substances)

Substance	Wavenumber [cm^{-1}]	Functional group
NMD	3293	Secondary amino group (N-H)
	1625	Aryl-substituted C=C
	1695	Carbonyl group (C=O)
	1523	Nitro group (NO_2)
	1090	Ether group (C-O-C)
EE	2820	Dimethyl amino group ($N(CH_3)_2$)
	1720	Carbonyl group (C=O)
	1150	Ether group (C-O-C)
HPMC	3443	Hydroxyl group (O-H)
	1069	Ether group (C-O-C)

3.3.3 UV-Visible Spectroscopy

The concentration of nimodipine released in dissolution testing is determined by recording absorbance spectra using a UV-Vis spectrophotometer (Lambda 950, PerkinElmer, USA). Measurements are made in 1 cm polymethyl methacrylate (PMMA) semi-micro cuvettes between 370 – 350 nm at every 1 nm. Each sample is measured against a blank of dissolution medium. Standards of concentrations ranging from 3 to 30 mg/L are prepared by diluting a 300 mg/L stock solution (nimodipine in methanol) with dissolution medium.

4 Results, Discussion and Conclusion

This chapter presents the findings of the performed studies. First, the characterization of the phase composition of the binary and ternary systems and the molecular arrangement is done. Second, the dissolution studies for VCM tablets and pellets are performed and discussed.

4.1 Characterization of Drug-Polymer Interactions

4.1.1 Phase Composition Studies (DSC)

Phase composition studies are made using differential scanning calorimetry. Physical mixtures (table 3-4) are analyzed in this work. The samples undergo a heating-cooling-heating cycles in DSC.

Information about miscibility of the binary and the ternary systems can be drawn from the first heating run. This is done by determining the area of the melting peak in the first heating curve. Melting peaks occur when crystalline API is present at its melting temperature. The smaller the area of the peak, the more API is dissolved prior to reaching this temperature. In case there is no peak detected, all crystalline API was dissolved in the polymeric melt before the melt temperature of the crystal is reached.

The second heating run gives information about whether or not a single glass transition temperature could be achieved. This gives insight in the phase arrangement in the amorphous system. A single T_g indicates a single-phase system in general. The T_g values determined experimentally are compared to theoretical values calculated using the Gordon-Taylor equation. A comparison again allows conclusions about the phase composition of the ASDs.

4.1.1.1 First Heating Run – Dynamic Heating

The first heating run of physical mixtures is performed using a dynamic heating rate of 10 °C/min. The following thermograms show the first heating runs of the binary mixtures and one ternary mixture (3:2; EE:HPMC) as examples, all containing 10% of API.
Figure 4-1 and figure 4-2 show the thermograms of the binary systems NMD and the polymers. For the binary system containing nimodipine and Eudragit® E, the glass transition of EE and an endothermic event (melting of NMD) can be detected. The binary system with HPMC on the other hand, shows an endothermic peak which refers to water, the melting peak of NMD and no glass transition of the polymer. In general, HPMC is known not to show

pronounced T_gs. The area of the melting peak of the system NMD and HPMC is broader. Figure 4-3 shows the water peak again with the overlapping T_g of EE, a small melting peak and the T_g of HPMC.

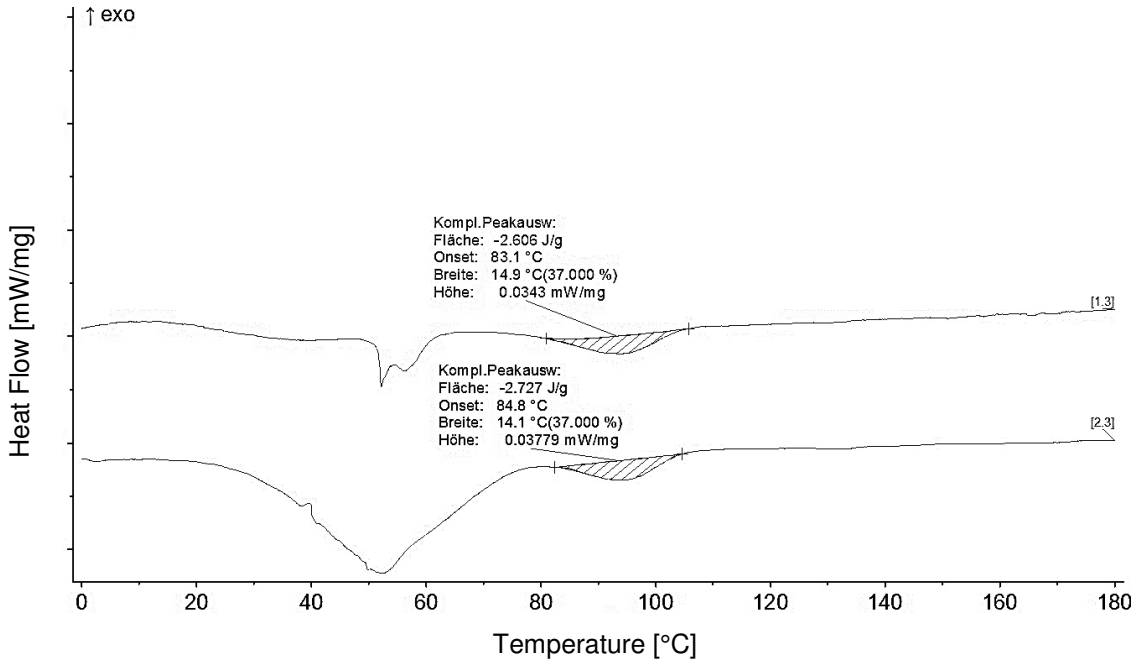

Figure 4-1 DSC-thermogram: first heating run of the binary system NMD and EE (10% API)

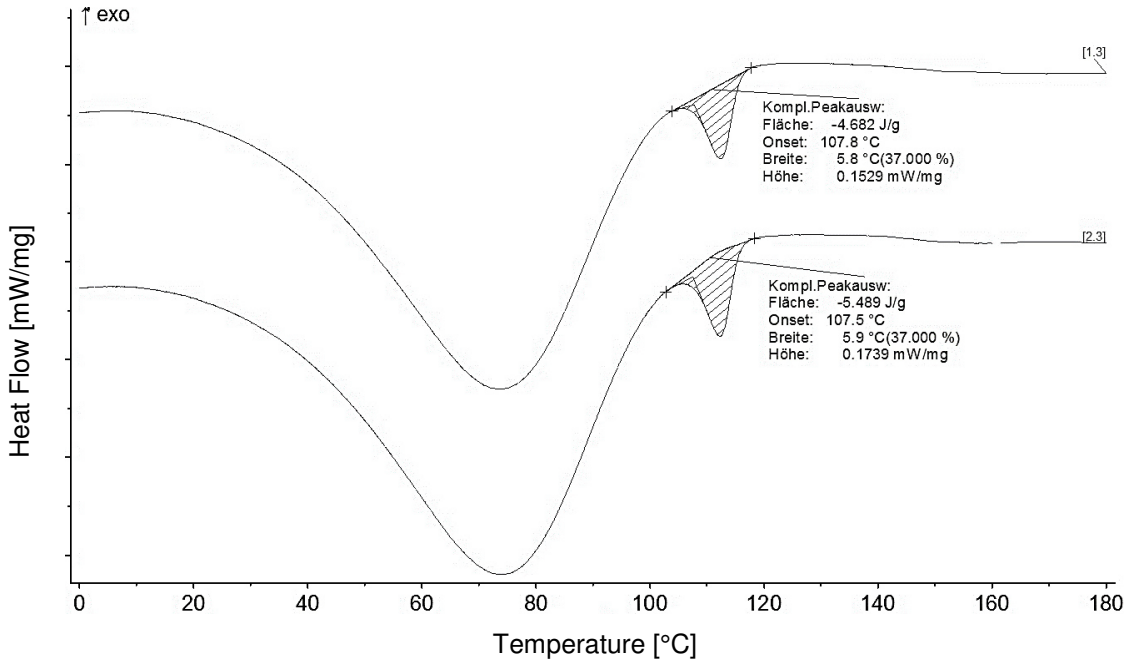

Figure 4-2 DSC-thermogram: first heating run of the binary system NMD and HPMC (10% API)

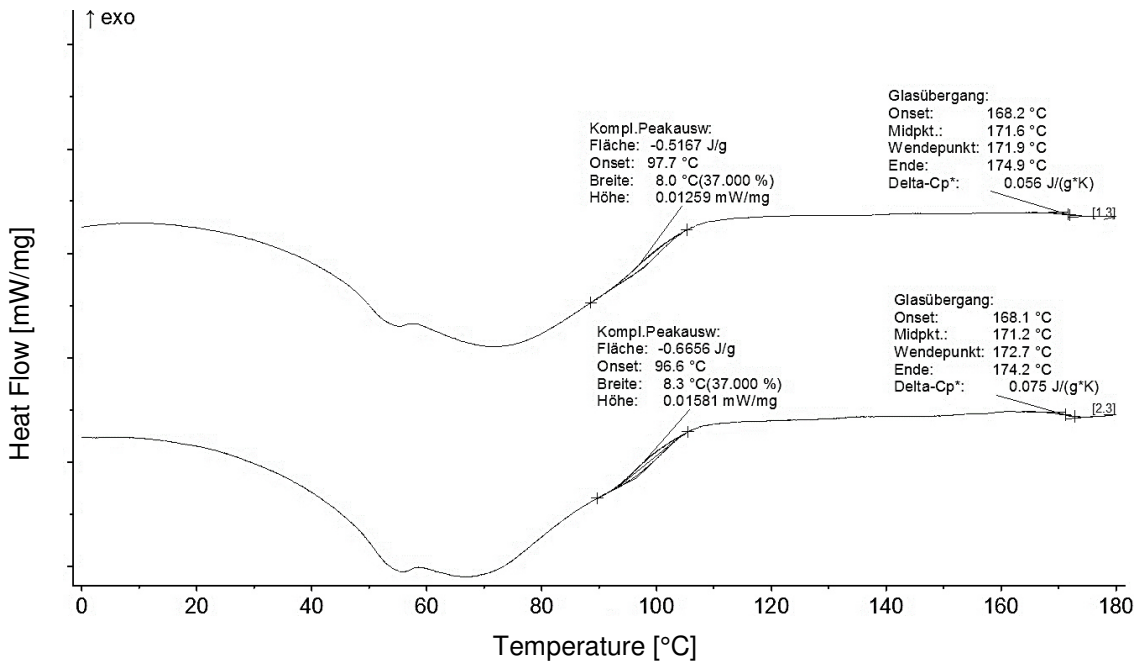

Figure 4-3 DSC-thermogram: first heating run of the ternary system NMD and EE:HPMC 3:2 (10% API)

From these three thermograms, it can be seen already, that the ternary system behaves different compared to the binary systems. The melting points of API for all compositions during the first heating scan are summarized in figure 4-4 and figure 4-5. They show the area under the melting peak and the onset temperature of the peak for each mixture containing 10% API over the EE content in the formulation. No EE (0%) shows the binary system of NMD and HPMC. The obtained peak area value of pure NMD is scaled to 10% in order to compare it with the blends (10% drug content).

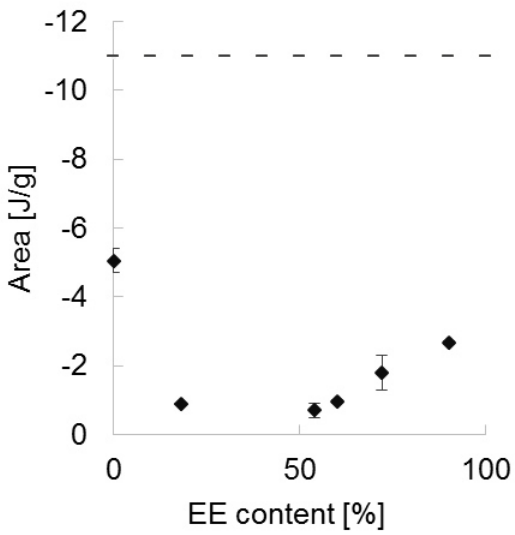

Figure 4-4 Evaluated area of melting peak (NMD) versus EE content; dashed line - NMD pure substance

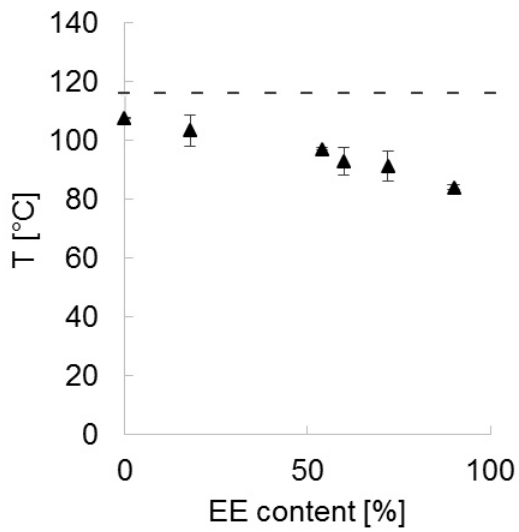

Figure 4-5 Onset temperature of area versus EE content; dashed line - NMD pure substance

The areas of the melting peak of the binary systems are larger compared to the ternary ones, whereas the onset temperature is decreasing with increasing EE content. The formulation without EE (0% EE) shows the highest peak area as well as the highest onset temperature. This indicates, that the interaction of NMD and HPMC below the melt temperature of NMD is very limited. Since HPMC is still in its glassy state at this temperature (T_g = 170-180 °C), this is plausible. The sample with 90% EE (without HPMC) represents solid-liquid solubility, since the T_g of EE (~45 °C) is far below the melt temperature of NMD. Thus, the melt point depression is most pronounced for this case and shows a steady trend with increasing EE content. Nevertheless, it is even more interesting to see, that the peak area does not correlate with this trend. The peak areas of the ternary systems are smaller compared to the binary systems. Assuming that the obtained data are reliable and neglecting the uncertainties originating from overlapped T_m*s* and with dehydration, a possible reason for this behavior could be the anomalous role change of EE depending on the composition as reported in literature. The anomalous role change is described as a composition depending change of the EE as H-acceptor between the carbonyl group forming H-bonds and the amino group forming ionic bonds. This could mean that the amount of HPMC influences the behavior of EE in this case. In absence of HPMC, EE possibly forms H-bonds with the carbonyl group and an increased amount of HPMC can lead to the mentioned role change to establish ionic interaction, explaining the better miscibility behavior [46].

Overall, the incongruence of composition dependent melting point depression and heat of melting as a function of HPMC to EE ratio points to the possible role of molecular level interaction as well as macroscopic properties on the observed effect. Since the peak area correlates to the amount of crystalline API at the given melt temperature, it seems that the solid HPMC that are not miscible in the system could phase separate out at some concentrations. Also, important to note is the presence of water and speciation of the same (free versus plasticizing fraction).

4.1.1.2 Second Heating Run – Modulated Heating

The second heating run gives information about the composition dependent T_g values of the ASD. The following thermograms (figure 4-6 to figure 4-8) show the second heating run of the binary mixtures and an example of one ternary mixture, all containing 10 % of API.

The evaluation of the T_g values was done using the first derivative of the reversing heat flow. The maximum of the peak in the first derivative curve helps in the visual determination of the correct T_g. It can be seen from the thermograms, that the detection of the T_g is not always straight forward. Figure 4-6 showing the second heat run for the binary system

containing NMD and EE only, indicates, that only one T_g is formed in this case and thus, a single-phasic amorphous system was achieved during the cooling cycle. In the case of the binary system with NMD and HPMC (figure 4-7), no T_g can be detected at all. Since HPMCs are known to show only poorly detectable T_g*s* this is not surprising, but it is also not possible to receive a signal from NMD. Thus, no clear conclusion can be drawn concerning the phase arrangement of this formulation. The generation of an amorphous system in the first heating and cooling cycle can be confirmed though, due to the absence of a melt peak.

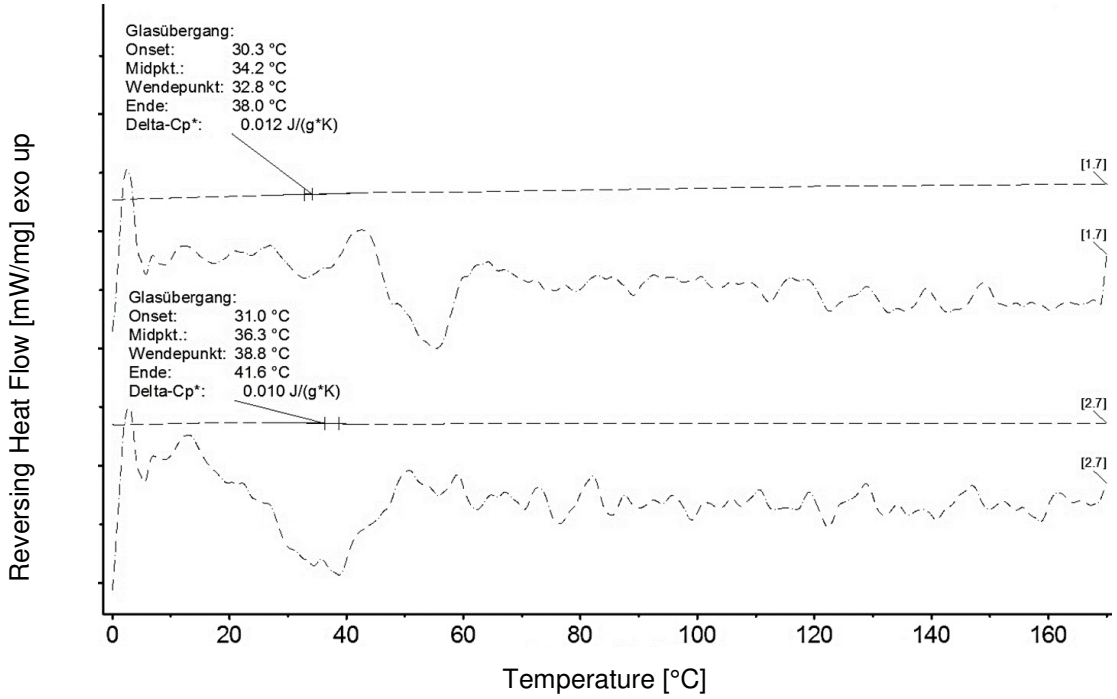

Figure 4-6 DSC-thermogram: second heat run - reversing heat flow of the binary system NMD and EE (10% API) and their derivatives (1.7 and 2.7)

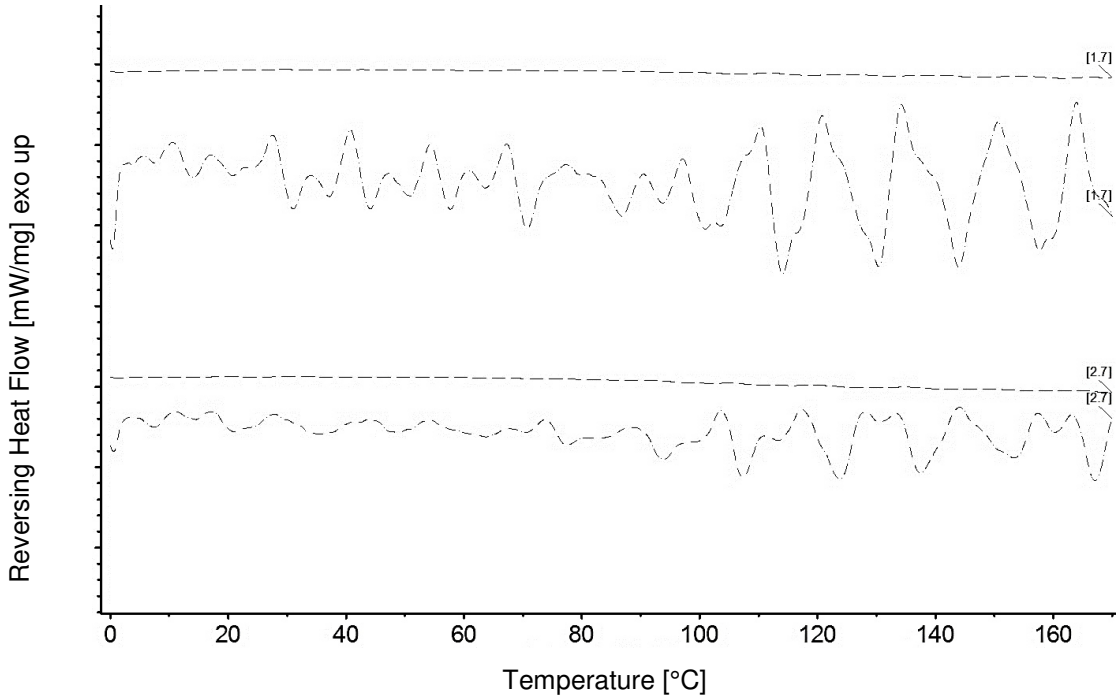

Figure 4-7 DSC-thermogram: second heating run of the binary system NMD and HPMC (10% API) and their derivatives (1.7 and 2.7)

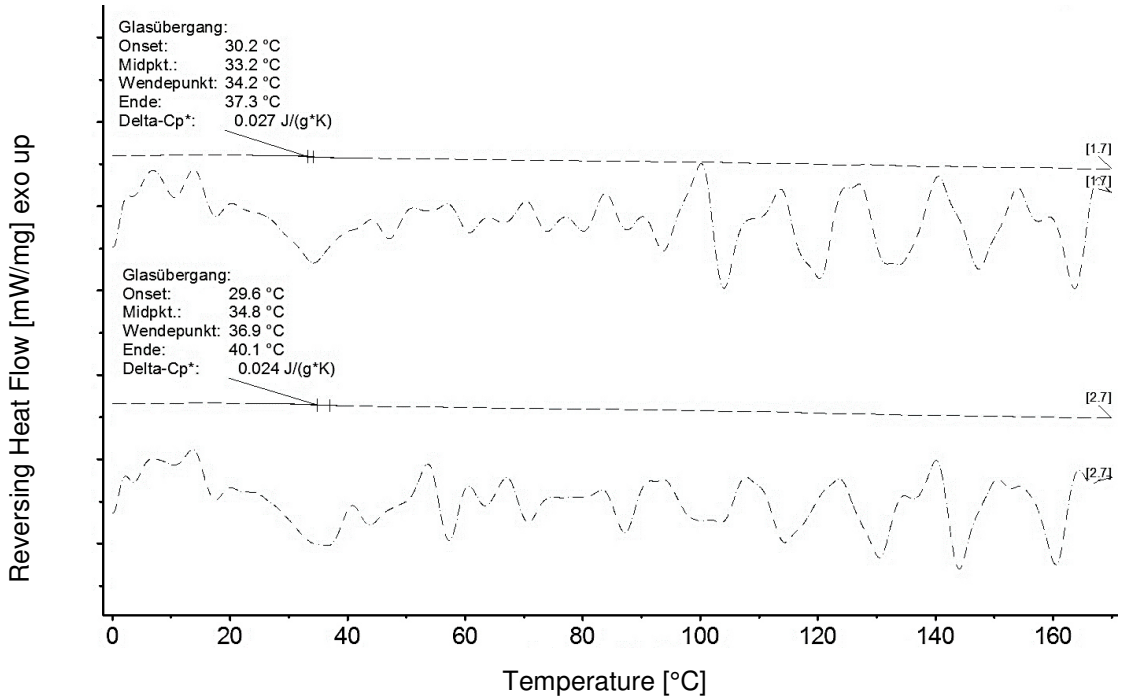

Figure 4-8 DSC-thermogram: second heating run of NMD and EE:HPMC 1:1 (10% API) and their derivatives (1.7 and 2.7)

In the case of the ternary system (figure 4-8), on the other hand, it is possible again to determine a T_g value. The position of the T_g is unexpectedly low though, similar to the T_g of the binary system with NMD and EE. The T_g of ternary systems can also be estimated by applying the Gordon-Taylor equation (equation 4-1). [26]

$$T_{g,mix} = \frac{w_1 T_{g,1} + K_1 w_2 T_{g,2} + K_2 w_3 T_{g,3}}{w_1 + K_1 w_2 + K_2 w_3}$$ **Equation 4-1**

$$K_1 = \frac{\rho_1 T_{g,1}}{\rho_2 T_{g,2}}$$ **Equation 4-2**

Table 4-1 Description of symbols used in equation 4-1 and equation 4-2

Symbol		Unit
$T_{g,mix}$	Glass transition temperature of mixture	[K]
W	Weight fraction of each component	-
T_g	Glass transition temperature of each component	[K]
K	K_1 (NMD & EE), K_2 (NMD & HPMC)	-
ρ	Density of each component	[g/cm^3]

The results are illustrated in figure 4-9 and deviate significantly from the experimental T_g values. This is an indication that HPMC does not contribute to the formation of ASDs. Therefore, the T_gs of the binary mixtures of API and EE are calculated as well and compared with the experimental data as shown in figure 4-10. The theoretical API content is calculated, neglecting the HPMC in the ternary blends and thus it increases with decreasing EE content (e.g. 10% NMD, 60% EE and 30% HPMC gives 14% NMD and 86% EE; w/w). In both cases, the experimental data deviates (slightly) negatively from the calculated values. A negative deviation from the predicted values can be taken as an indication of predominant entropic interactions for molecular mixing. [47]

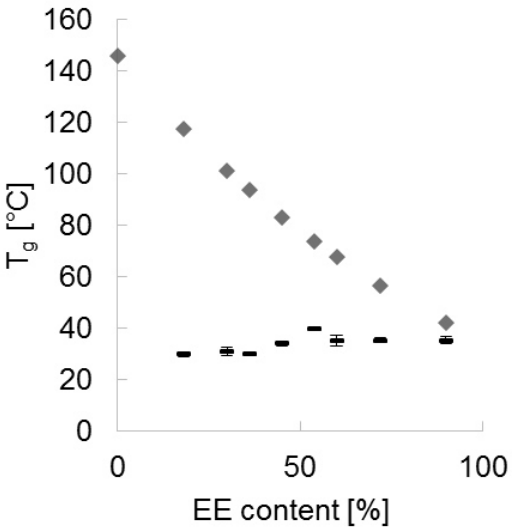

Figure 4-9 Experimental values (-) of T_g versus theoretical values (♦) using Gordon-Taylor model for ternary mixtures

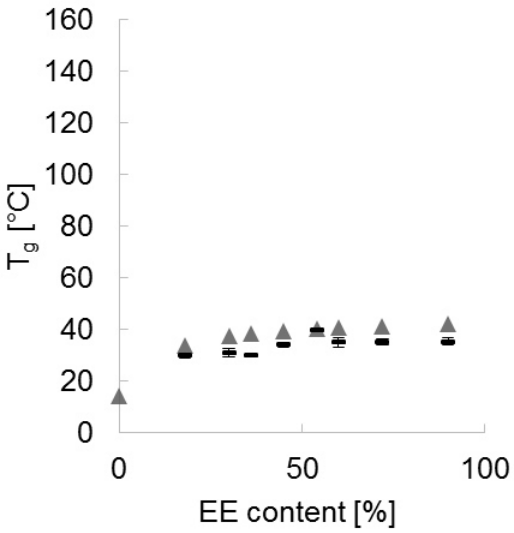

Figure 4-10 Experimental values (-) of T_g versus theoretical values (▲) using Gordon-Taylor model for binary mixtures (NMD and EE)

The T_g value of the binary system NMD and EE can be compared to the experimental data, as well as the T_g values for the ternary system. However, the T_g of NMD and HPMC cannot be determined. The approach of using the Gordon-Taylor equation for the binary system (NMD and EE) is in good agreement to the experimentally determined values for the ternary system. Thus, it could be assumed, that HPMC is possibly present as an inert carrier only for the present ASD.

Conclusion

Regarding the miscibility behavior due to the obtained data of DSC, it is better using a ternary system of API and two polymers than only using binary system. Further, the more equal the amount of the polymer ratio (e.g. 1:1) the smaller the melting peak area becomes which is regarded to be an indicator for better miscibility.

The T_g is decreasing with increasing HPMC content, even though the T_g of HPMC is high compared to NMD and EE and should increase the T_g of the ternary systems. It is assumed that HPMC does not participate in forming the solid dispersion due to high thermal viscosity (without mechanical treatment) and only NMD and EE form a solid dispersion as the empirical data of the binary system and experimental data suggest. The negative deviation from the experimental T_g values from the empirical ones can be supposed to weaker drug-polymer interactions than drug-drug and polymer-polymer interactions [48].

4.1.2 Molecular Arrangement (FTIR-Spectroscopy)

The main target of this work is to investigate the molecular arrangement in this ternary formulation. Therefore, interactions of functional groups between API and polymeric carries are investigated via infrared spectroscopy. This section is divided into 3 parts: pure substances, binary mixtures, ternary mixtures.

4.1.2.1 Pure Substances

The spectra of the pure substances (powder and processed samples (VCM)) are recorded to identify characteristic absorbed bands for identifying interactions the ASDs prepared via the VMC technology. The focus of this subsection lies on evaluating the spectra of crystalline and amorphous API.

API

Functional groups or bonds of interest regarding the API are the secondary amine group (N-H), the carbonyl group (C=O), the C=C double bonds from the aromatic rings and the nitro group (NO_2), all circled in the following structure.

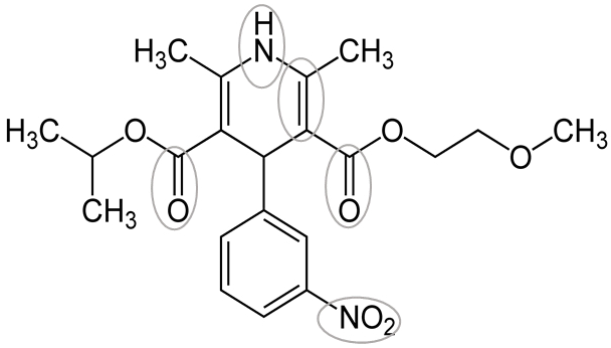

Figure 4-11 Chemical structure of NMD – groups of interest are tagged

These groups are likely to interact with groups of the polymers by forming ionic bonds or hydrogen bonds. The following figures show the spectra of crystalline and amorphous NMD. The mentioned bands appear at 3269 cm^{-1} (N-H), 1695 cm^{-1} (C=O), 1625 cm^{-1} (C=C) and 1523 cm^{-1} (NO_2) in the spectrum of crystalline NMD.

Table 4-2 Bands of interest in IR-spectra

Substance	Wavenumber [cm^{-1}]	Functional group
	3293	Secondary amino group (N-H)
	1625	Aryl-subsituted C=C
NMD	1695	Carbonyl group (C=O)
	1523	Nitro group (NO_2)
	1090	Ether group (C-O-C)

In order to identify the characteristic API peaks for its amorphous form, the spectra of the pure amorphous drug substance are recorded and compared to the spectra of the crystalline API (figure 4-12 to figure 4-14). [49]

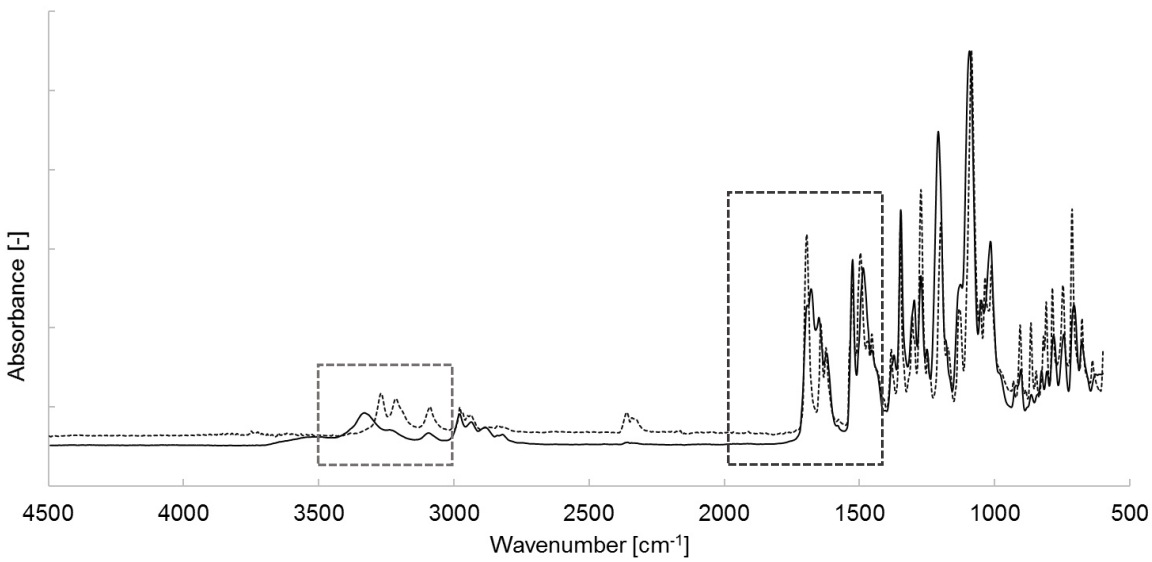

Figure 4-12 Averaged FTIR-spectra (n=3) of crystalline (dotted line) and amorphous (solid line) NMD revealing characteristic differences in two regions

The spectrum of the amorphous material show shifting of the bands of the amine group, the carbonyl group and the C=C double bond. The bands of the nitro group appear at the same wavenumbers. This leads to the assumption that the nitro group will not be involved in interacting with the polymers. Figure 4-13 shows a detailed view of the spectra within the wavenumber range of 3000 – 3500 cm^{-1}. It can be seen that the NH-band shifts to higher wavenumbers from crystalline state to the amorphous one. This indicates that the drug-drug hydrogen bonds present in the crystalline form are broken during amorphization [50].

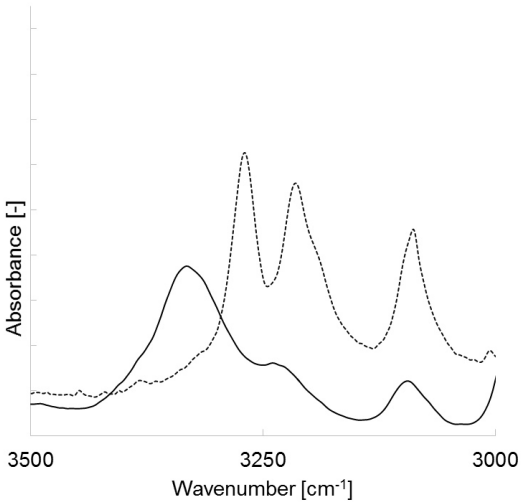

Figure 4-13 Averaged FTIR-spectra (n=3) of crystalline (dotted line) and amorphous (solid line) NMD – detailed view of the single bond stretch region

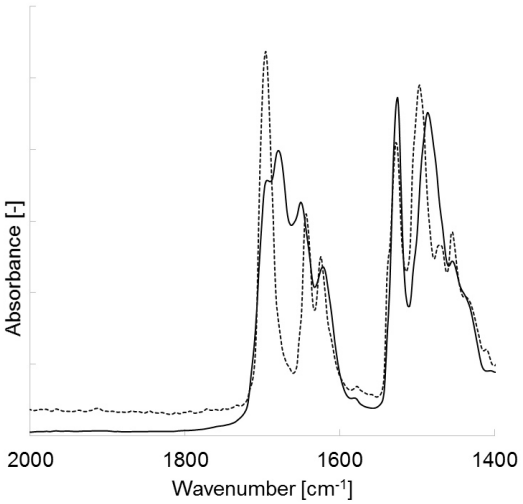

Figure 4-14 Averaged FTIR-spectra (n=3) of crystalline (dotted line) and amorphous (solid line) NMD - detailed view of the double bond stretch region

Figure 4-14 shows a detailed view of the spectra within the wavenumber range of 1400-2000 cm^{-1}. It reveals shifts to lower wavenumbers of the C=O bond and the C=C bond of the dihydropyridine ring, also indicating a weakening of intermolecular H-bonds within drug molecules.

Polymers

Functional groups of interest occurring in the spectra of the polymeric carriers are the dimethylamine group ($-N(CH_3)_2$) occurring at 2820 cm^{-1} and the carbonyl group (C=O) at 1720 cm^{-1} for EE as well as the hydroxyl group of HMPC occurring at 3443 cm^{-1} [51].

Table 4-3 Bands of interest in IR-spectra of polymers

Substance	Wavenumber [cm^{-1}]	Functional group
EE	2820	Dimethyl amino group ($N(CH_3)_2$)
	1720	Carbonyl group (C=O)
	1150	Ether group (C-O-C)
HPMC	3443	Hydroxyl group (O-H)
	1069	Ether group (C-O-C)

The following spectra (figure 4-15 and figure 4-16) show the peaks of the powder materials compared to the VCM prepared samples. The spectra of powder and VCM prepared samples are superposed without any peak shifts, indicating no change due to the VCM process.

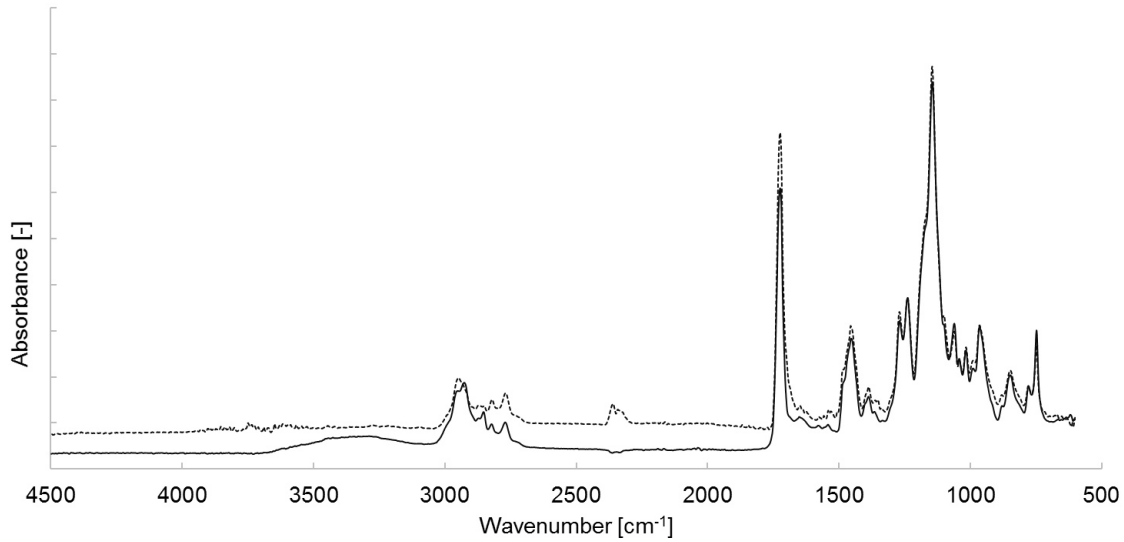

Figure 4-15 Averaged FTIR-spectra (n=3) of EE powder (dotted line) and VCM prepared sample (solid line)

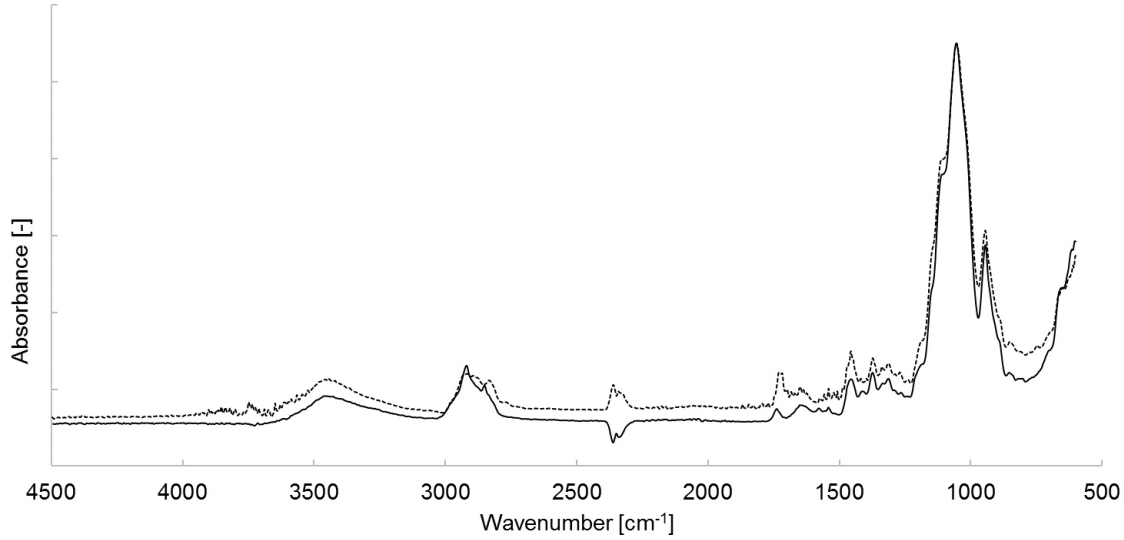

Figure 4-16 Averaged FTIR-spectra (n=3) of HPMC powder (dotted line) and VCM prepared sample (solid line)

4.1.2.1 Binary Mixtures

Spectra of ASDs of binary blends (API + polymer) are investigated by comparing the spectra of the pure substances with the digitally generated spectra of the binary blends (figure 4-17 to figure 4-19). Grey spectra are from the amorphous, pure substances, black and green show the binary mixtures and red shows a ternary blend of EE: HPMC 1:1. Moreover, digital mixtures are illustrated for the binary blends, calculated by proportional addition of the pure substance spectra, to allow a direct evaluation of peak shifts due to interactions.

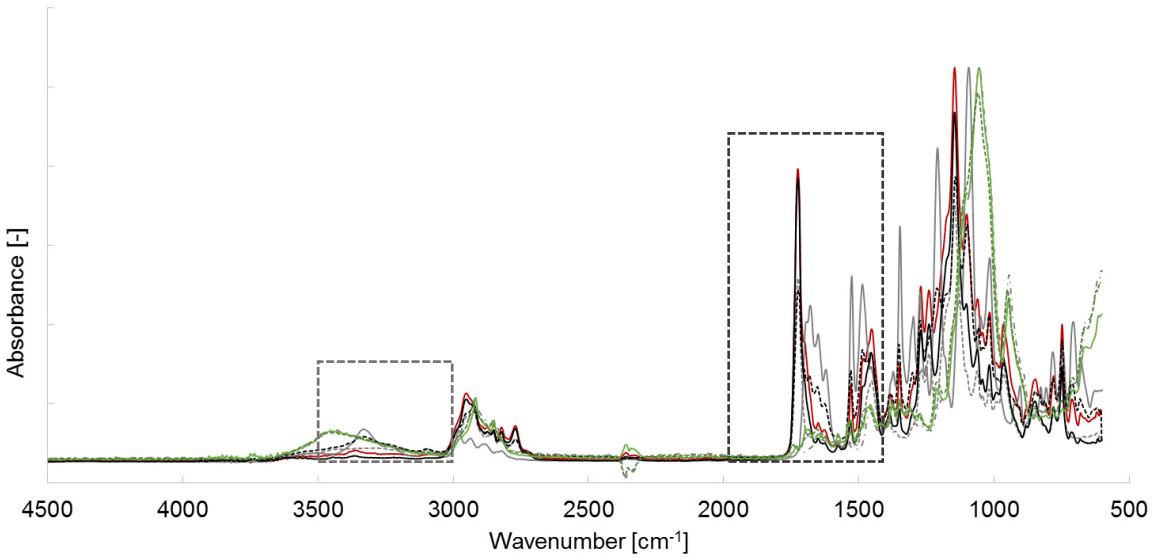

Figure 4-17 Averaged FTIR-spectra (n=3) of pure substances: amorphous NMD (grey, solid line), VCM prepared polymers – EE grey, dashed line; HPMC grey, chain dotted line, binary mixtures: API + EE black, solid = ASD, dotted = digital blend, API + HPMC green, solid = ASD, dotted = digital blend, ternary system: API + EE:HPMC 1:1, red solid line

Figure 4-18 and figure 4-19 show a detailed view of the spectra within the wavenumber range of 3000 – 3500 cm^{-1} and 1400 – 2000 cm^{-1}. They reveal that NMD is in its amorphous state in all VCM samples, since the drug-drug H-bonds were weakened. This is indicated by the redshift of the characteristic NH-band at 3293 cm^{-1} in the binary mixture with EE (3366 cm^{-1}) and the ternary mixture (3362 cm^{-1}). Moreover, this is supported when comparing the digital binary mixture of NMD and EE (black, dotted line) with the measured spectra (black, solid line). It is again clear to see that the NMD peak is redshifted the measured sample. However, specific functional interactions between drug-polymer molecules are not shown according to the IR spectra. There is no shift of the carbonyl group (C=O) of EE at 1720 cm^{-1} giving evidence that EE and NMD do not seem to form H-bonds.

For the binary mixture with HPMC (green, solid line), it is not possible to detect the characteristic NH-band of NMD in the spectrum. It seems to be overlapped with the hydroxyl group, which can be due to H-bonds between the molecules. Looking at the digital blend (green, dotted line) though, this seems to be due to the dilution effect, since this peak can also not be found there. The hydroxyl group (3443 cm^{-1}) of HPMC seems to be slightly shifted to the right when comparing the measured spectrum to the digital blend. The possible reason for this could be that HPMC contained some moisture in powder (that was used to create digital spectrum) which is eliminated upon processing. Thereby, dispersions might have un-plasticized HPMC OH region. The potential C=O side group of EE (1720 cm^{-1}) for interaction though, does not show any shift when changing from a binary to a ternary system. On the other hand, the C=O side group of NMD (1695 cm^{-1}) is slightly

redshifted for the measured system compared to the digital blend. This could indicate an interaction between HPMC and NMD.

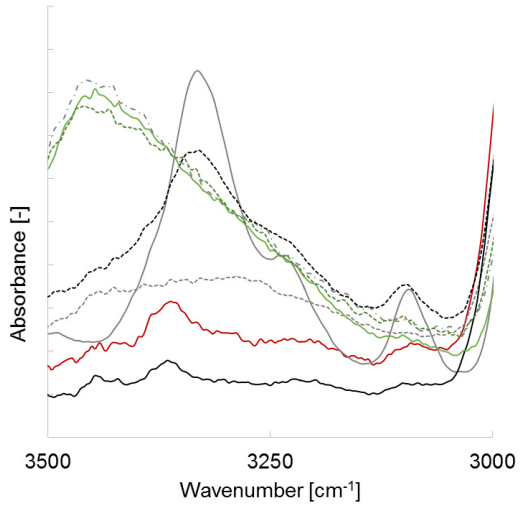

Figure 4-18 Averaged FTIR-spectra (n=3) of pure amorphous substances (grey, NMD solid, EE dotted, HPMC chain dotted), prepared (solid) and digital (dotted) binary systems (black for EE; green for HPMC) and the ternary system EE:HPMC 1:1 (red) – detailed view (3000 – 3500 cm^{-1})

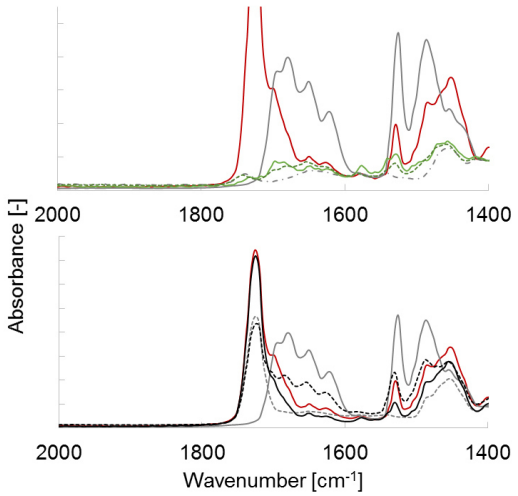

Figure 4-19 Averaged FTIR-spectra (n=3) of pure amorphous substances (grey, NMD solid, EE dotted, HPMC chain dotted), prepared (solid) and digital (dotted) binary systems (black for EE; green for HPMC) and the ternary system EE:HPMC 1:1 (red) – detailed view (1400 – 2000 cm^{-1})

When comparing the spectra to the ternary system, it seems likely that the drug molecules are dispersed in the carrier matrix in its amorphous form without forming intermolecular bonds.

4.1.2.2 *Ternary Mixtures*

Spectra of ASDs of ternary blends are investigated by comparing the spectra of pure NMD with the digitally generated spectra of the ternary blends (figure 4-20 and figure 4-21). The grey spectra are from the amorphous NMD, black and green show the ternary mixtures. Figure 4-7 compares the spectra of two contrary mixtures (4:1 and 1:4) with 10 % API.

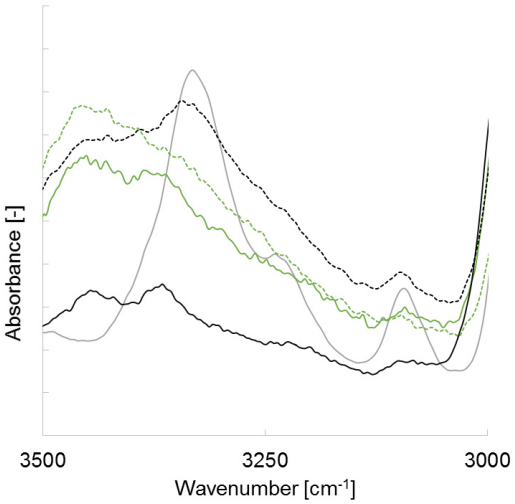

Figure 4-20 Averaged FTIR-spectra (n=3) of pure amorphous NMD (grey, solid) prepared (solid) and digital (dotted) ternary systems (black for more EE; green for more HPMC) – detailed view (3000- 3500 cm^{-1})

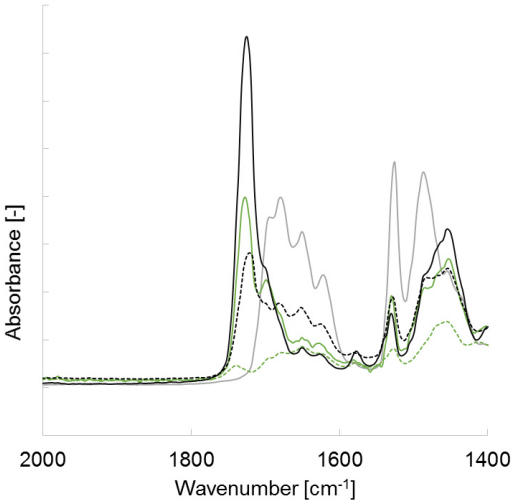

Figure 4-21 Averaged FTIR-spectra (n=3) of pure amorphous NMD (grey, solid) prepared (solid) and digital (dotted) ternary systems (black for more EE; green for more HPMC) – detailed view (1400- 2000 cm^{-1})

Conclusion

The FTIR-spectra helped in revealing the amorphous state of the API in the VCM prepared samples of binary and ternary mixtures. The drug molecules are dispersed in the polymeric carriers, however, the spectra do not give compelling evidence of specific functional interactions (like H-bonding) with polymers. The amorphous state of the drug molecule and hence improving its solubility is achieved. There are no drug-polymer interactions when preparing the samples with VCM technology. However, this might be different when preparing ASD via HME, i.e. there could still be possibility of drug-polymer H-bonding.

4.2 Characterization of Drug Release

The in vitro release of API from ASDs prepared via VCM technology and tabletop extrusion is investigated in dissolution studies. This section provides results of the dissolution tests performed under sink (ASDs and pellets) and non-sink conditions (ASDs).

4.2.1 Intrinsic Dissolution Studies

Intrinsic dissolution studies are performed under sink conditions (with respect to crystalline drug solubility in the selected medium). This means the total drug content in the VCM prepared tablets is below the solubility concentration of NMD and there will be no driving force of recrystallization of dissolved API. Samples of binary and ternary systems (table 3- 4) are prepared and processed to homogeneous disc shaped ASDs. Dissolution studies are performed in triplicates (n=3). Intrinsic dissolution studies are made to calculate the intrinsic release rate and to allow an estimation of the API release profile from different geometries. figure 4-22 and figure 4-23 show the dissolution profiles of systems with 10% API.

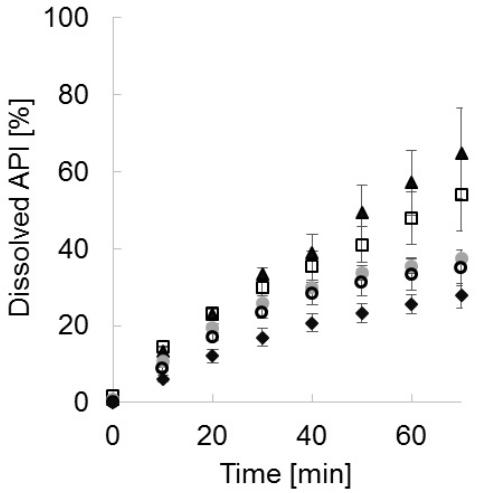

Figure 4-22 dissolution profiles of formulations with 10% API and more EE: (▲) EE; (□) 4:1 EE:HPMC; (●)2:1 EE:HPMC; (○)3:2 EE:HPMC; (♦)1:1 EE:HPMC

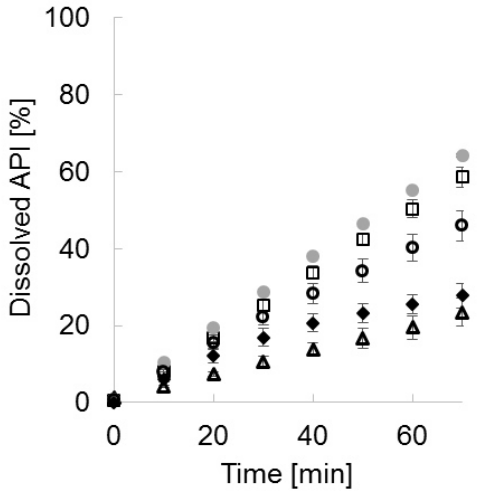

Figure 4-23 dissolution profiles of formulations with 10% API and more HPMC: (●) 1:2 EE:HPMC; (□)1:4 EE:HPMC; (○)2:3 EE:HPMC; (♦)1:1 EE:HPMC; (△) HPMC

The binary mixture of NMD and EE and the ternary systems with more HPMC (1:2 and 1:4) exhibit the highest dissolution rates. The binary mixture of NMD and HPMC, however, is the slowest. Moreover, the trend of the dissolution rate over the formulation composition is not inconsistent. Especially for the formulations containing more HPMC, where the ranking of the fastest to the slowest formulation is the 1:2, 1:4, 2:3, 1:1 EE:HPMC with the binary system of NMD and HPMC being last. Another interesting observation is that the ternary

system with a polymer ratio of 1:1 is very slow, even though the mixtures with slightly more or less EE or HPMC exhibit significantly higher dissolution rates. This erratic behavior could be an effect of the different dissolution mechanism of the two polymers used in this study. HPMC is a swelling polymer, releasing the API from a gel like surface via diffusion, whereas EE (erodible polymer) releases the API via surface erosion. An intrinsic dissolution profile from an erosion controlled system is linear, since the dissolution happens layer by layer. A swelling polymer develops a gel layer first and then, the drug release will be controlled by diffusion through this layer, representing the case of bulk erosion. This effect can be seen for the samples with 2:1, 3:2 and 1:1 EE: HPMC ratio. Interestingly, the drug release of NMD from higher HPMC containing samples was linear though. When investigating a sample of NMD – HPMC dispersions after being exposed to dissolution medium under a polarized light microscope (figure 4-35 to figure 4-30), it was found that the samples showed recrystallization of the API at the surface. Thus, the drug dissolution was not controlled only by the behavior of the polymer, but by the kinetics of crystallization towards equilibrium and dissolution at the polymer surface. However, this hypothesis certainly deserves further in depth investigation.

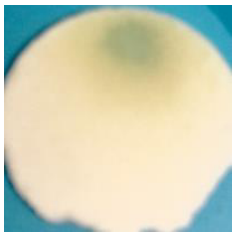

Figure 4-24 VCM prepared sample of NMD (10 %) and HPMC (90 %)

Figure 4-25 VCM prepared sample of HPMC (pure polymer)

Figure 4-26 VCM prepared sample of NMD (10 %) and HPMC (90 %) after dissolution testing

Figure 4-27 PLM before dissolution testing

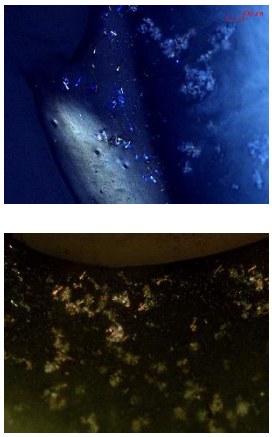

Figure 4-28 PLM after 20' dissolution testing

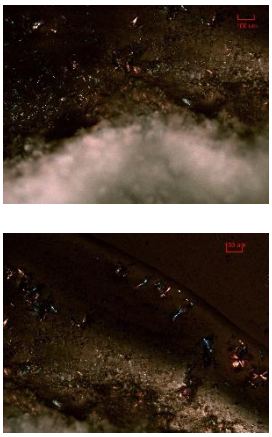

Figure 4-29 PLM after 45' dissolution testing

Figure 4-30 PLM after 70' dissolution testing

Since the dissolution profiles show an almost linear trend for dissolved drug concentration over time, the intrinsic dissolution rate is calculated by linear regression for all formulations.

The next figure shows the instrinsic dissolution rates plotted against the EE content to reveal the above mentioned observations. In short, the ternary system with a 1:1 EE:HPMC ratio is very slow whereas mixtures with slightly more or less EE or HPMC exhibit significantly higher dissolution rates. The effects of the different dissolution behaviors are illustrated with trend lines, revealing a steeper elevation on the swelling controlled side. Thus, it can be assumed that the swelling mechanism is contributing more to the dissolution process than the erosion mechanism.

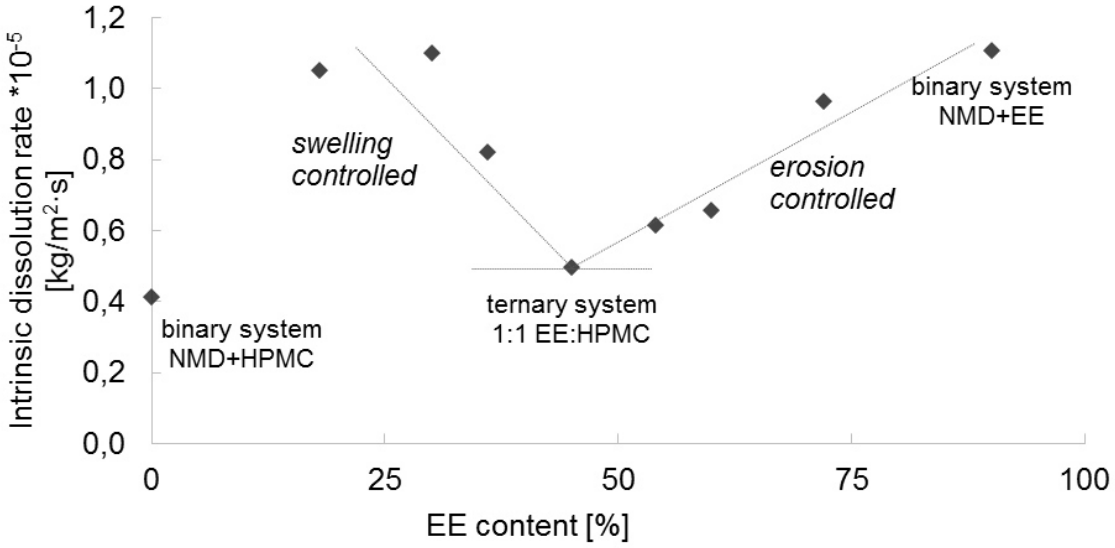

Figure 4-31 Plot of the intrinsic dissolution rates against the EE content.

4.2.2 Dissolution Studies of Pellets

Pellets of both binary mixtures and three ternary mixtures are prepared and tested under sink conditions. Figure 4-32 and figure 4-33 show the dissolution profiles of the tested pellets and the dissolution profiles of the VCM prepared tablets with the same formulation, respectively.

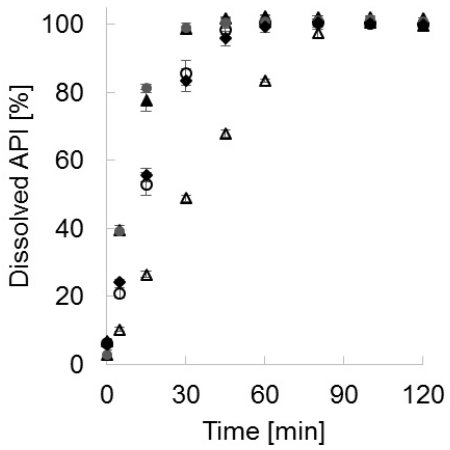

Figure 4-32 Pellet dissolution profiles of formulations with 10% API: (▲) EE; (●) 2:1 EE:HPMC ; (♦)1:1 EE:HPMC; (○)2:3 EE:HPMC; (Δ) HPMC

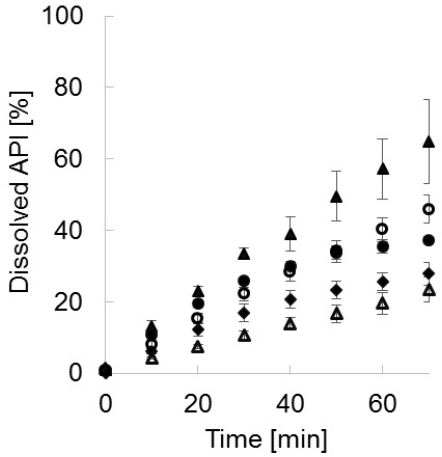

Figure 4-33 Intrinsic dissolution profiles (VCM) of formulations with 10% API: (▲) EE; (●) 2:1 EE:HPMC ; (♦)1:1 EE:HPMC; (○)2:3 EE:HPMC; (Δ) HPMC

The following table compares the released drug content of the pellets (tabletop extruded) to the VCM prepared tablets. This is done to compare the ASD prepared by the VCM technology as a miniaturization approach in an early development phase. Again, the binary mixture of NMD and EE shows a high dissolution rate. The same applies to the ternary mixture with a polymer ratio of EE: HPMC 2:1 (more EE). The binary system of NMD and HPMC is the slowest also for the pellets. The mixture with a polymer ratio of 1:1 shows a significantly increased dissolution velocity compared to the VCM prepared tablets.

Table 4-4 Dissolution results of extruded pellets compared to intrinsic dissolution results

Ratio of Polymers EE:HPMC	API release rate [mg/min]	Ranking		Intrinsic API release rate [mg/min]
EE	2.17	1	1	0.89
2:1	1.78	3	3	0.51
1:1	1.85	4	4	0.39
2:3	2.17	1	2	0.64
HPMC	1.48	5	5	0.31

4.2.3 Dissolution Studies under Non-Sink Conditions

Disc shaped VCM samples of 1 g (equivalent to 100 mg API) and 25 mm diameter are prepared. 100 mg ($2.389*10^{-4}$ mol) equal 2.3 times the solubility of crystalline API. The (quasi) equilibrium solubility (after 24 h) of crystalline NMD in dissolution medium is $1.025*10^{-4}$ mol/L. For one ternary system (2:3 EE: HPMC), the physical mixture is also tested and shows that the dissolution of NMD increased due to the amorphisation of the API during processing compared to the crystalline API (figure 4-34).

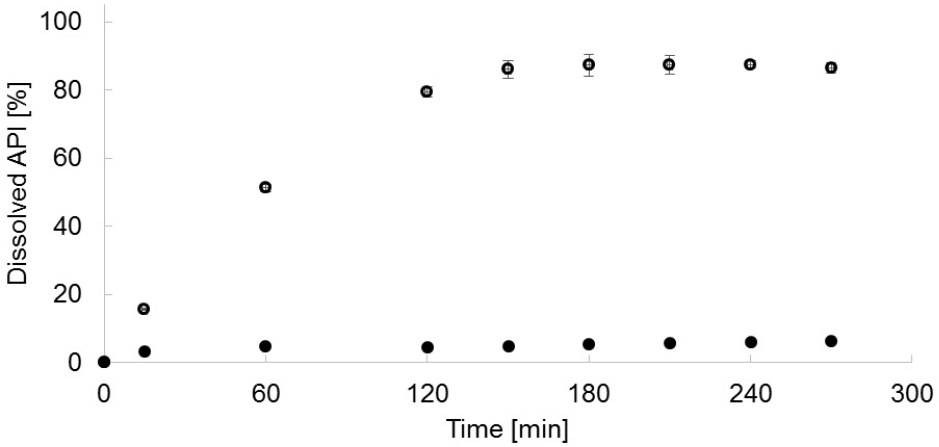

Figure 4-34 Dissolution profiles under non-sink condition: (○) 2:3 EE:HPMC ASD; (●)2:3 EE:HPMC physical mixture

The next figure (figure 4-35) shows the release profiles all formulations tested under non-sink conditions. The binary system of NMD and HPMC is (again) the slowest and reaches the lowest end concentration. The ternary systems reveal an API concentration to stationary state before reaching 100% (at 150'). It is assumed that predominant surface recrystallization occurs by this point so that the dissolution rate could not increase furthers.

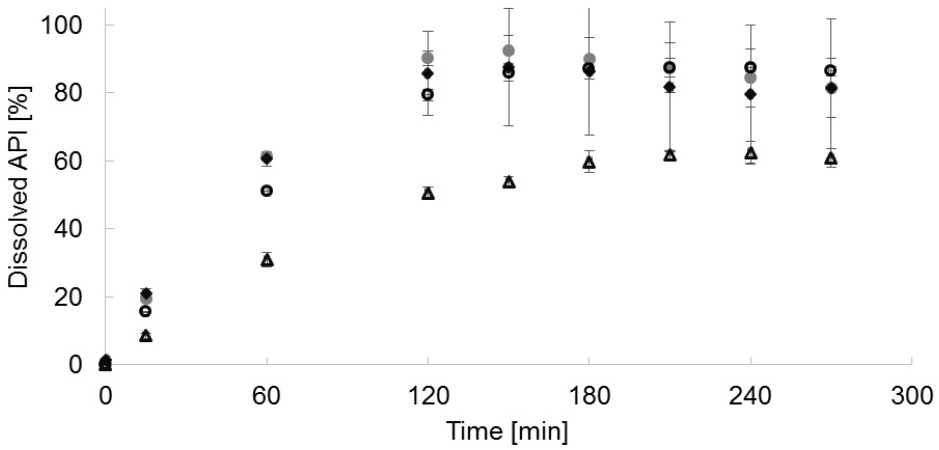

Figure 4-35 Dissolution profiles of formulations with 10% API: (●) 2:1 EE:HPMC ; (♦)1:1 EE:HPMC; (○)2:3 EE:HPMC; (∆) HPMC

The amorphous solubility is determined empirically as the following equation shows.

$$S_a = S_c \, e^{\frac{\Delta S_f}{R} ln \frac{T_f}{T}} \qquad \textbf{Equation 4-3}$$

Table 4-5 Description of symbols used in equation 4-3

Symbol			Unit
S_a	Solubility of amorphous NMD		[mol/L]
S_c	Solubility of crystalline NMD		[mol/L]
ΔS_f	Entropy of fusion	124.57	[J/mol·K]
R	Universal gas constant	8.314	[J/mol·K]
T_f	Temperature of fusion	390	[K]
T	Temperature	310	[K]

Both T_f and ΔS_f are obtained from DSC data of crystalline drug material. The enthalpy of fusion is represented by the area of the melting peak (H = 48.9 kJ/mol) and the temperature of fusion or melting temperature (T_f = 116.7 °C) is the onset temperature of this peak. R is the universal gas constant, the solubility experiment is carried out at 37 °C (T) and the determined solubility after 24 hours is S_c (1.025*10^{-4} mol/L). [52]

ΔS_f is calculated using the following equation:

$$\Delta G = 0 = H - T_f \cdot \Delta S_f \qquad \textbf{Equation 4-4}$$

$$S_a = S_c \cdot 31.18$$

It is assumed that if the amorphous form of NMD is stabilized in the dissolved polymeric environment, the solubility can be 30 times higher than the solubility of the crystalline form. However, this approach does not consider the stability of the plasticized amorphous form when in contact with dissolution medium. The theoretical solubility value (31.975*10^{-4} mol/L) compared to the experimental maximum concentration reached under non-sink conditions (4.445*10^{-4} mol/L) for the ternary system 2:1 EE:HPMC, is seven-fold higher. Thus, stability of the formulation during dissolution can be the limiting factor considering the propensity of solid-state or solution mediated recrystallization.

Conclusion

Different compositions of binary and ternary ASD systems of a BCS II drug are tested whether or not they can achieve the desired performance in in vitro dissolution testing. Firstly, the intrinsic dissolution rate of different formulations (mostly with 10% API) is determined. This is made via testing VCM prepared tablets that cover most of the surface and are only accessible for the solvent at a defined area. The evaluation of the released concentration versus time reveals linear correlation and thus indicates a “layer-wise” dissolution from the tablet. Secondly, some formulations of interest are hot-melt extruded and also tested. The release rate is compared to the intrinsic ones. This is made to compare the VCM technology to extrusion and to evaluate this technology as a possible way to test formulations in an early development phase.

5 Summary and Outlook

Combining the obtained information from different characterization methods, it was possible to evaluate miscibility, possible molecular interactions and dissolution behavior in different formulation compositions. It was found that the binary system of API and EE achieves moderate phase miscibility after thermal treatment only (in the miniaturized screening), a single T_g at low temperature, amorphous dispersed drug in the polymer and fast dissolution behavior. The dissolution rates of VCM prepared and tabletop extruded samples were the fastest. The binary system of API and HPMC suggests poor miscibility behavior after thermal treatment in the VCM, the T_g of the ASD is experimentally not evaluable, drug molecules are dispersed in amorphous form according to IR spectra and a slow dissolution is found including recrystallization at the surface of the specimen in the dissolution medium. In this case, the hot-melt extruded samples behave differently in dissolution testing. Thus, the dissolution rate depends on the applied process as shown in the difference between VCM prepared samples and pellets made via hot-melt extrusion. In all cases though, the solubility is increased significantly compared to the crystalline form of the API. The miscibility of the ternary systems becomes better, the more equal the ratio of the polymers. The T_g of the systems decreases with increasing HPMC amount. It is assumed that the HPMC does not form a homogeneous blend with the other substances with thermal treatment only due to its yield point. The intrinsic dissolution studies of the VCM tablets lead to the conclusion that the swelling mechanism (HPMC content) contributes more to the dissolution that the erosion mechanism (EE content). Moreover, the dissolution studies under non-sink condition show that 100 % API release cannot be reached and thus, stability of the formulation during dissolution can be the limiting factor considering the propensity of solid-state or solution mediated recrystallization.

The investigations of molecular interactions using FT-IR, show that the drug molecules are in amorphous state in the carrier matrix, however, evidence of molecular interactions is not given. The bands of functional groups, that are likely to interact between drug and polymer molecules, do not show shifts in the spectra. This leads to the conclusion that the API molecules are dispersed in the polymers without H-bond formation or ionic interactions. By the dispersion of the amorphous API molecules in the polymeric carrier, recrystallization is hindered in solid state, but not necessarily during dissolution.

The results from this thesis can be used to define a formulation window for the hot-melt extrusion process with desired drug dissolution profile based in thorough understanding of

the contribution of each formulation component. Processability of the different formulations has to be considered as well of course before selecting the final formulation. The VCM technology was found to be a useful tool to test HME formulations in an early development phase, even though results cannot be directly translated in all cases. Still, the material needed for this technology is low and the time-consumption for formulation screening can be reduced significantly.

In the future, additional physical stability studies of the amorphous systems in solid state should be done.

6 Appendix

6.1 Additional DSC-Thermograms

6.1.1 First Heating Run

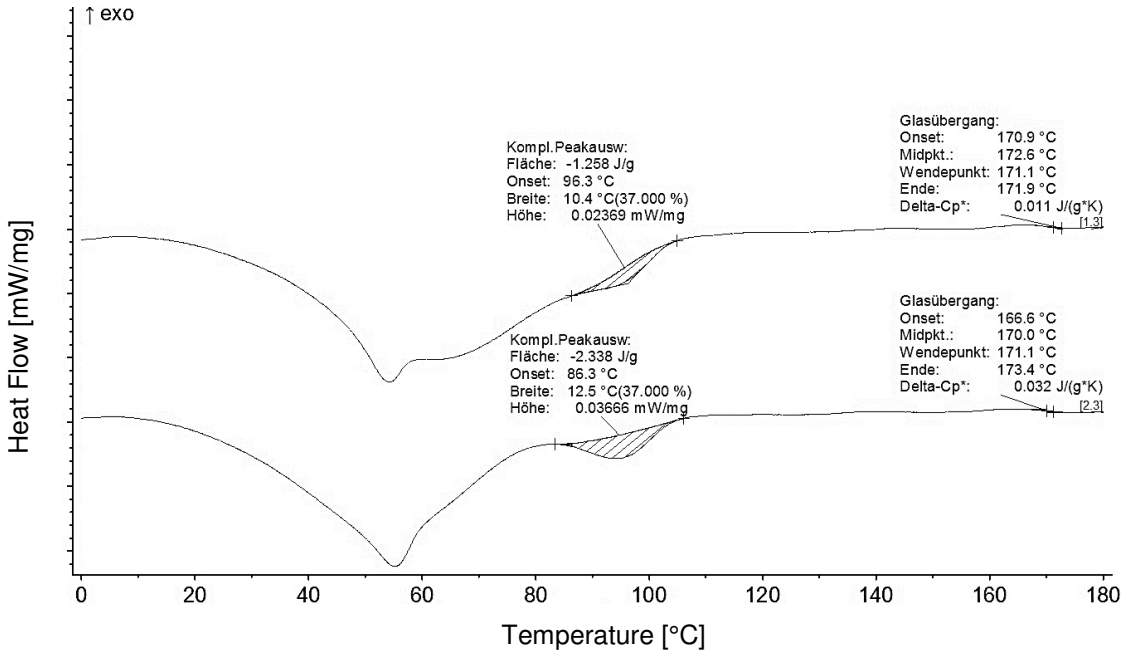

Figure 6-1 DSC-thermogram: first heating run of the ternary system EE:HPMC 4:1 (10% API)

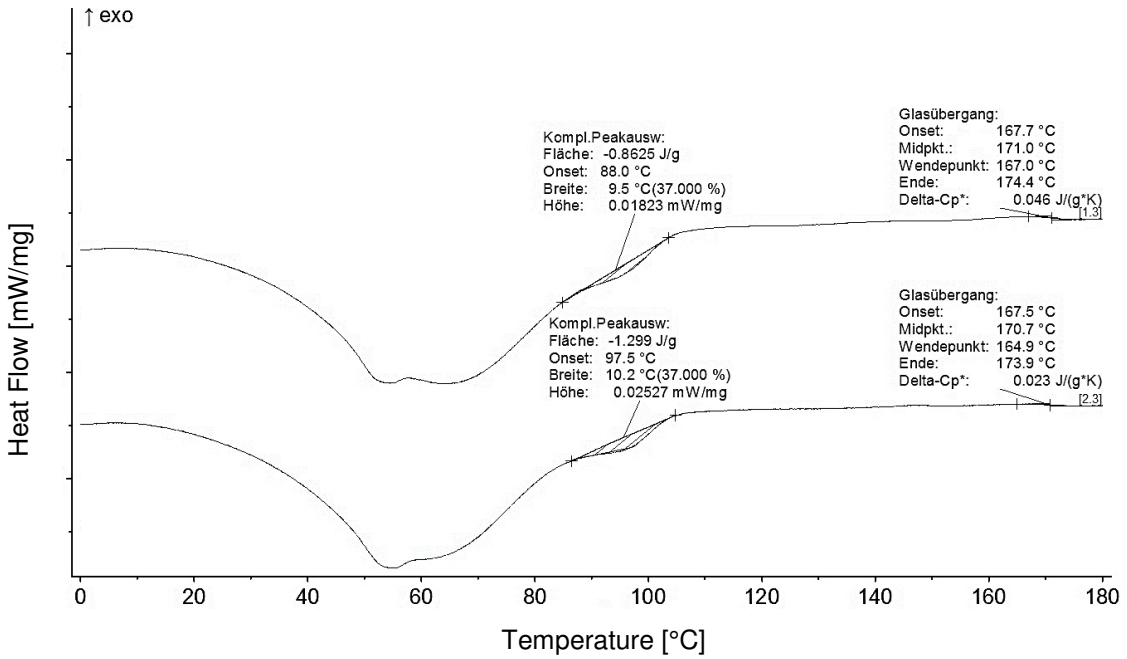

Figure 6-2 DSC-thermogram: first heating run of the ternary system EE:HPMC 2:1 (10% API)

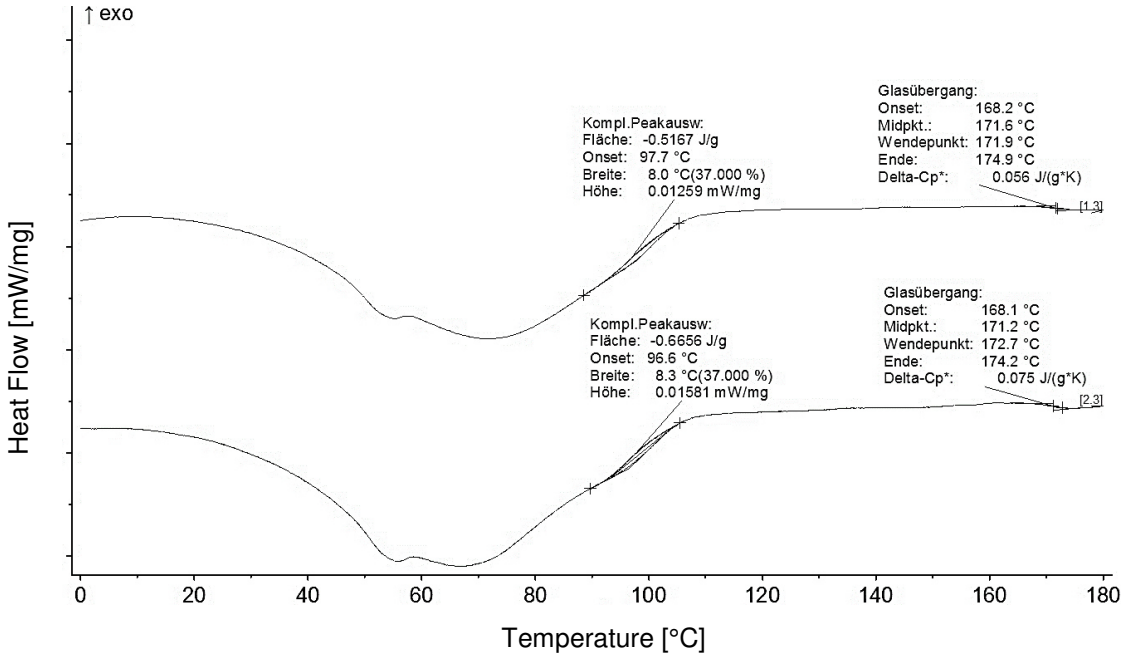

Figure 6-3 DSC-thermogram: first heating run of the ternary system EE:HPMC 3:2 (10% API)

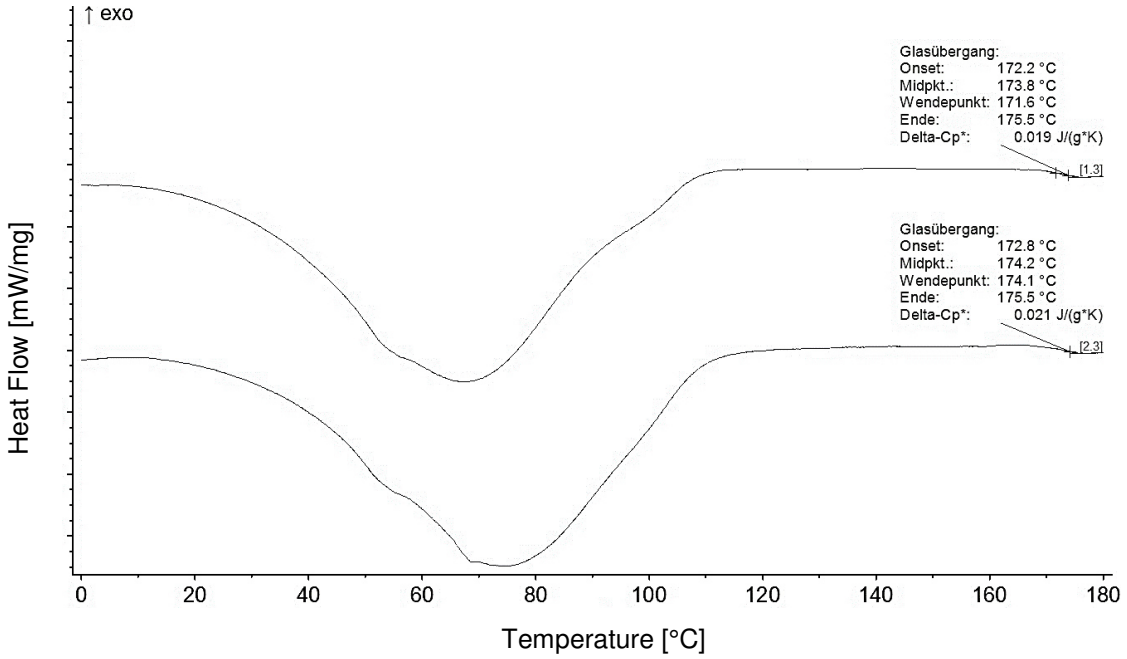

Figure 6-4 DSC-thermogram: first heating run of the ternary system EE:HPMC 2:3 (10% API)

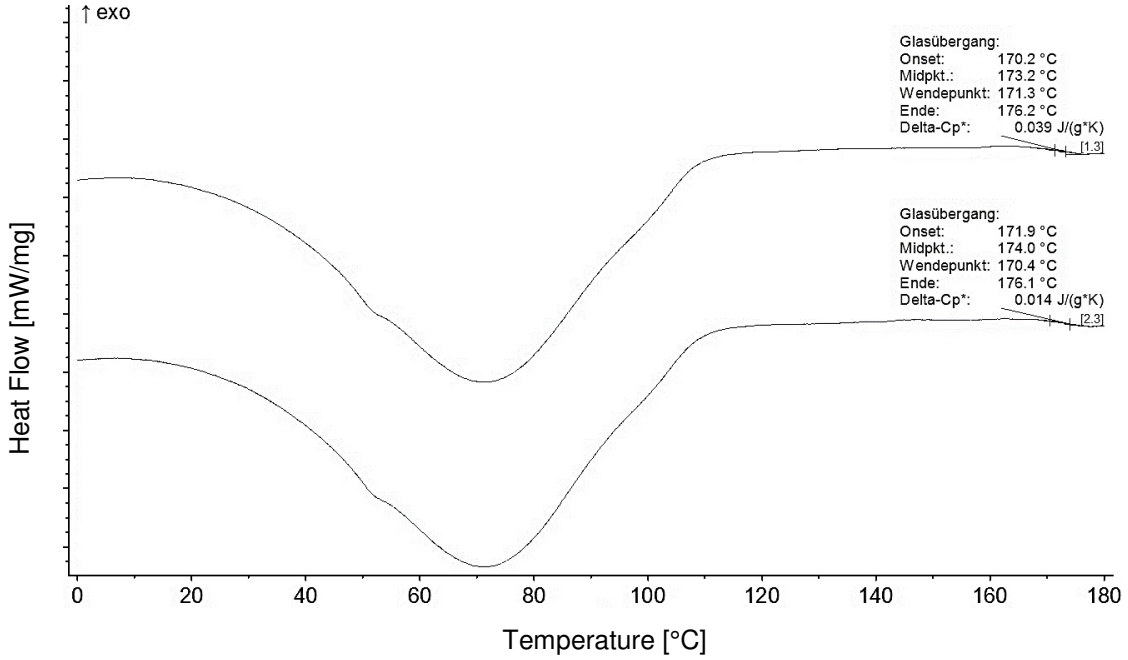

Figure 6-5 DSC-thermogram: first heating run of the ternary system EE:HPMC 1:2 (10% API)

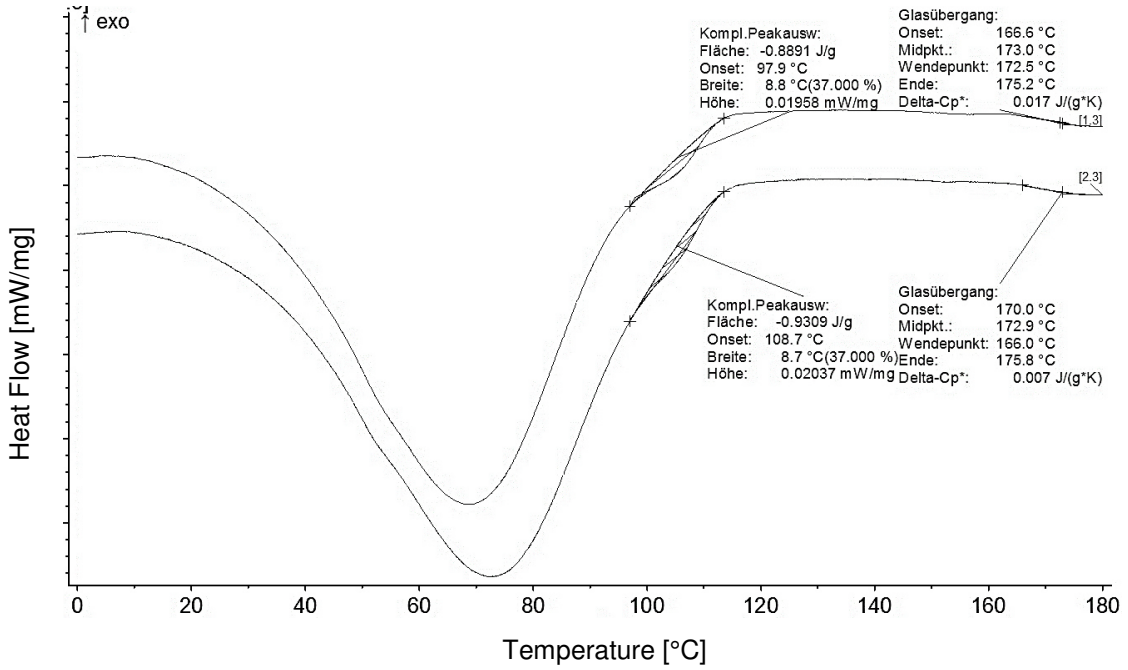

Figure 6-6 DSC-thermogram: first heating run of the ternary system EE:HPMC 1:4 (10% API)

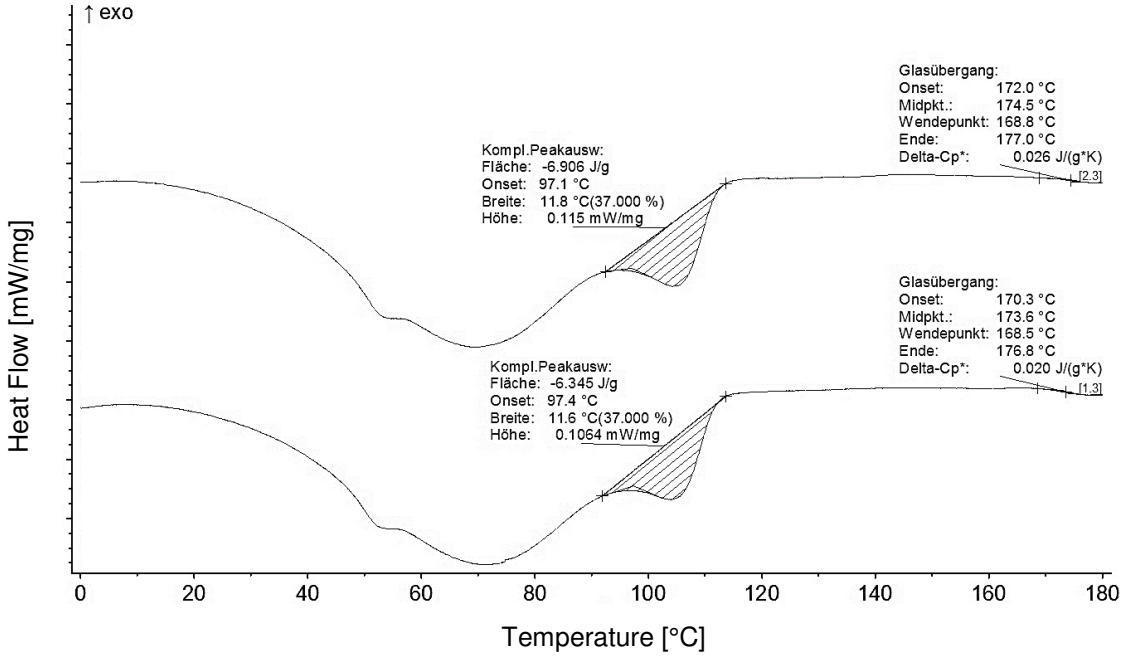

Figure 6-7 DSC-thermogram: first heating run of the ternary system EE:HPMC 1:1 (20% API)

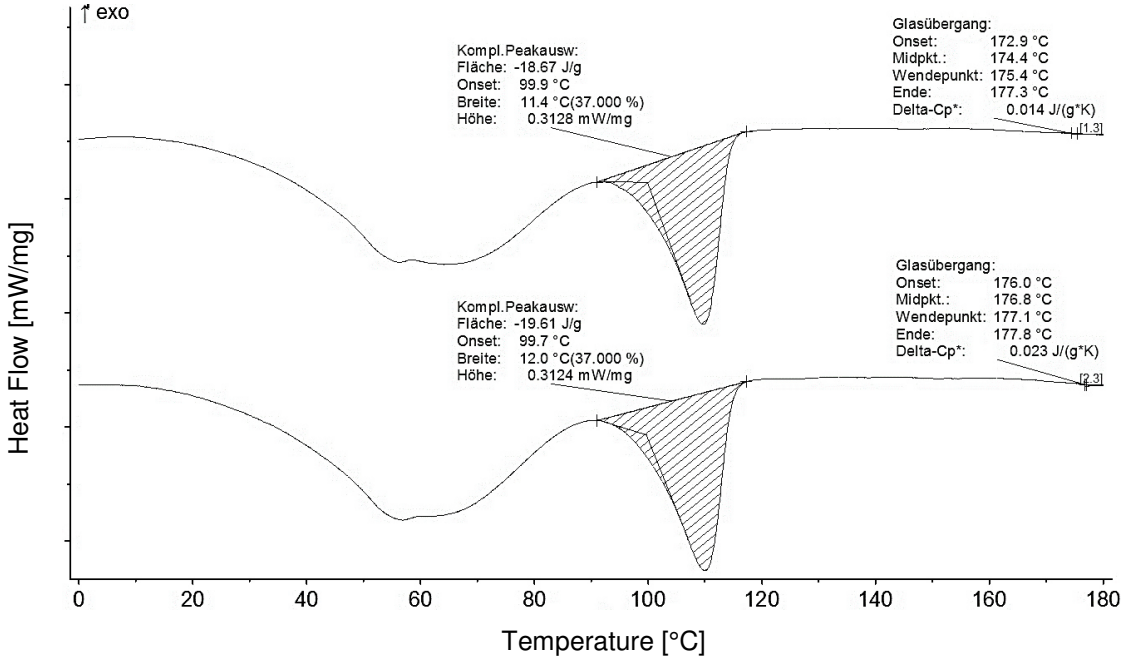

Figure 6-8 DSC-thermogram: first heating run of the ternary system EE:HPMC 1:1 (30% API)

6.1.2 Second Heating Run

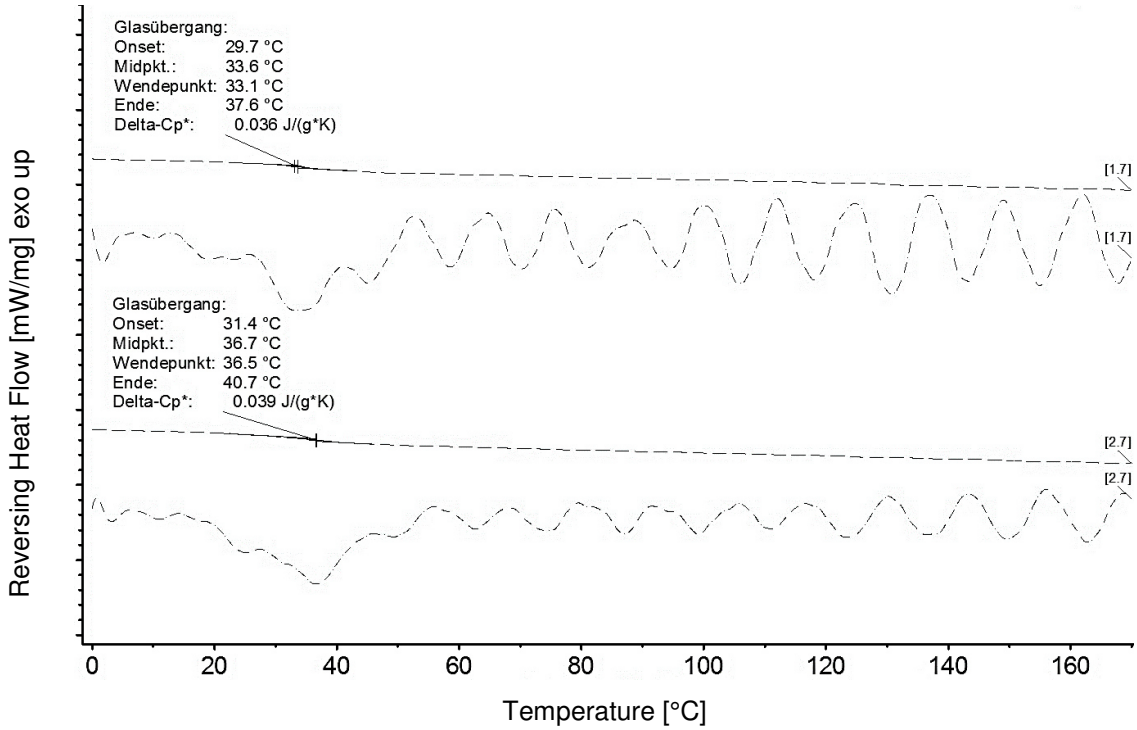

Figure 6-9 DSC-thermogram: second heating run of the ternary system EE:HPMC 4:1 (10% API) and their derivatives (1.7 and 2.7)

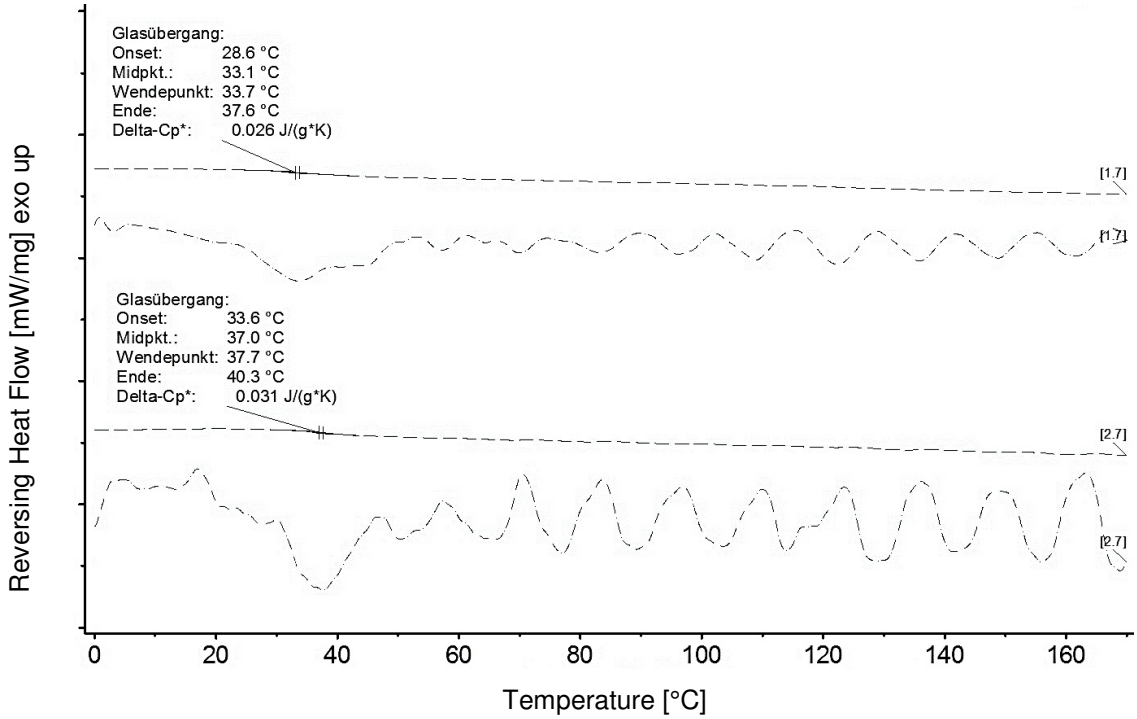

Figure 6-10 DSC-thermogram: second heating run of the ternary system EE:HPMC 2:1 (10% API) and their derivatives (1.7 and 2.7)

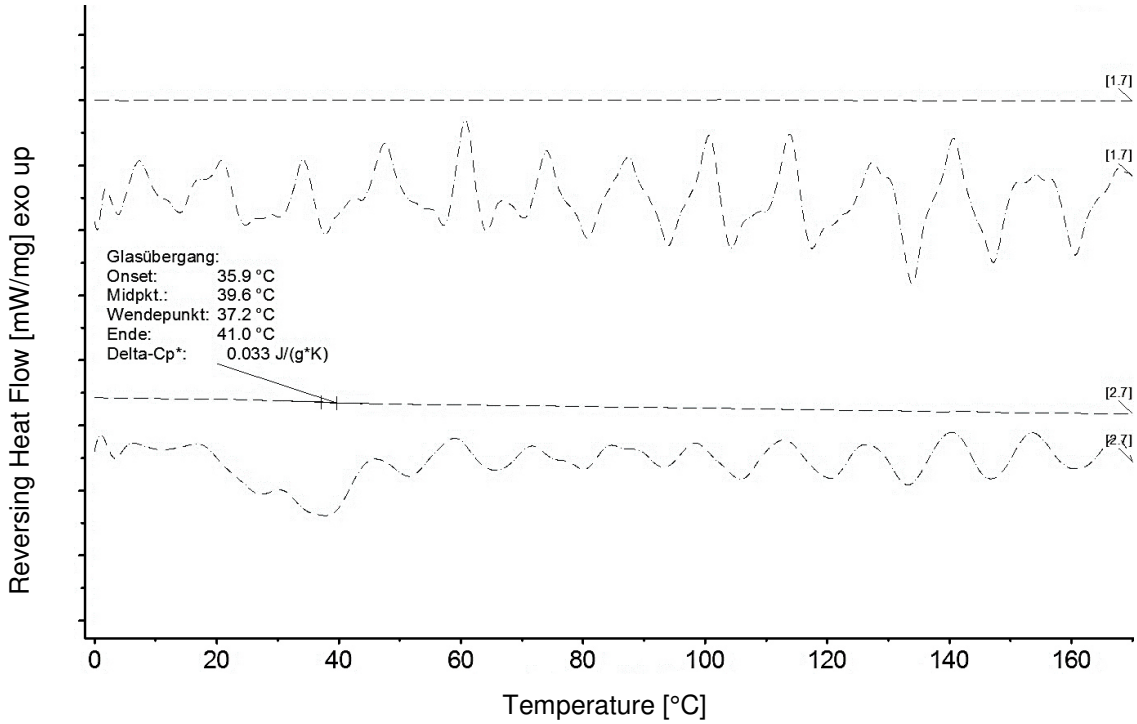

Figure 6-11 DSC-thermogram: second heating run of the ternary system EE:HPMC 3:2 (10% API) and their derivatives (1.7 and 2.7)

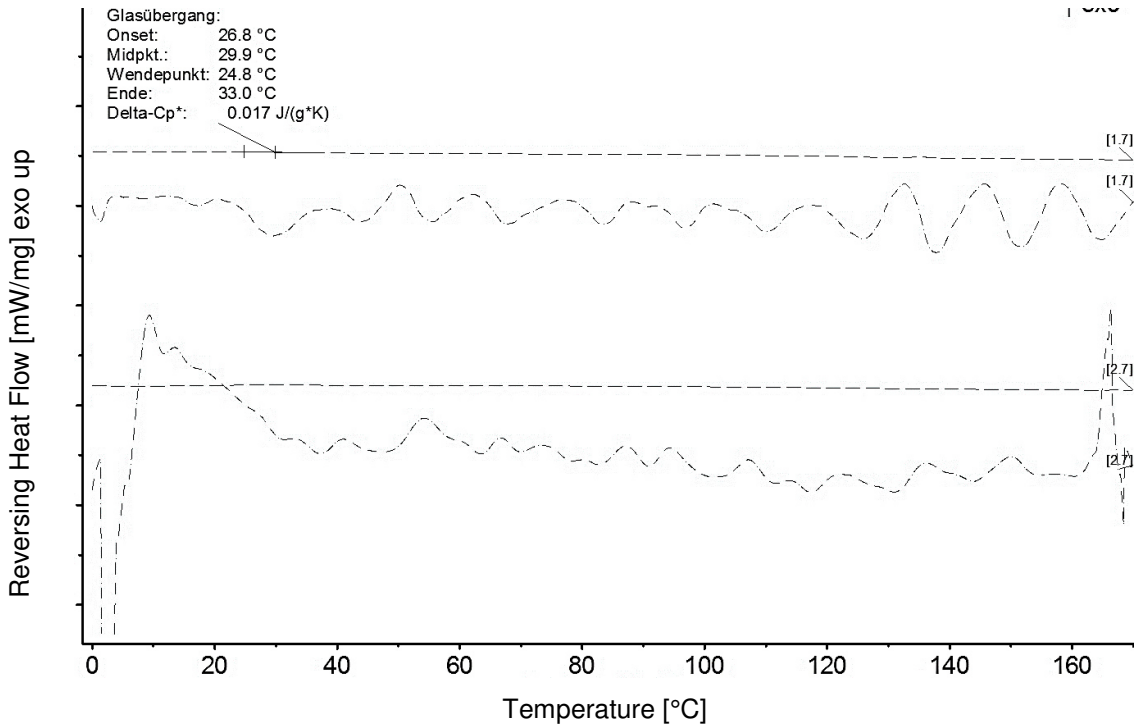

Figure 6-12 DSC-thermogram: second heating run of the ternary system EE:HPMC 2:3 (10% API) and their derivatives (1.7 and 2.7)

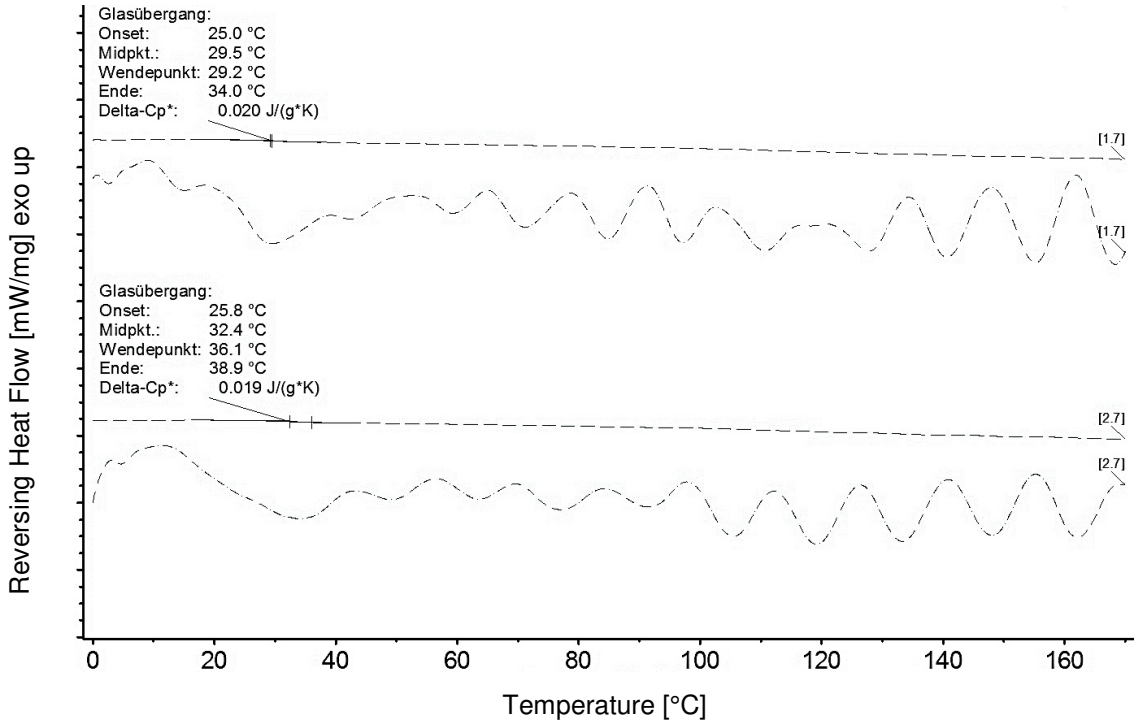

Figure 6-13 DSC-thermogram: second heating run of the ternary system EE:HPMC 1:2 (10% API) and their derivatives (1.7 and 2.7)

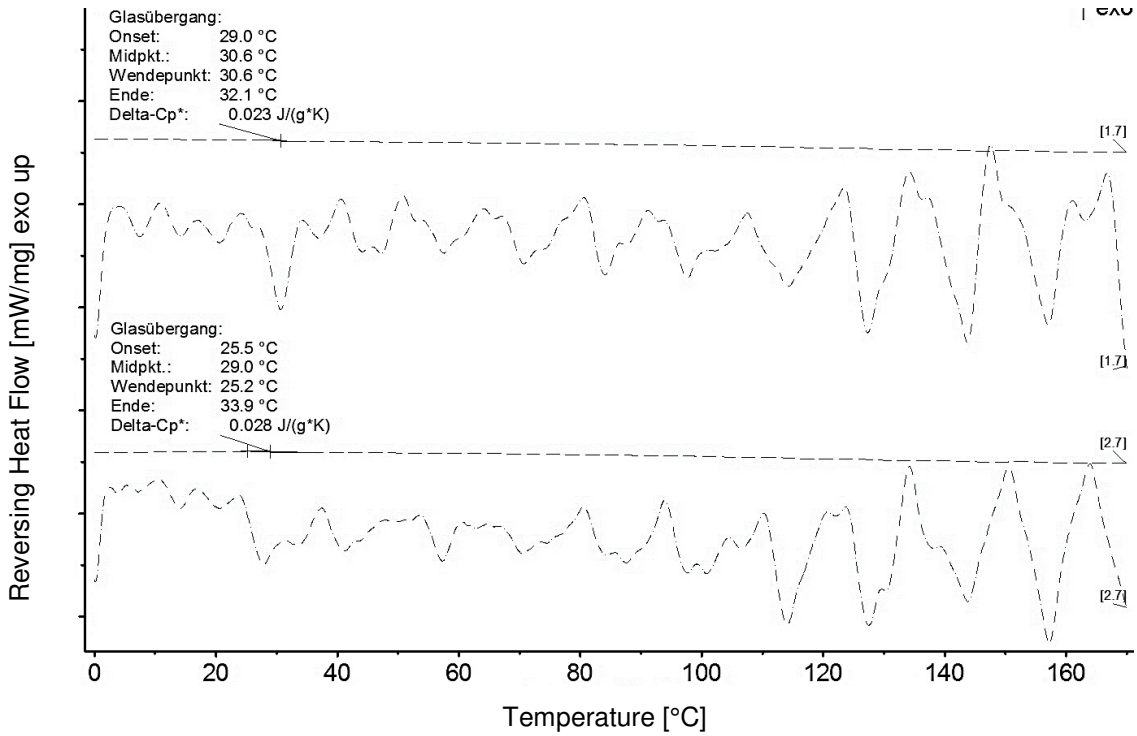

Figure 6-14 DSC-thermogram: second heating run of the ternary system EE:HPMC 1:4 (10% API) and their derivatives (1.7 and 2.7)

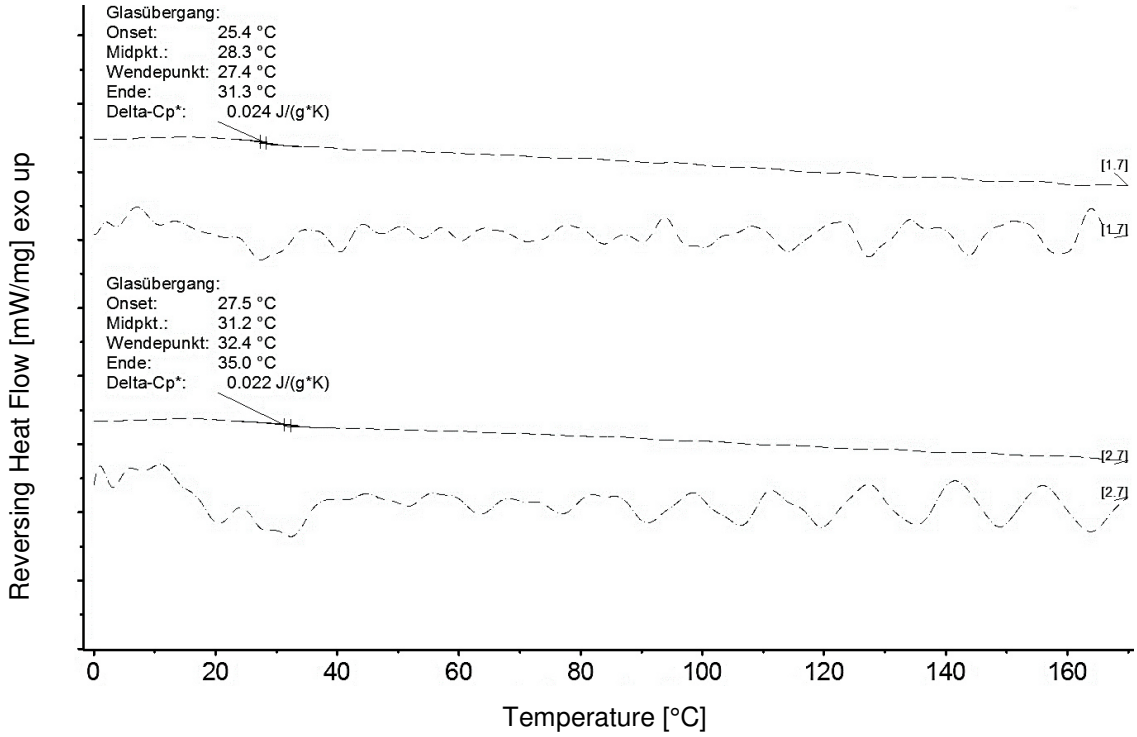

Figure 6-15 DSC-thermogram: second heating run of the ternary system EE:HPMC 1:1 (20% API) and their derivatives (1.7 and 2.7)

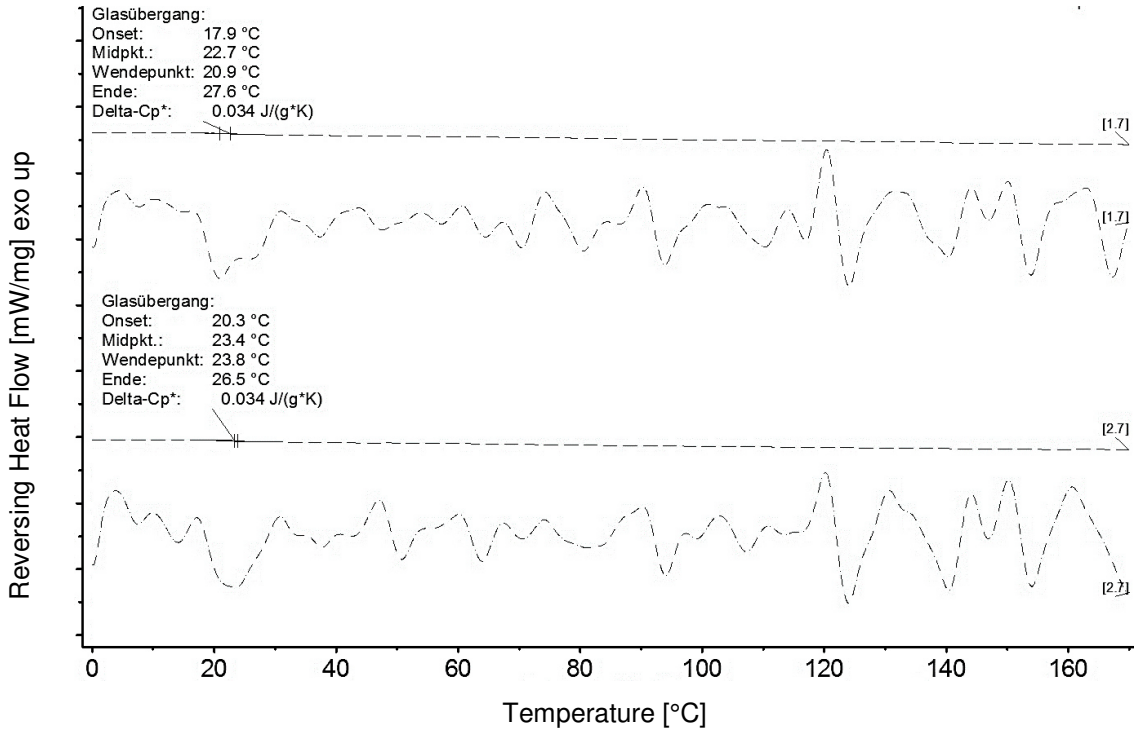

Figure 6-16 DSC-thermogram: second heating run of the ternary system EE:HPMC 1:1 (30% API) and their derivatives (1.7 and 2.7)

6.1.3 Experimental and Empirical T_g Values

Table 6-1 Experimental and empirical *Tg* values

API content [%]	Ratio of Polymers EE:HPMC	T_g experimental	T_g empirical ternary system	T_g empirical binary system	Remarks
10	EE	35.3	42.0	42.0	More EE
10	4:1	35.2	56.6	41.3	
10	2:1	35.0	67.7	40.7	
10	3:2	39.6	73.6	40.2	
10	2:3	29.9	93.6	38.3	More HPMC
10	1:2	31.0	101.0	37.3	
10	1:4	29.8	117.3	34.0	
10	HPMC	-	146.0	14.2	
10	1:1	34.0	83.2	39.4	Different API content
20	1:1	29.5	74.0	34.7	
30	1:1	23.1	65.3	30.7	

6.2 Additional FTIR-Spectra

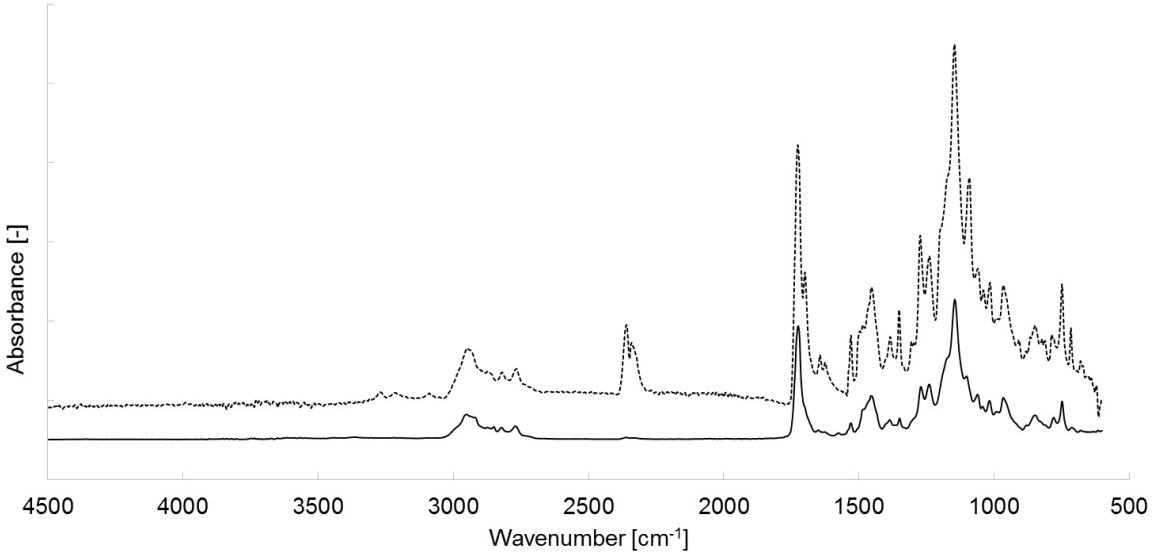

Figure 6-17 Averaged FTIR-spectra (n=3) of binary mixture (NMD and EE); dotted line – powder blend, solid line – VCM prepared sample

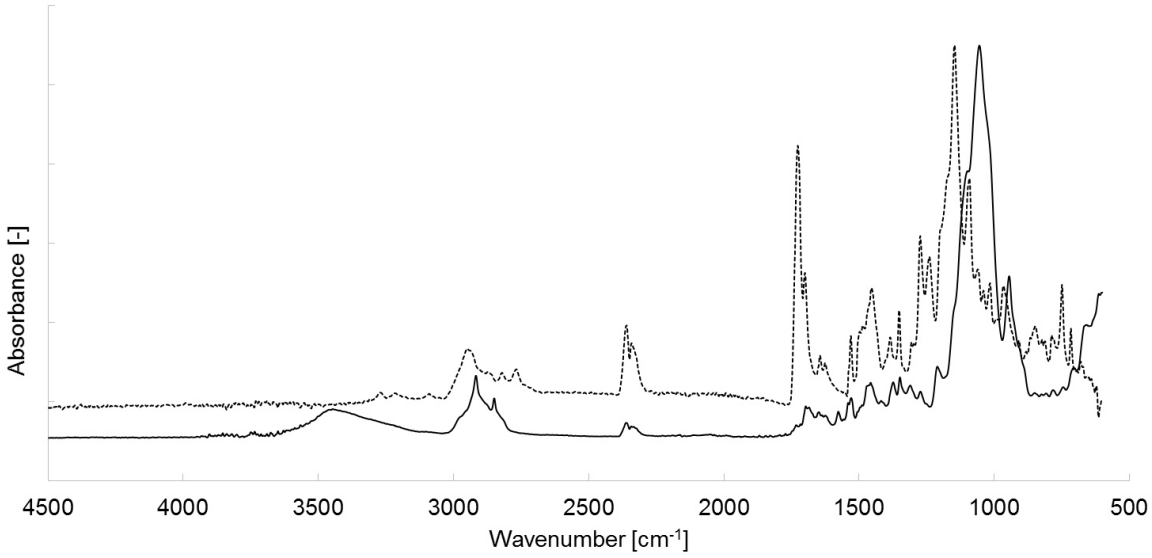

Figure 6-18 Averaged FTIR-spectra (n=3) of binary mixture (NMD and HPMC); dotted line – powder blend, solid line – VCM prepared sample

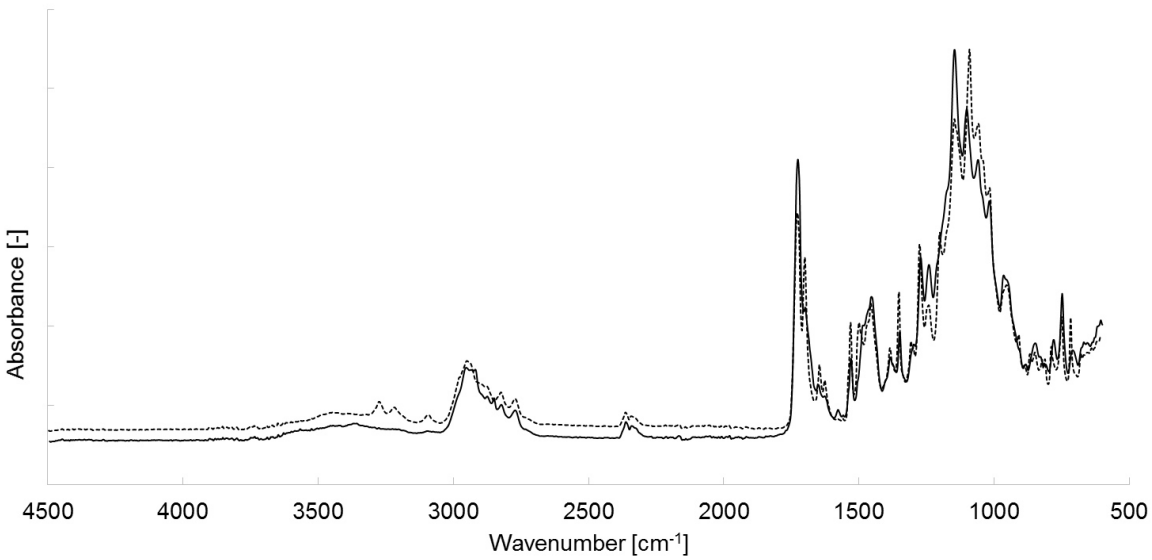

Figure 6-19 Averaged FTIR-spectra (n=3) of ternary mixtures (10% API 1:2 EE:HPMC); (black) solid line – VCM sample, (grey) dotted line – physical mixture

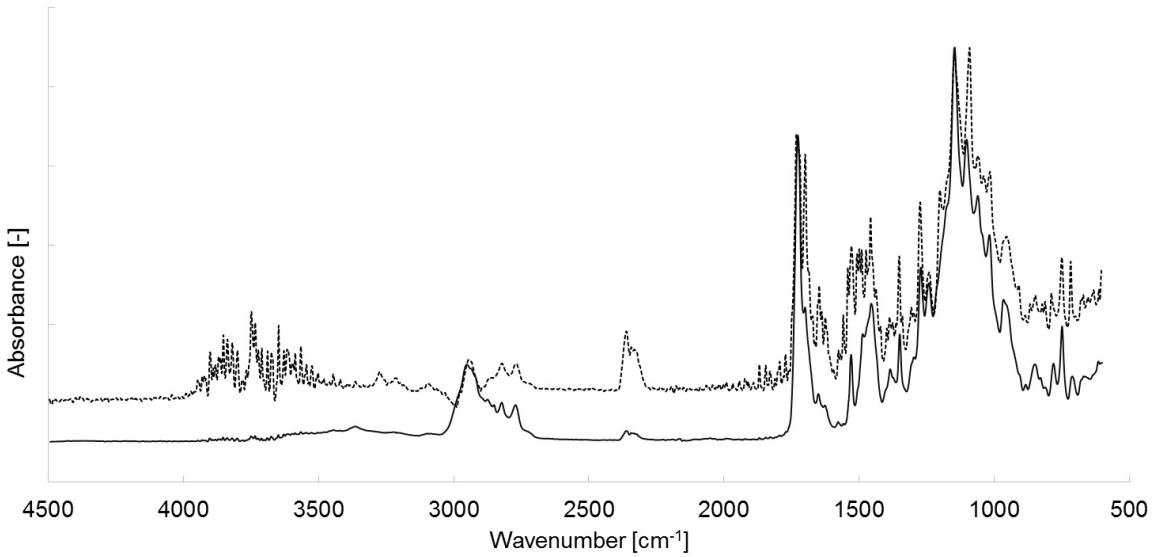

Figure 6-20 Averaged FTIR-spectra (n=3) of ternary mixtures (10% API 2:3 EE:HPMC); (black) solid line – VCM sample, (grey) dotted line – physical mixture

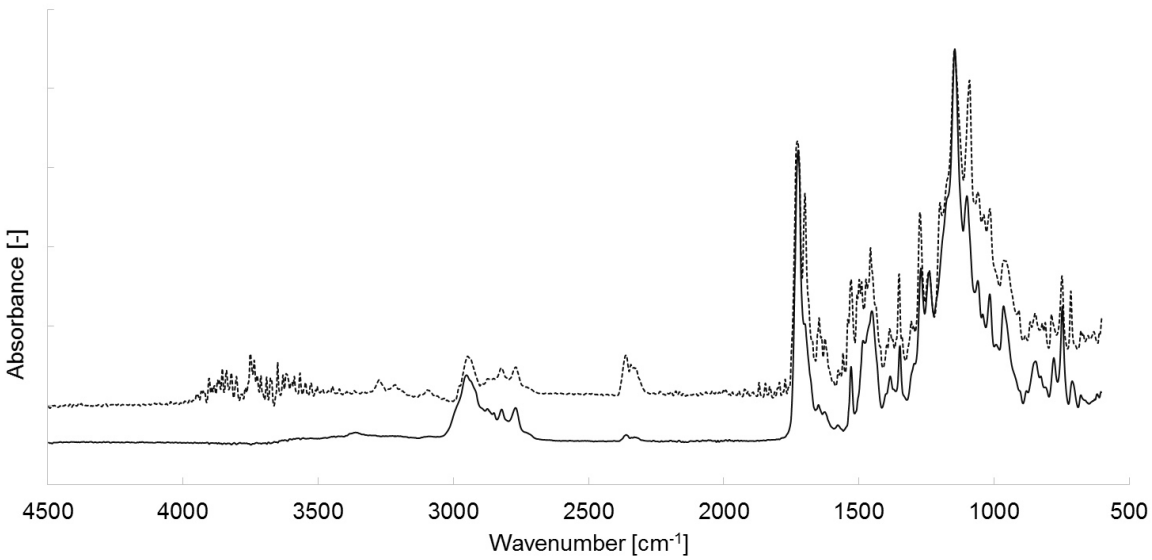

Figure 6-21 Averaged FTIR-spectra (n=3) of ternary mixtures (10% API 1:1 EE:HPMC); (black) solid line – VCM sample, (grey) dotted line – physical mixture

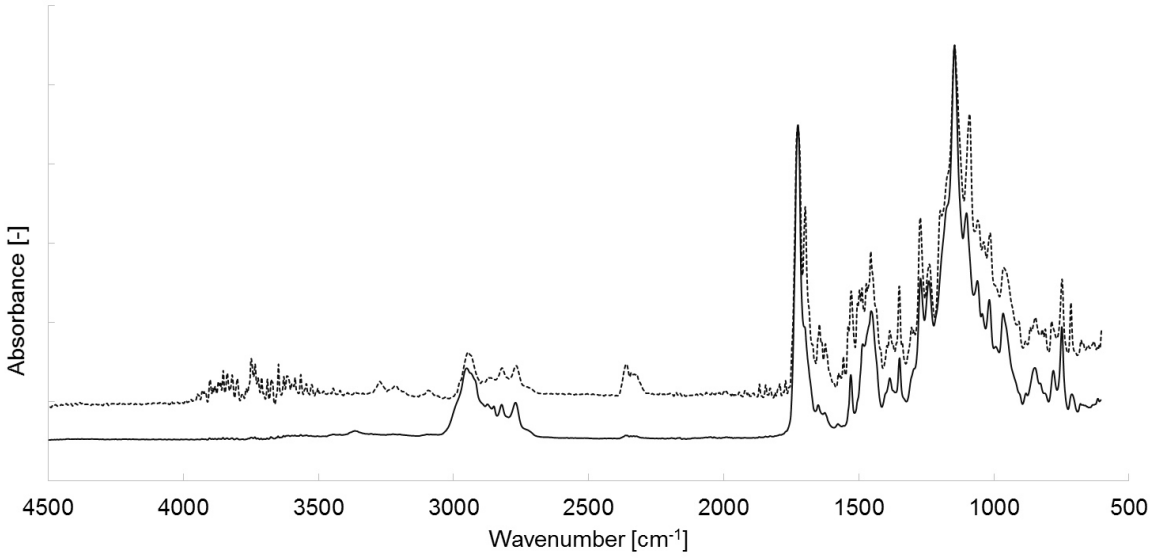

Figure 6-22 Averaged FTIR-spectra (n=3) of ternary mixtures (10% API 3:2 EE:HPMC); (black) solid line – VCM sample, (grey) dotted line – physical mixture

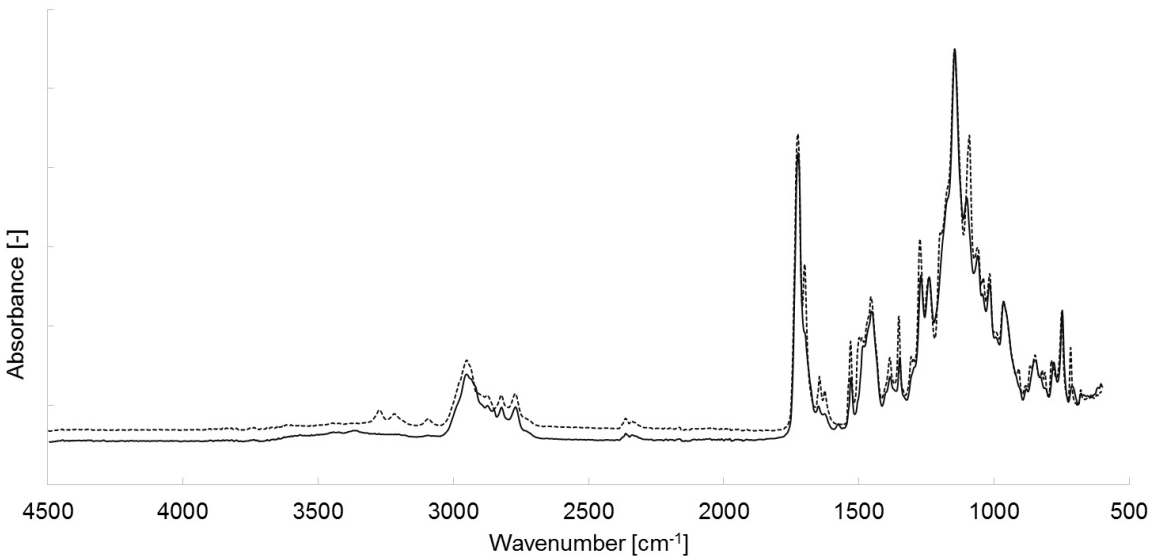

Figure 6-23 Averaged FTIR-spectra (n=3) of ternary mixtures (10% API 2:1 EE:HPMC); (black) solid line – VCM sample, (grey) dotted line – physical mixture

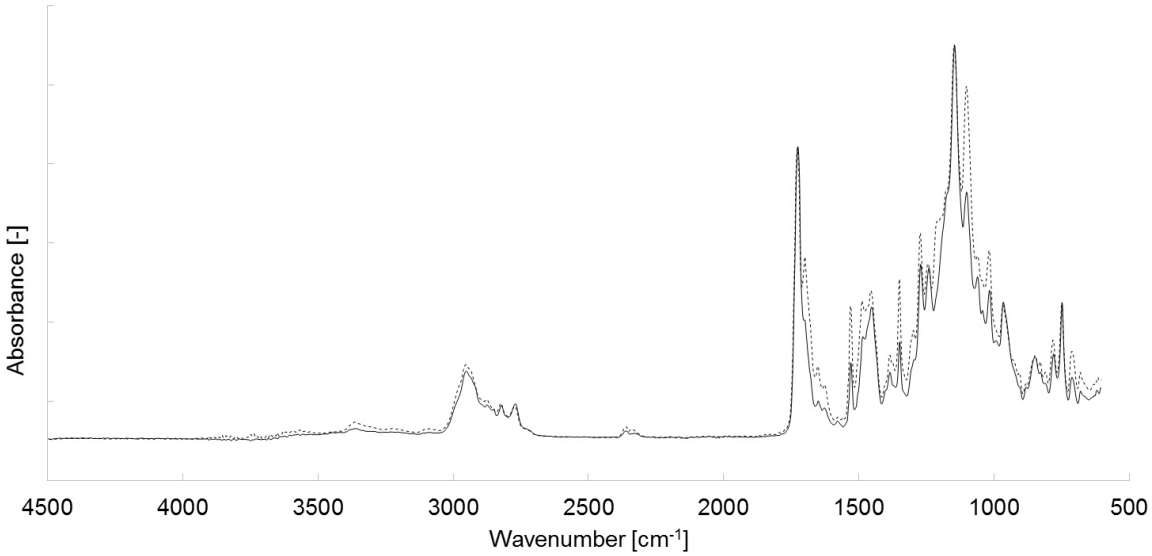

Figure 6-24 Averaged FTIR-spectra (n=3) of ternary mixtures (20% API 1:1 EE:HPMC); (black) solid line – VCM sample, (grey) dotted line – physical mixture

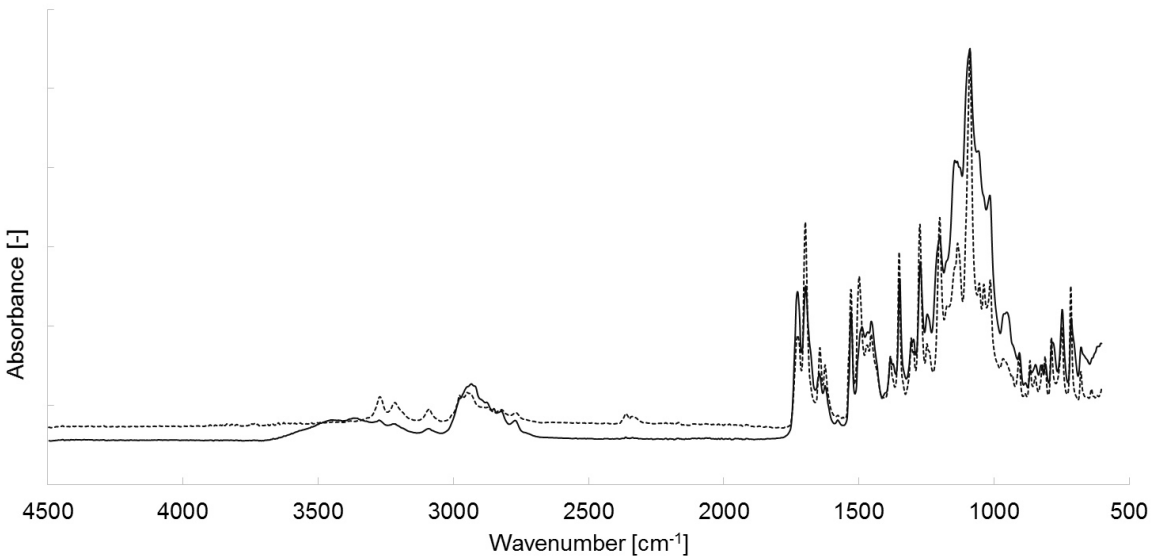

Figure 6-25 Averaged FTIR-spectra (n=3) of ternary mixtures (30% API 1:1 EE:HPMC); (black) solid line – VCM sample, (grey) dotted line – physical mixture

6.3 Dissolution Testing of VCM Tablets

Table 6-2 Released API content and intrinsic dissolution rate

API content [%]	Ratio of Polymers EE:HPMC	Dissolved API @ 75 min [%]	Intrinsic dissolution rate 10^{-5} [kg/m²·s]	Remarks
10	EE	64.9	1.108	More EE
10	4:1	53.9	0.965	
10	2:1	37.4	0.658	
10	3:2	35.0	0.615	
10	2:3	45.9	0.820	More HPMC
10	1:2	64.4	1.100	
10	1:4	58.2	1.050	
10	HPMC	23.5	0.413	
10	1:1	27.8	0.496	Different API amount
20	1:1	51.8	1.700	
30	1:1	70.8	3.799	

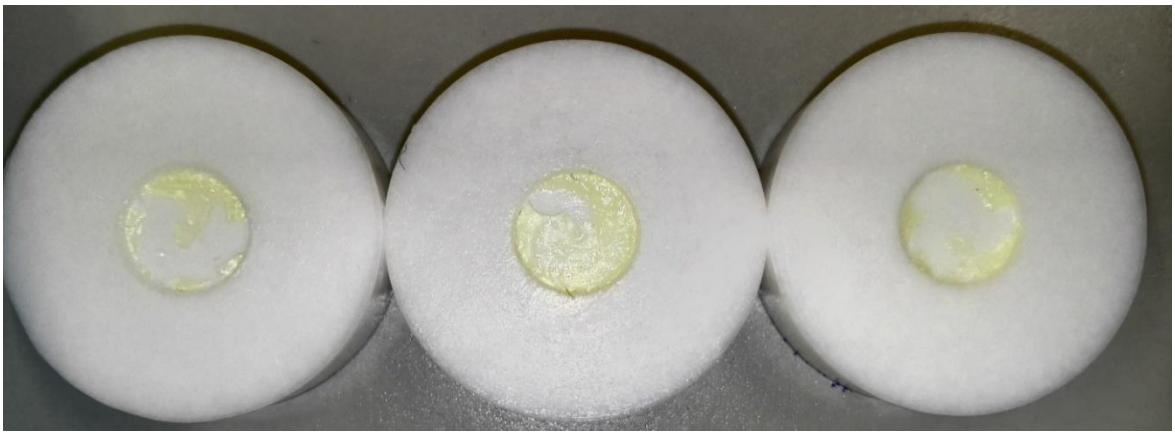

Figure 6-26 10% API with EE; picture taken after dissolution testing (70‘)

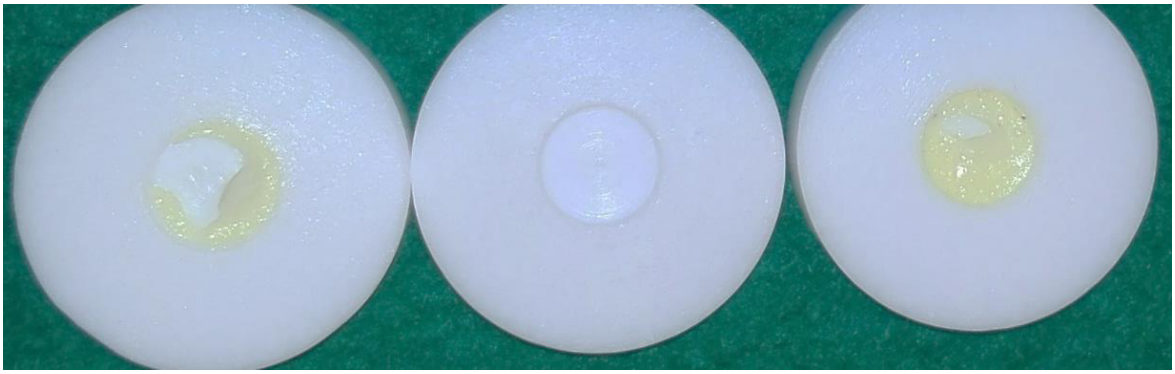

Figure 6-27 10% API with 4:1 EE:HPMC; picture taken after dissolution testing (70‘)

Figure 6-28 10% API with 2:1 EE:HPMC; picture taken after dissolution testing (70‘)

Figure 6-29 10% API with 3:2 EE:HPMC; picture taken after dissolution testing (70‘)

Figure 6-30 10% API with HPMC; picture taken after dissolution testing (70‘)

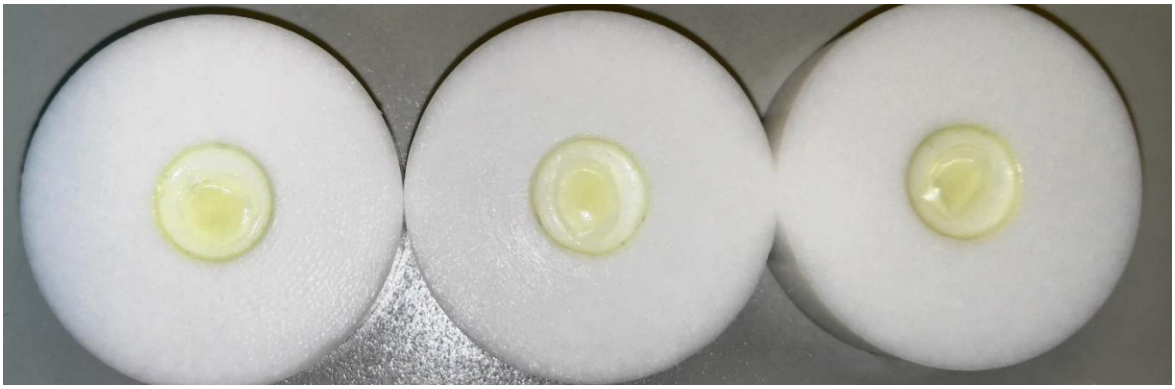

Figure 6-31 10% API with 1:4 EE:HPMC; picture taken after dissolution testing (70‘)

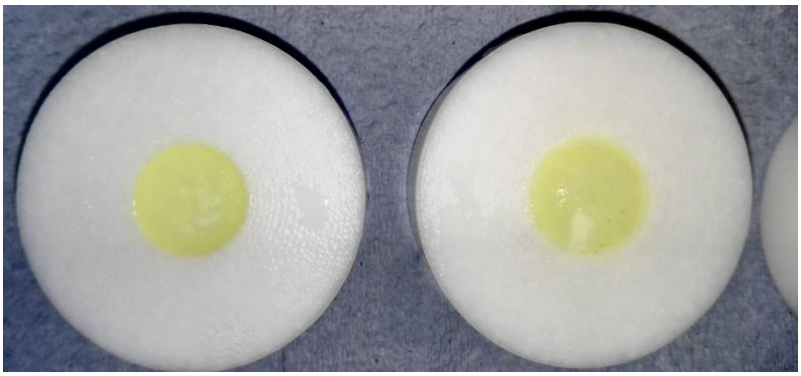

Figure 6-32 10% API with 1:2 EE:HPMC; picture taken after dissolution testing (70‘)

Figure 6-33 10% API with 2:3 EE:HPMC; picture taken after dissolution testing (70‘)

Figure 6-34 10% API 1:1 EE:HPMC; picture taken after dissolution testing (70‘)

7 References

[1] J. Khinast, “Pharmaceutical Engineering II: Drug Products and Manufacturing Science,” Graz University of Technology, 2016.

[2] U. Fagerholm, “Evaluation and suggested improvements of the Biopharmaceutics Classification System (BCS),” *J. Pharm. Pharmacol.*, vol. 59, no. 6, pp. 751–757, Jun. 2007.

[3] S. Baghel, H. Cathcart, and N. J. O’Reilly, “Polymeric Amorphous Solid Dispersions: A Review of Amorphization, Crystallization, Stabilization, Solid-State Characterization, and Aqueous Solubilization of Biopharmaceutical Classification System Class II Drugs,” *J. Pharm. Sci.*, vol. 105, no. 9, pp. 2527–2544, Sep. 2016.

[4] B. T. Smith, *Remington Education: Physical Pharmacy:* Pharmaceutical Press, 2015.

[5] H. D. Williams *et al.*, “Strategies to Address Low Drug Solubility in Discovery and Development,” *Pharmacol. Rev.*, vol. 65, no. 1, pp. 315–499, Feb. 2013.

[6] A. Paudel, “Formulation and Process Considerations in Manufacturing Spray-Dried Amorphous Solid Dispersions: A Case Study with Naproxen-Polyvinylpyrrolidone,” University of Leuven, 2013.

[7] B. C. Hancock, G. T. Carlson, D. D. Ladipo, B. A. Langdon, and M. P. Mullarney, “Comparison of the mechanical properties of the crystalline and amorphous forms of a drug substance,” *Int. J. Pharm.*, vol. 241, no. 1, pp. 73–85, 2002.

[8] S. Janssens and G. Van den Mooter, “Review: physical chemistry of solid dispersions,” *J. Pharm. Pharmacol.*, vol. 61, no. 12, pp. 1571–1586, Dec. 2009.

[9] Y. Qiu, Y. Chen, G. G. Z. Zhang, L. Liu, and W. Porter, *Developing Solid Oral Dosage Forms: Pharmaceutical Theory and Practice*. Elsevier Science, 2009.

[10] G. Van den Mooter, “The use of amorphous solid dispersions: A formulation strategy to overcome poor solubility and dissolution rate,” *Drug Discov. Today Technol.*, vol. 9, no. 2, pp. e79–e85, Jun. 2012.

[11] H. Patil, R. V. Tiwari, and M. A. Repka, “Hot-Melt Extrusion: from Theory to Application in Pharmaceutical Formulation,” *AAPS PharmSciTech*, vol. 17, no. 1, pp. 20–42, Feb. 2016.

[12] S. C. Fox, *Pharmaceutics*. London: Pharmaceutical Press, 2014.

[13] A. Sosnik and K. P. Seremeta, “Advantages and challenges of the spray-drying technology for the production of pure drug particles and drug-loaded polymeric carriers,” *Adv. Colloid Interface Sci.*, vol. 223, pp. 40–54, Sep. 2015.

[14] M. M. Crowley *et al.*, “Pharmaceutical Applications of Hot-Melt Extrusion: Part I,” *Drug Dev. Ind. Pharm.*, vol. 33, no. 9, pp. 909–926, Jan. 2007.

[15] J. Breitenbach, “Melt extrusion: from process to drug delivery technology,” *Eur. J. Pharm. Biopharm.*, vol. 54, no. 2, pp. 107–117, 2002.

[16] C. Brown *et al.*, “Hot-melt extrusion for solid dispersions: composition and design considerations,” in *Amorphous Solid Dispersions*, Springer, 2014, pp. 197–230.

[17] D. Markl, “Demonstration of a Hot Melt Extrusion Process with SIPAT,” Graz University of Technology, 2012.

[18] J. Rantanen and J. Khinast, “The Future of Pharmaceutical Manufacturing Sciences,” *J. Pharm. Sci.*, vol. 104, no. 11, pp. 3612–3638, Nov. 2015.

[19] L. Saerens, C. Vervaet, J. P. Remon, and T. De Beer, “Process monitoring and visualization solutions for hot-melt extrusion: a review: PAT in hot-melt extrusion,” *J. Pharm. Pharmacol.*, vol. 66, no. 2, pp. 180–203, Feb. 2014.

[20] C. Schiessl, “Thermische Analyse-Möglichkeiten zur Untersuchung von dentalen Kunststoffen,” 2009.

[21] K. Mohomed and D. A. Bohnsack, “Differential Scanning Calorimetry (DSC) as an Analytical Tool in Plastics Failure Analysis,” *Am. Lab.*, vol. 45, no. 3, pp. 20–23, 2013.

[22] G. Buckton, “Applications of isothermal microcalorimetry in the pharmaceutical sciences,” *Thermochim. Acta*, vol. 248, pp. 117–129, 1995.

[23] M. E. Brown and P. K. Gallagher, Eds., *Handbook of thermal analysis and calorimetry. Vol. 1: Principles and practice*, 2. impr. Amsterdam [u.a.]: Elsevier, 2003.
[24] A. Gregorova, “Application of Differential Scanning Calorimetry to the Characterization of Biopolymers,” in *Applications of Calorimetry in a Wide Context - Differential Scanning Calorimetry, Isothermal Titration Calorimetry and Microcalorimetry*, A. A. Elkordy, Ed. InTech, 2013.
[25] P. Gill, T. T. Moghadam, and B. Ranjbar, “Differential scanning calorimetry techniques: applications in biology and nanoscience,” *J Biomol Tech*, vol. 21, no. 4, pp. 167–193, 2010.
[26] A. Paudel, J. Meeus, and G. V. den Mooter, “Structural Characterization of Amorphous Solid Dispersions,” in *Amorphous Solid Dispersions*, N. Shah, H. Sandhu, D. S. Choi, H. Chokshi, and A. W. Malick, Eds. New York, NY: Springer New York, 2014, pp. 421–485.
[27] C. Leuner and J. Dressman, “Improving drug solubility for oral delivery using solid dispersions,” *Eur. J. Pharm. Biopharm.*, vol. 50, no. 1, pp. 47–60, Jul. 2000.
[28] M. K. Haque, K. Kawai, and T. Suzuki, “Glass transition and enthalpy relaxation of amorphous lactose glass,” *Carbohydr. Res.*, vol. 341, no. 11, pp. 1884–1889, Aug. 2006.
[29] M. H. Gey, *Instrumentelle Analytik und Bioanalytik*. Berlin, Heidelberg: Springer Berlin Heidelberg, 2015.
[30] J. Coates, “Interpretation of Infrared Spectra, A Practical Approach,” in *Encyclopedia of Analytical Chemistry*, R. A. Meyers, Ed. Chichester, UK: John Wiley & Sons, Ltd, 2006.
[31] K.-P. Möllmann and M. Vollmer, “Fourier transform infrared spectroscopy in physics laboratory courses,” *Eur. J. Phys.*, vol. 34, no. 6, pp. S123–S137, Nov. 2013.
[32] J. X. Wu, M. Yang, F. van den Berg, J. Pajander, T. Rades, and J. Rantanen, “Influence of solvent evaporation rate and formulation factors on solid dispersion physical stability,” *Eur. J. Pharm. Sci.*, vol. 44, no. 5, pp. 610–620, Dec. 2011.
[33] O. Planinšek, B. Kovačič, and F. Vrečer, “Carvedilol dissolution improvement by preparation of solid dispersions with porous silica,” *Int. J. Pharm.*, vol. 406, no. 1–2, pp. 41–48, Mar. 2011.
[34] B. D. Ulery, L. S. Nair, and C. T. Laurencin, “Biomedical applications of biodegradable polymers,” *J. Polym. Sci. Part B Polym. Phys.*, vol. 49, no. 12, pp. 832–864, Jun. 2011.
[35] K. E. Uhrich, S. M. Cannizzaro, R. S. Langer, and K. M. Shakesheff, “Polymeric Systems for Controlled Drug Release,” *Chem. Rev.*, vol. 99, no. 11, pp. 3181–3198, Nov. 1999.
[36] D. Bartis and J. Pongracz, “Three dimensional tissue cultures and tissue engineering,” University of Pécs, 2011.
[37] D. E. Alonzo, G. G. Z. Zhang, D. Zhou, Y. Gao, and L. S. Taylor, “Understanding the Behavior of Amorphous Pharmaceutical Systems during Dissolution,” *Pharm. Res.*, vol. 27, no. 4, pp. 608–618, Apr. 2010.
[38] G. Ragno, “Analysis of nimodipine and its photodegradation product by derivative spectrophotometry and gas chromatography,” *Int. J. Pharm.*, vol. 119, no. 1, pp. 115–119, May 1995.
[39] I. Coulter, *Pharmaceutical nimodipine compositions*. Google Patents, 2008.
[40] A. Grunenberg, B. Keil, and J.-O. Henck, “Polymorphism in binary mixtures, as exemplified by nimodipine,” *Int. J. Pharm.*, vol. 118, no. 1, pp. 11–21, 1995.
[41] K. Nollenberger and J. Albers, “Poly(meth)acrylate-based coatings,” *Int. J. Pharm.*, vol. 457, no. 2, pp. 461–469, Dec. 2013.
[42] P. Vibhooti, G. Rajan, and B. Seema, “Eudragit and Chitosan–The Two Most Promising Polymers for Colon Drug Dilevery,” 2010.
[43] S. B. Makwana, V. A. Patel, and S. J. Parmar, “Development and characterization of in-situ gel for ophthalmic formulation containing ciprofloxacin hydrochloride,” *Results Pharma Sci.*, vol. 6, pp. 1–6, 2016.
[44] J. L. Ford, “Design and Evaluation of Hydroxypropyl Methylcellulose Matrix Tablets for Oral Controlled Release: A Historical Perspective,” in *Hydrophilic Matrix Tablets for Oral*

Controlled Release, vol. 16, P. Timmins, S. R. Pygall, and C. D. Melia, Eds. New York, NY: Springer New York, 2014, pp. 17–51.
[45] D. Treffer, A. Troiss, and J. Khinast, “A novel tool to standardize rheology testing of molten polymers for pharmaceutical applications,” *Int. J. Pharm.*, vol. 495, no. 1, pp. 474–481, Nov. 2015.
[46] H. Ueda, S. Wakabayashi, J. Kikuchi, Y. Ida, K. Kadota, and Y. Tozuka, “Anomalous Role Change of Tertiary Amino and Ester Groups as Hydrogen Acceptors in Eudragit E Based Solid Dispersion Depending on the Concentration of Naproxen,” *Mol. Pharm.*, vol. 12, no. 4, pp. 1050–1061, Apr. 2015.
[47] P. Tong and G. Zografi, “A study of amorphous molecular dispersions of indomethacin and its sodium salt,” *J. Pharm. Sci.*, vol. 90, no. 12, pp. 1991–2004, 2001.
[48] Y. Li *et al.*, “Interactions between drugs and polymers influencing hot melt extrusion: Drug-polymer interactions in HME,” *J. Pharm. Pharmacol.*, vol. 66, no. 2, pp. 148–166, Feb. 2014.
[49] X. Zheng, R. Yang, X. Tang, and L. Zheng, “Part I: Characterization of Solid Dispersions of Nimodipine Prepared by Hot-melt Extrusion,” *Drug Dev. Ind. Pharm.*, vol. 33, no. 7, pp. 791–802, Jan. 2007.
[50] K. Drużbicki *et al.*, “In search of the mutual relationship between the structure, solid-state spectroscopy and molecular dynamics in selected calcium channel blockers,” *Eur. J. Pharm. Sci.*, vol. 85, pp. 68–83, Mar. 2016.
[51] R. I. Moustafine, I. M. Zaharov, and V. A. Kemenova, “Physicochemical characterization and drug release properties of Eudragit® E PO/Eudragit® L 100-55 interpolyelectrolyte complexes,” *Eur. J. Pharm. Biopharm.*, vol. 63, no. 1, pp. 26–36, May 2006.
[52] S. Janssens, A. De Zeure, A. Paudel, J. Van Humbeeck, P. Rombaut, and G. Van den Mooter, “Influence of Preparation Methods on Solid State Supersaturation of Amorphous Solid Dispersions: A Case Study with Itraconazole and Eudragit E100,” *Pharm. Res.*, vol. 27, no. 5, pp. 775–785, May 2010.